

Bulletin 152



New Mexico Bureau of Mines & Mineral Resources

A DIVISION OF
NEW MEXICO INSTITUTE OF MINING & TECHNOLOGY

Geology, mineralogy, geochemistry, and geothermometry of Kelly Limestone jasperoids, Magdalena mining district, New Mexico

Jacques Renault¹, Augustus K. Armstrong², John E. Repetski³, and Robert L. Oscarson²

¹New Mexico Bureau of Mines & Mineral Resources, Socorro, New Mexico 87801; ²U.S. Geological Survey, Menlo Park, California 94025; ³U.S. Geological Survey, Reston, Virginia 22092

NEW MEXICO INSTITUTE OF MINING & TECHNOLOGY

Daniel H. Lopez, *President*

NEW MEXICO BUREAU OF MINES & MINERAL RESOURCES

Charles E. Chapin, *Director and State Geologist*

BOARD OF REGENTS

Ex Officio

Gary Johnson, *Governor of New Mexico*
 Alan Morgan, *Superintendent of Public Instruction*

Appointed

J. Michael Kelly, *President, 1992-1997, Roswell*
 Steve Torres, *Secretary/Treasurer, 1991-1997, Albuquerque*
 Charles Zimmerly, *1991-1997, Socorro*
 Diane D. Denish, *1992-1997, Albuquerque*
 Delilah A. Vega, *Student Member, 1995-1997, Socorro*

BUREAU STAFF

ORIN J. ANDERSON, *Senior Geologist*
 RUBEN ARCHULETA, *Metallurgical Lab. Tech.*
 GEORGE S. AUSTIN, *Senior Industrial Minerals Geologist*
 ALBERT BACA, *Maintenance Carpenter II*
 JAMES M. BARKER, *Assistant Director, Senior Industrial Minerals Geologist, Supervisor, Cartography Section*
 PAUL W. BAUER, *Field Economic Geologist*
 LYNN A. BRANDVOLD, *Senior Chemist*
 RON BROADHEAD, *Assistant Director, Senior Petroleum Geologist, Head, Petroleum Section*
 RITA CASE, *Administrative Secretary (Alb. Office)*
 STEVEN M. CATHER, *Field Economic Geologist*
 RICHARD CHAMBERLIN, *Field Economic Geologist*
 RICHARD R. CHAVEZ, *Assist. Head, Petroleum Section*
 RUBEN A. CRISPIN, *Garage Supervisor*
 NELIA DUNBAR, *Analytical Geochemist*
 ROBERT W. EVELETH, *Senior Milling Engineer*
 NANCY S. GILSON, *Assistant Editor*

KATHRYN G. GLESENER, *Manager, Cartography Section*
 DEBBIE GOERING, *Staff Secretary*
 IBRAHIM GUNDLER, *Senior Metallurgist*
 WILLIAM C. HANEBERG, *Assistant Director, Engineering Geologist*
 JOHN W. HAWLEY, *Senior Environmental Geologist, Manager, Albuquerque Office*
 LYNN HEIZLER, *Assistant Curator*
 MATT HEIZLER, *Geochronologist*
 LYNNE HEMENWAY, *Computer Pub./Graphics Spec.*
 CAROL A. HIELLMING, *Associate Editor*
 GRETCHEN K. HOFFMAN, *Senior Coal Geologist*
 GLEN JONES, *Manager, Digital Cartography Laboratory*
 PHILIP KYLE, *Geochemist/Petrologist*
 ANN LANNING, *Executive Secretary*
 ANNABELLE LOPEZ, *Petroleum Records Clerk*
 THERESA L. LOPEZ, *Receptionist/Staff Secretary*
 DAVID W. LOVE, *Senior Environmental Geologist*
 JANE A. CALVERT LOVE, *Editor*
 VIRGIL LUETHI, *Mineralogist/Economic Geologist*

FANG LUO, *Research Associate/Petroleum Engineer*
 WILLIAM MCINTOSH, *Volcanologist/Geochronologist*
 CHRISTOPHER G. MCKEE, *X-ray Facility Manager*
 VIRGINIA T. MCLEMORE, *Senior Economic Geologist*
 NORMA J. MEEKS, *Director of Publications Office*
 LISA PETERS, *Lab Technician*
 BARBARA R. POPP, *Biotechnologist*
 MARSHALL A. RENTER, *Senior Geophysicist*
 JACQUES R. RENAULT, *Senior Geologist*
 CINDIE A. SALISBURY, *Cartographic Drafter II*
 SANDRA SWARTZ, *Chemical Lab. Technician*
 TERRY TELLES, *Technical Secretary*
 REBECCA J. TITUS, *Senior Cartographer*
 JUDY M. VAIZA, *Business Sero. Coordinator*
 MANUEL J. VASQUEZ, *Mechanic II*
 SUSAN J. WELCH, *Manager, Geologic Extension Service*
 MICHAEL WHITWORTH, *Hydrogeologist*
 MAUREEN WILKS, *Bibliographer*
 JIRI ZIDEK, *Chief Editor/Senior Geologist*

ROBERT A. BIEBERMAN, *Emeritus Sr. Petroleum Geologist*
 FRANK E. KOTTLAWSKI, *Emeritus Director/State Geologist*

SAMUEL THOMPSON III, *Emeritus Sr. Petroleum Geologist*
 ROBERT H. WEBER, *Emeritus Senior Geologist*

Research Associates

WILLIAM L. CHENOWETH, *Grand Junction, CO*
 CHARLES A. FERGUSON, *Univ. Alberta, CAN*
 JOHN W. GEISSMAN, *UNM*
 LELAND H. GILE, *Las Cruces*
 CAROL A. HILL, *Albuquerque*
 BOB JULYAN, *Albuquerque*
 SHARI A. KELLEY, *SMU*
 WILLIAM E. KING, *NMSU*

BARRY S. KUES, *UNM*
 MICHAEL J. KUNK, *USGS*
 TIMOTHY F. LAWTON, *NMSU*
 DAVID V. LEMONE, *UTEP*
 SPENCER G. LUCAS, *NMMNH&S*
 GREG H. MACK, *NMSU*
 NANCY J. McMILLAN, *NMSU*
 HOWARD B. NICKELSON, *Carlsbad*

GLENN R. OSBURN, *Washington Univ.*
 ALLAN R. SANFORD, *NMT*
 JOHN H. SCHILLING, *Reno, NV*
 WILLIAM R. SEAGER, *NMSU*
 EDWARD W. SMITH, *Tesque*
 JOHN F. SUTTER, *USGS*
 RICHARD FL. TEDFORD, *Amer. Mus. Nat. Hist.*
 TOMMY B. THOMPSON, *CSU*

Graduate Students

ROBERT APPELT
 ULVI CETIN
 DAVID ENNIS

RICHARD ESSER
 JOHN GILLENFINE
 MICHAEL HEYNEKAMP

TINA ORTIZ
 DAVID J. SIVILS
 JOE STROUD

Plus about 30 undergraduate assistants

Original Printing

Published by Authority of State of New Mexico, NMSA 1953 Sec. 63-1-4
 Printed by University of New Mexico Printing Services, August 1995

Available from New Mexico Bureau of Mines & Mineral Resources, Socorro, NM 87801 Published as public domain, therefore reproducible without permission. Source credit requested.

Contents

Abstract	5
Introduction	5
Geology of the Magdalena mining district	6
Proterozoic	7
Paleozoic	7
Mississippian	8
Pennsylvanian	8
Permian	12
Mesozoic	13
Tertiary	13
Intrusive activity	13
Mineralization	14
Jasperization	16
Definition and formation of jasperoids	16
Mineralogy of Kelly Limestone jasperoids	17
Geochemistry of Kelly Limestone jasperoids	25
Opportunistic sampling	25
Systematic sampling of two outcrops	27
Interpretation of jasperoid geochemistry	28
Geothermometry	31
Thermal effect of a dike intrusion on Kelly Limestone chert	31
Silica-crystallite analysis of other cherts and jasperoids	33
Summary of geothermometry study	34
Summary and conclusions	34
Acknowledgments	35
Appendix 1. Theory and calibration of silica-crystallite geothermometer	35
Appendix 2. Conodont descriptions	39
Appendix 3. Sample locations	43
Appendix 4. Chemical analyses	46
References	48
Figures	
1. Index map of west-central New Mexico showing location of Magdalena Mountains	5
2. Skylab photo of west-central New Mexico	6
3. Generalized geology of Magdalena mining district	7
4. Light-microscope photomicrographs of Kelly Limestone	9
5. Stratigraphic section showing lithology, environments of deposition, and age of Kelly Limestone and Sandia Formation	10
6. Paleokarst features at top of zone 14	11
7. Cavity or paleokarst feature in Ladron Member	12
8. Diagram illustrating burial history of Kelly Limestone through time	13
9. Rhyolite dike cutting Kelly Limestone-related jasperoid	14
10. Kelly Limestone and jasperoid at top of section	15
11. Texture of jasperoid in outcrop	16
12. Diagrammatic illustration of unconformity, karst development, rhyolite dike, and jasperoid	17
13. SEM photomicrographs of jasperoid mineralogy	19
14. SEM photomicrographs of jasperoid mineralogy	22
15. SEM photomicrographs of jasperoid mineralogy	23
16. Element variation in two jasperoid outcrop sections	26
17. Ni vs. Co, Cr vs. Fe, Cu vs. Pb, Ag vs. Pb, and Ag vs. Au scatter diagrams for two jasperoid outcrop sections	29
18. Variation of [212] crystallite temperature in sedimentary chert as a function of distance from white rhyolite dike contact	32
19. Variation of silica-crystallite temperature with reciprocal distance from center of white rhyolite dike	32
20. Variation of [212]/[104] crystallite sizes in Kelly Limestone cherts	37
21. Variation of [212]/[104] crystallite sizes in Kelly Limestone jasperoids	37
22. Calibration curve of silica-crystallite size to temperature	38
23. SEM photomicrographs of conodont specimens from top beds Kelly Limestone	40

22. Calibration curve of silica-crystallite size to temperature 38
23. SEM photomicrographs of conodont specimens from top beds Kelly Limestone **40**
24. SEM photomicrographs of conodont specimens from the Waldo mine and the crest of the Magdalena Mountains **41**
25. SEM photomicrographs of conodont specimens from outcrops of Kelly Limestone near crest of Magdalena Mountains **42**
26. Location of specimens for geochemical, SEM, and petrographic study **44**

Tables

1. Mineralogy of Magdalena mining district jasperoids **20**
2. Summary statistics for spectrographic analysis of 43 jasperoids, Magdalena district **25**
3. Correlation-coefficient table of selected elements **27**
4. Summary of conodont CAI data **31**
5. Silica-crystallite geothermometry of Kelly Limestone early diagenetic cherts 33
6. Silica-crystallite geothermometry of Magdalena district Kelly Limestone jasperoids 33
7. The [212] and [104] crystallite sizes for Kelly Limestone jasperoids 37
8. The [212] and [104] crystallite sizes for Kelly Limestone cherts 38
9. Calibration data 39
10. Geochemical analyses **46**

Abstract—The Magdalena Mountains consist of westward-tilted and faulted Carboniferous and Permian sedimentary rocks that lie on a basement of Proterozoic supracrustal rocks and are covered with Tertiary volcanic rocks associated with volcanic calderas. Mesozoic sedimentary rocks are not preserved beneath the Oligocene unconformity. Tertiary rocks are a thick sequence of volcanic rocks, caldera pyroclastics, and sedimentary rocks. Several Oligocene intrusions of mafic to felsic compositions intersect the Paleozoic rocks. The Kelly mining district is well known for its Tertiary base-metal deposits. Zinc was the most important, but lead, copper, and small amounts of silver and gold have contributed to the economy of New Mexico.

Jasperoid, a microcrystalline silica rock, occurs in bold outcrops along the crest of the Magdalenas and along the west-facing dip slope. It is the focus of this study, because in similar settings in Nevada it is frequently associated with economically important deposits of very fine-grained gold. In the Magdalenas jasperoid extensively replaces the Mississippian Kelly Limestone and fills Mississippian karst openings beneath Pennsylvanian black shale and siltstone. The mineralogy of the jasperoids displays strongly oxidized pyrite with internal zones of silver and copper sulfides. Galena and sphalerite follow pyrite in the paragenesis. A small amount of sulfur-isotope work on euhedral pyrite incompletely replaced by hematite/goethite in the jasperoids suggests that pyrite is inherited from the replaced carbonate rocks. Micrometric cassiterite grains were found in minute cavities of the jasperoids.

The geochemistry of the jasperoids was investigated by opportunistic sampling throughout the district and by systematic sampling of cliff faces at the crest of the Magdalenas. The geochemical data are compared with crustal abundance data and are found to be consistent with a model of partial melting of crustal rocks followed by differentiation and evolution of late-stage hydrothermal fluids. The geochemistry of the systematically sampled jasperoids suggests that silicification of the limestones occurred in a single event. Unlike the jasperoids of Nevada, good evidence of meteoric-water origin was not found for the Kelly Limestone jasperoids. In the opportunistically sampled jasperoids, gold ranged in concentration from 2 to 2100 ppb, averaging 274 ppb. In the same samples, silver ranged from 2 to 200 ppm, averaging 22.3 ppm. Gold and silver in the systematically sampled sections follow about the same statistics.

The geothermometry of the jasperoids was investigated by conodont color-alteration index and by silica-crystallite size. Background temperature prior to silicification reached between 190 and 223°C. The mean maximum temperatures of the cherts and jasperoids were 293 and 348°C, respectively. These high temperatures are consistent with the association of the silicification with proximal intrusive activity. The temperature data imply that heat was advected through open space by the silicification event, and the field relationships indicate that silica-rich fluids were carried into the karsted carbonate rocks of the Kelly Limestone along faults and dikes. The fluids were prevented from reaching higher in the section by an impermeable seal of Pennsylvanian black shales and siltstones.

Introduction

The Magdalena mining district is located in the northern part of the Magdalena Mountains, 3-5 mi (4.8-8.0 km) southeast of the town of Magdalena, Socorro County, New Mexico (Fig. 1). The mining district is accessible by four-wheel drive vehicle and foot trails from New Mexico Highway 60. The study area covers about 3 mi² (7.8 km²) between latitudes 34°03'00" and 34°06'30"N and longitudes 107°10'30" and 107°12'00"W, and lies entirely within the

boundaries of the Magdalena 7.5 minute quadrangle. Elevations in the map area range from 5955-10179 ft (1815-3103 m).

According to Loughlin and Koschmann (1942, p. 2), ore was discovered in the mining district in 1866 and the first shipments were made in 1881. Until 1900 output from the mining district consisted of lead with subordinate silver and a little gold. Copper then became the principal metal until 1903, when zinc-carbonate ores were first recognized and zinc became the dominant metal, coming mainly from carbonate ores until 1908 and from complex sulfide ores thereafter. The mining district was especially active during World War I. Operations nearly ceased during the depression of 1921. The Waldo and Lynchburg mines were in production during World War II and mining continued at the Lynchburg from 1950 until 1957.

Previous geologic studies include the classic study of Loughlin and Koschmann (1942), who described the stratigraphy, structure, and ore deposits and provided a 1:24,000 geologic map of the mining district. Iovenitti (1977) studied the geochemistry and history of the jasperoids. Blakestad (1978) made a detailed study of the geology and produced a geologic map of the Kelly mining district. Manrique and Campbell (1987) did a fluid-inclusion study and produced a genetic model for ore deposition at the Waldo—Graphic mine. Bobrow et al. (1983), Chapin et al. (1978), Chapin (1989), and McIntosh et al. (1991) studied the Cenozoic calderas and volcanic history of the Magdalena Mountains.

Silicification of the upper part of the Mississippian Kelly Limestone in the northern Magdalena Mountains appears to be related to the thermal and hydrothermal processes that occurred during evolution of the 32.1 Ma Socorro caldera and 28.9 Ma Sawmill—Magdalena caldera which both overlapped the Magdalena mining district (Fig. 2). However, it may be related to younger intrusions not exposed at

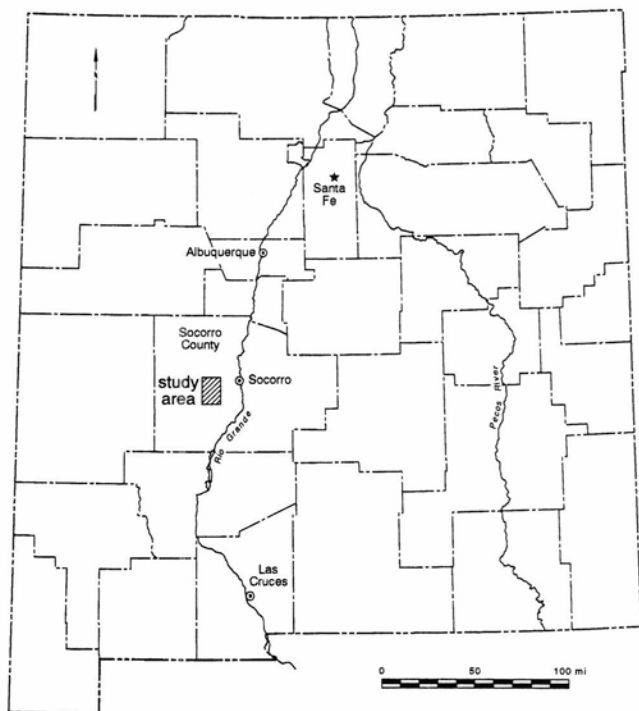


FIGURE 1—Index map of New Mexico showing location of the Magdalena Mountains and Magdalena mining district.

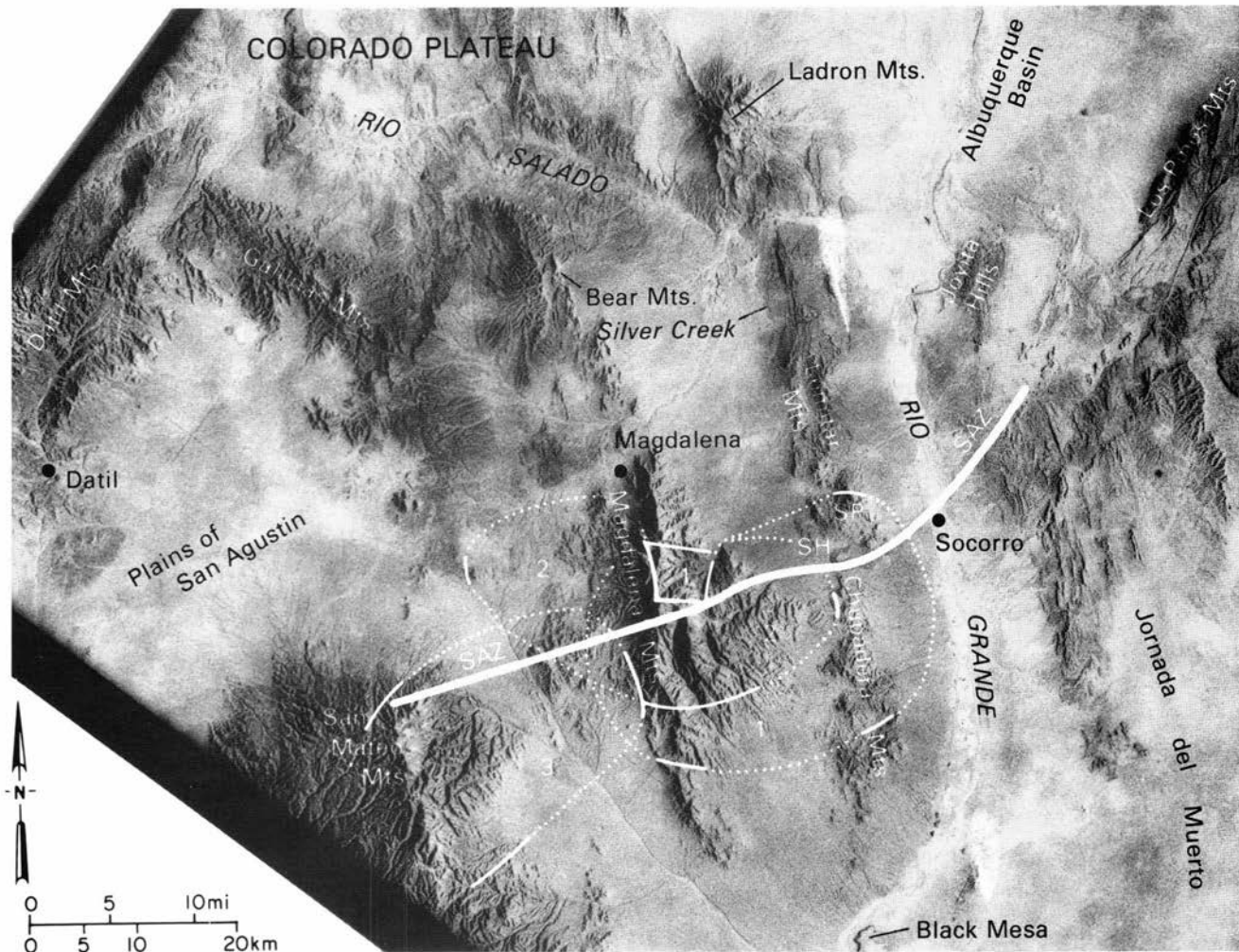


FIGURE 2—Skylab photograph of west-central New Mexico showing location of the Socorro accommodation zone (SAZ), domains of domino-style faulting, and the following early-rift calderas and their respective ash-flow tuffs: (1) Socorro caldera—Hells Mesa Tuff (32 Ma), (2) Sawmill Canyon—Magdalena caldera—La Jencia Tuff (28.8 Ma), and (3) Mt. Withington caldera—South Canyon Tuff (27.3 Ma). Note that the SAZ is approximately perpendicular to the structural grain of the synrift faults evident in the topography. From Chapin (1989, fig. 4).

the surface. In caldera settings mineralization is often much later and related to intrusions into the ring-fracture zone which provides the structural pathway for mineralizing fluids. An example is the Mogollon mining district in southwestern New Mexico, where the mineralization is some 10 Ma younger than the caldera (McIntosh, written comm. 1994).

Studies in other mining districts show that geochemical analysis of jasperoids has been useful in identifying metal anomalies that are related to economic sulfide-ore deposits (Theodore and Jones, 1992; Lovering and McCarthy, 1978; Lovering and Heyl, 1974). Theodore and Jones (1992) stated that gold concentrations in jasperoids are typically very spotty because sedimentary-hosted Au—Ag deposits along the Carlin trend of north-central Nevada contain jasperoids commonly showing insignificant gold concentrations in one sample and anomalously high concentrations in another sample only several meters away. Recent studies of jasperoids from the northern Great Basin also confirmed an extreme variability in elemental concentrations in suites of samples obtained from a single deposit (Holland et al., 1988). In addition, many of the sedimentary-hosted Au—Ag deposits along the Carlin trend and the Preble—Pinso—Getchell alignment show a zonation from distal carbonate veins, through mixed carbonate—jasperoid veins, to jasperoid-only

mineralized veins proximal to the deposits (Madrid and Bagby, 1988). In north-central Nevada, anomalous concentrations of gold appear to be concentrated mainly in the jasperoid parts of the mixed carbonate—jasperoid veins. Field studies for this report were done in 1988–1989 by Armstrong and in 1990–1992 by Renault and Armstrong. Renault studied the geochemistry and the silica-crystallite geothermometry of the jasperoids. Armstrong did the petrographic analysis, facies and porosity, and cathode—luminescence investigations of the Carboniferous rocks. Repetski established conodont stratigraphy and color and textural alteration for the temperature history of the carbonate rocks. Oscarson conducted SEM studies of the jasperoid porosity and mineralogy. The carbonate-rock classification used in this report follows Dunham (1962).

Geology of the Magdalena mining district

The Magdalena Mountains are of the Basin and Range type. They consist of westward-tilted and faulted Carboniferous and Permian sedimentary rocks (Fig. 3) that lie on a basement of Proterozoic supracrustal rocks and are partially covered with Tertiary volcanic rocks of the Socorro (32.1 Ma) and Sawmill—Magdalena (28.9 Ma) calderas.

Mississippian—The Kelly Limestone is exposed in the Ladron, Lemitar, Magdalena, and Chupadera Mountains of west-central New Mexico (Armstrong, 1958). In the Magdalena Mountains, the Kelly Limestone was measured and sampled at the head of Jordan Canyon near the north end of the range. A stratigraphic column with the microfacies, environment of deposition, and microfossil zones is shown in Fig. 5. Sando's (1984, fig. 3) Mississippian time scale for the western United States, which is based on biozones and their radiometric ages, is used in this study to estimate the length of two hiatuses within the Kelly Limestone. (See also Figs. 9, 10.)

The Kelly Limestone was deposited 5-10°S of the equator (Christopher R. Scotese, written comm. 1991). The climate was hot and arid in the Tournaisian, with increasing rainfall in the Viséan and Namurian. The Kelly Limestone is separated from the peneplained Proterozoic igneous and metamorphic rocks by a hiatus of 0.85-1.3 Ga. A pre-Kelly regolith several meters deep is developed below the unconformity in the Proterozoic rocks. The Kelly Limestone consists, in ascending order, of the Caloso and Ladron Members. The Caloso Member rests unconformably on the surface of Proterozoic metamorphic and igneous rocks. Its basal beds are 0-2 ft (0-0.6 m) thick and can be either quartz conglomerate and sandstone or microbial-mat lime mudstone. These are overlain by 33 ft (10 m) of microbial-mat dolomitic-lime mudstone and ostracode-echinoderm peloid packstone containing the calcareous alga *Asphaltinella* (Figs. 4A-D). Conodonts were collected from the lower 2 ft (0.6 m) of the Caloso Member. They contain *Gnathodus texanus* Roundy, which supports Mamet's conclusion based on foraminifera (Armstrong and Mamet, 1976) that the base of the Caloso Member is zone 8, Tournaisian.

The lower part of the overlying Ladron Member is zone 9, Tournaisian. A short hiatus separates the Caloso Member from the Ladron Member. During this hiatus the Caloso was subjected to vadose weathering and calcite cementation. The base of the Ladron Member is a 1 inch (2.5 cm) thick bed of 0.5-1.0 mm spherical quartz-grain sand cemented by lime mud and overlain by 10 ft (3 m) of poorly sorted crinoidal packstone. This is followed by a 6 ft (1.8 m) shoaling-upward sequence of microbial mats and stromatolitic-dolomitic lime mudstones. This olive-brown dolomitic to dolostone unit is the "silver pipe" of Loughlin and Koschmann (1942). The 43 ft (13 m) of limestone above the "silver pipe" are thick-bedded crinoidal wackestones and packstones with nodular white to light-gray chert (Fig. 4E). Within the member is a cryptic disconformity that encompasses zones 10 through 13. This hiatus may represent some 12 m.y., during which the zone 9 Tournaisian part of the Ladron Member was subjected to vadose and phreatic cementation and porosity reduction. Krukowski (1988) was the first to recognize that the upper 8-10 ft (2.5-3.0 m) sequence of the Ladron Member is Viséan in age, belonging to zone 14 (middle to upper Meramecian). The limestones are thin- to medium-bedded, well sorted, gray to brownish-gray echinoderm-brachiopod wackestone to packstone (Fig. 4F) containing brownish-gray nodular chert. Conodonts identified by Repetski and Robert G. Stamm from these highest beds are *Cavusgnathus unicornis* Youngquist and Miller (Pa elements), *Gnathodus texanus* Roundy (Pa elements), *Hindeodus scitulus* (Hinde) (Pa

elements), and *Taphrognathus varians* Branson and Mehl (Pa elements).

Meyers (1978, 1988) studied the cementing and paleokarst histories of the Kelly Limestone and described the diagenetic evolution and development of porosity in the upper limestone beds as follows (1988, p. 307): "The pre-Sandia Formation paleokarst features developed on skeletal Kelly Limestone which was composed mainly of crinoidal calcarenites. These paleokarst features developed on partly cemented crinoidal limestones with high intergranular porosities and permeabilities". The karst processes generally affected the upper meter or two of the formation, but in some cases penetrated to several tens of meters below the unconformity.

Paleokarst features are present in a vertical profile of progressively more intense alteration upward. This profile consists of (ascending):

- a. Etching of pre-Pennsylvanian calcite cements.
- b. Plugging of partly cemented intergranular pores by micrite and microspar, which are interpreted to be a combination of eluviated carbonate sediment and neomorphic microspar.
- c. Plugging of etched, partly cemented intergranular pores and small dissolution cavities by eluviated clay and detrital-quartz silt.
- d. Fragmented host limestones forming rubble-and-fissure fabrics in which nodules of host rock are surrounded by anastomosing veinlets and fissures filled with "weathering calcarenite," clay, and detrital quartz silt.

The restriction of much of the alteration processes in the Kelly Limestone to intergranular pores and relatively small dissolution cavities within a relatively thin interval, measuring only meters to tens of meters, contrasts with the large bedding- and joint-controlled caves and passages extending over thick intervals (hundreds of meters) characteristic of conventional extant karst.

Meyers (1985) thought the Kelly karst developed mainly in the vadose zone. Our studies indicate, however, that zone 9 beds of the Ladron Member were cemented by vadose and phreatic waters during the hiatus between zones 9 and 14. The zone 9 carbonates had a low porosity prior to deposition of the thin-bedded calcarenites of zone 14. The pre-Pennsylvanian paleokarst profile (Figs. 6, 7) developed mainly in the zone 14 crinoidal limestones that were partly cemented but had high intergranular porosity and permeability.

Pennsylvanian—The Ouachita deformation in the region was generally Early to Middle Pennsylvanian in age (Ross and Ross, 1985). The large graben-like structures present in west Texas, New Mexico, and Arizona (on the late Paleozoic cratonic shelf) resulted from the collision of South America with North America during the Late Carboniferous to mid-Wolfcampian time. In the Magdalena Mountains, the Ouachita deformation resulted in terrigenous marine sedimentation which produced the Sandia Formation and is very dissimilar to that of the Mississippian. The Kelly Limestone is composed of bioclastic carbonate sands deposited on an extensive, stable, subtidal shelf. In contrast, the Early Pennsylvanian is marked by crustal instability, reflected in the Sandia Formation by an influx of clastic sediments which formed black shales and quartz silts and sands. These tectonically derived terrigenous clastics formed a nearly impervious seal above the echinoderm

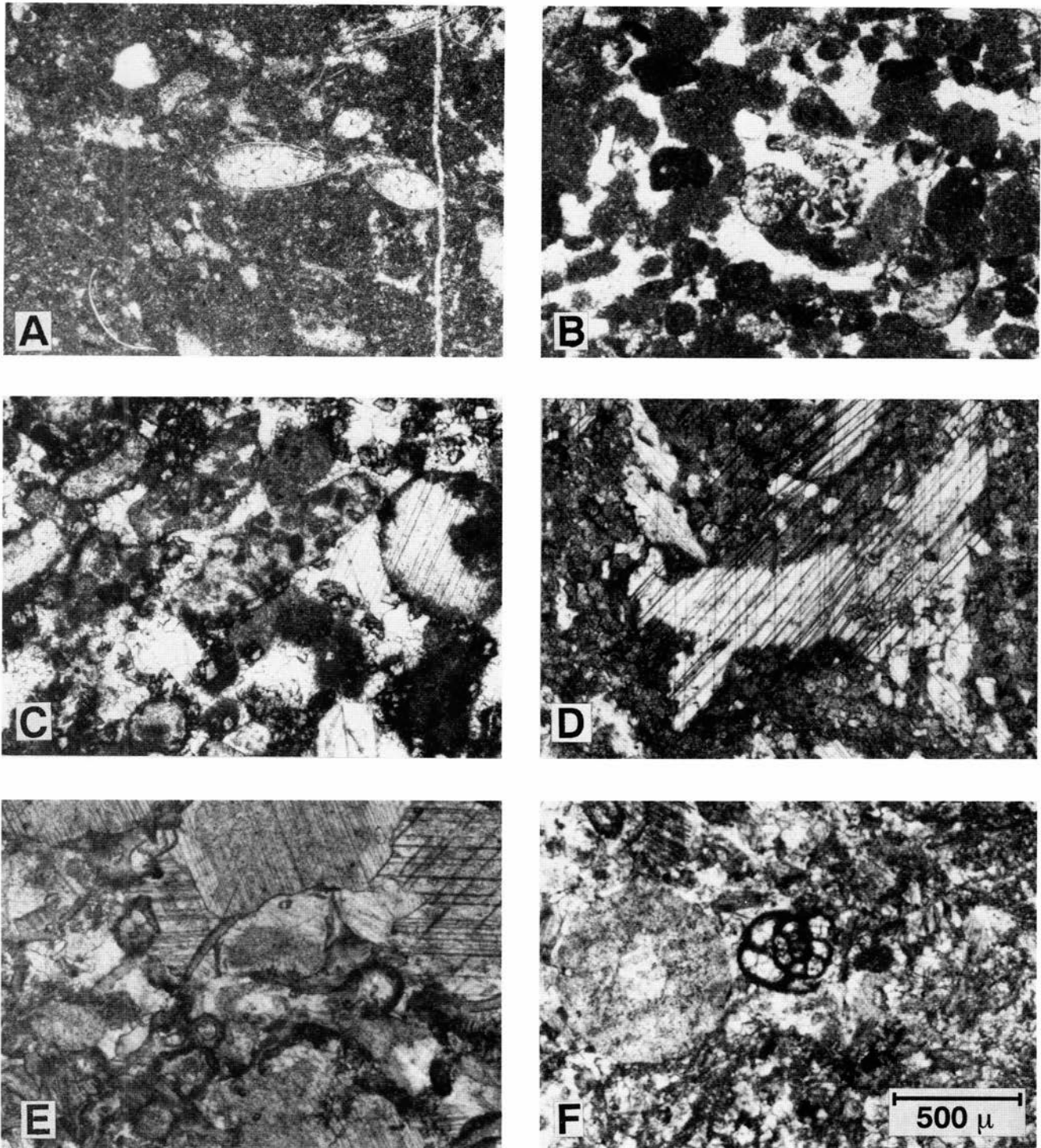


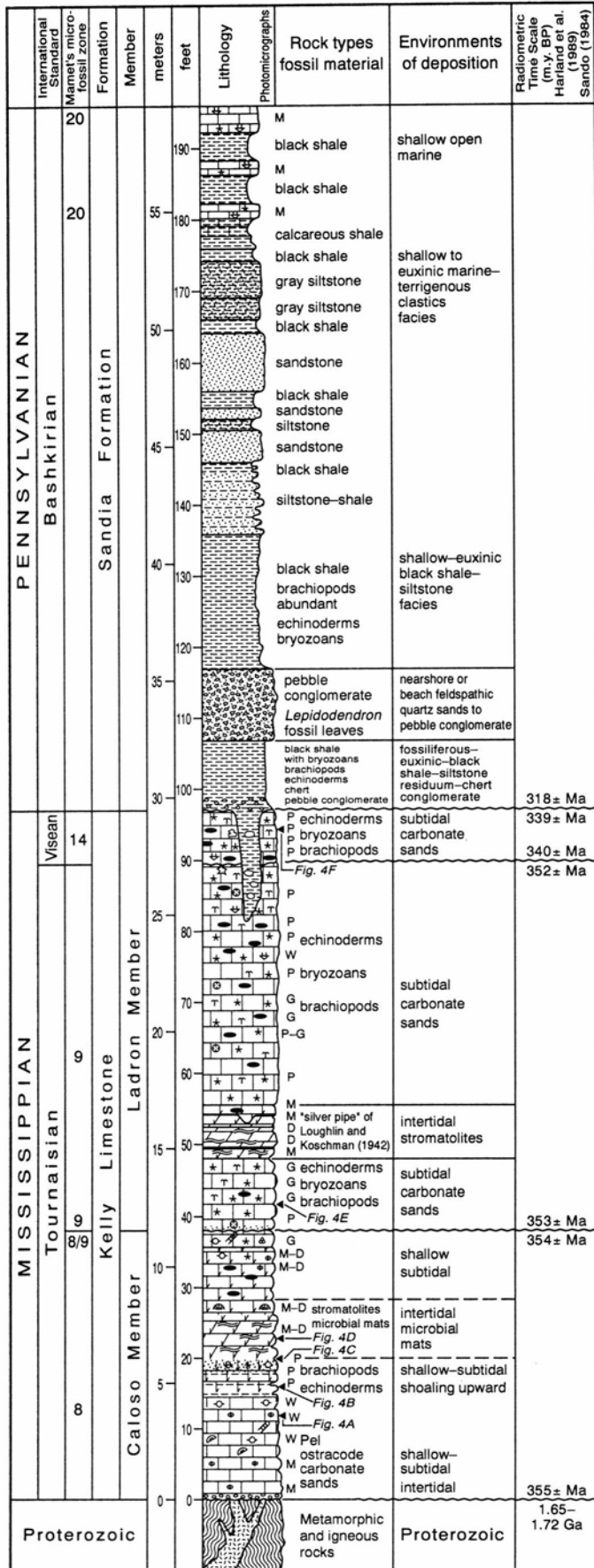
FIGURE 4—Photomicrographs, plane polarized light, Kelly Limestone. **A**, Ostracode–pellet lime mudstone, ostracode interiors filled by spar calcite, some detrital quartz sand. Environment of deposition was subtidal marine. 88N–1+3. **B**, Ostracode–calcareous algae–quartz–peloid packstone to grainstone. Quartz grains are silt size. Low faunal diversity. The calcareous algae *Asphaltinella* sp. and *Ortonella* sp. are abundant. Shallow subtidal depositional environment. 88N–1+19. **C**, Echinoderm–ostracode–quartz–peloid grainstone. The peloids are in part dolomitized. Calcite spar cement. Shallow subtidal depositional environment. 88N+1+20. **D**, Dolomitic calcite, calcite pseudomorphs of anhydrite/gypsum, dolomite rhombs, with iron oxides between rhombs, microbial mats and small stromatolites in outcrop, small channel cut and fill. High intertidal to low supratidal depositional environment. 88N–1+23. **E**, Echinoderm–bryozoan packstone–grainstone. The fossil fragments are poorly sorted, with stylolitic contact between and syntaxial overgrowth on the crinoid fragments. Bryozoans have spar-calcite pore fillings. 88N–1+43. **F**, Echinoderm–endothyrid packstone. Crinoid fragments are angular and poorly sorted. Matrix consists of small abraded bryozoan fragments and lime mud. 88N–1+96.

packstones and grainstones of the Ladoron Member of the Kelly Limestone, which had been subjected to pre-Pennsylvanian **karsting** and ground-water solution.

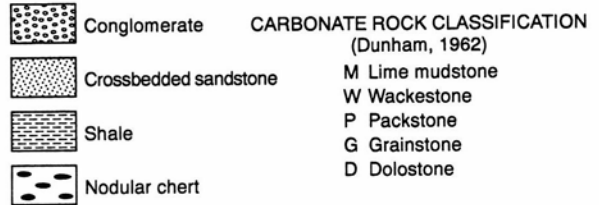
The Sandia Formation (Fig. 5) was studied at a number of outcrops along the crest and on the west flank of the range.

The best continuous exposure is in the Waldo mine tunnel.

The erosional hiatus between the Mississippian and Pennsylvanian encompasses Mamet's zones 15 to 20, Viséan to early Bashkirian time. The hiatus spans at least 21 m.y. (Fig. 5). The lower part of the Sandia Formation



EXPLANATION



CARBONATE PARTICLES OTHER THAN FOSSILS

Size	Millimeters	Mud	Coated Particles	
			One Coat	More than one coat
Silt	0.063	⊕	⊖ Superficial ooid	⊙
Sand		⊖		⊙
Granule	2.0	⊕	⊖ Superficial ooid	⊙
Pebble	4.0	⊖		⊙

ROCK TYPES

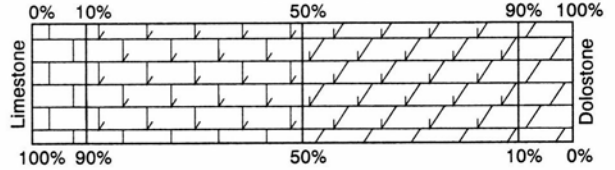


FIGURE 5—Stratigraphic section of the Kelly Limestone and the lower part of the Sandia Formation showing lithology and environments of deposition. Section measured is the Jordan Canyon road exposure, near the crest of the range at an altitude of 8800 ft (2682 m).



FIGURE 6—Paleokarst features at top of zone 14, Ladron Member, Kelly Limestone. Pennsylvanian black shales and siltstones overlying the paleokarst which is filled in part by terra rossa. The crinoidal packstones have a small sinkhole that was filled with terra-rossa soil. Barite crystals were deposited in the sinkhole and cavities by Tertiary hydrothermal fluids. Outcrop at north side of Jordan Canyon road, elevation 8800 ft (2682 m).

is some 80 ft (24 m) thick and is composed of black shales, siltstones, and quartz sandstones overlain by thin lime mudstones (micrites) (Fig. 5). Much of the terra-rossa soil that developed on top of zone 14 beds was removed by wave action of the transgressive Sandia sea. However, the terra rossa is preserved in limestone karst features. The basal Sandia Formation sedimentary rocks are chert conglomerate and dark-gray siltstone that rest on the eroded

and karsted surface of zone 14 beds of the Ladron Member. These basal conglomerates are from a few inches (several cm) to several feet (approximately 1 m) thick. The basal Sandia Formation chert conglomerate was derived from the Kelly Limestone residuum that developed during this long interval of subaerial erosion and karst development. The chert conglomerate fills channels cut into the Kelly crinoidal limestone. These are overlain by dark-gray to black



FIGURE 7—Cavity or paleokarst feature in the Ladron Member, Kelly Limestone crinoidal packstone. Bottom of the cavity is filled with calcareous terra-rossa soil which contains rounded limestone cobbles and pebbles. Upper part of cavity is still a void. Walls of cavity and the limestone clasts are lined with small barite crystals of Tertiary age. Outcrop at north side of Jordan Canyon road, elevation 8800 ft (2682 m).

siltstones and fissile shales which contain the molds of brachiopods, echinoderms, molluscs, and bryozoans. Above the black shales are 10 ft (3 m) of crossbedded quartz-pebble sandstone which contains numerous "*Lepidodendron*" leaves and tree-trunk impressions. These feldspar—quartz sands appear to have been deposited in a nearshore or beach environment (Fig. 5).

The Sandia Formation is overlain by the Madera Limestone which is 650-1750 ft (229-533 m) thick. Upward

coarsening cyclothems only 30-90 ft (9-27 m) thick are present in the section. They begin with argillaceous wackestones or lime mudstones and grade upward through fossiliferous wackestones-packstones to grainstones which may be oolitic. The cyclothems are interpreted as upward-shoaling sequences (Wilson, 1989, p. 13). Interbedded gray shales are interpreted as the deep-water basal parts of each shoaling-upward cycle capped by fossiliferous limestones.

Permian—The Permian in the area is represented by red

arkosic sandstones, siltstones, and shales of the Abo Formation which is 0-700 ft (0-213 m) thick (Siemers, 1973). Lower Permian red beds in New Mexico were deposited in a series of basins largely controlled by the distribution of late Paleozoic positive elements (McKee, 1967). During late Virgilian and early Wolfcampian times many uplifts, formed dominantly by Proterozoic basement, were rejuvenated and vast amounts of detritus was shed into adjoining basins and troughs (Hunt, 1983).

Mesozoic

No Mesozoic rocks are preserved beneath the Oligocene unconformity in the Magdalena Mountains. Triassic and Cretaceous rocks are present to the east in the Los Pinos Mountains and to the northwest near Riley. An extrapolation of Mesozoic cover over the Magdalena Mountains suggests that there were 600 ft (183 m) of Triassic and 2000 ft (610 m) of Cretaceous sedimentary rocks present at the end of the Mesozoic. Depth of burial at the end of the Mesozoic was approximately 7200 ft (2195 m) (Fig. 8).

Tertiary

The Eocene Baca Formation of Wilpolt et al. (1946) is exposed in west-central New Mexico along a discontinuous arc that extends from the Bear Mountains north of the town of Magdalena westward to the New Mexico—Arizona border (Lucas, 1983). The Baca Formation is a red-bed sequence of mudstone, sandstone and conglomerates but is absent in the Magdalena Mountains area, which was a highland during the early Tertiary and served as a source for deposition of Baca sediments further north (Cather, 1980, 1989). Chapin (1989) found above deeply eroded upper Paleozoic rocks the Oligocene Spears Formation (Cather, 1986), which is a sequence of volcanic conglomerates, mudflow deposits, and volcanoclastic sandstones 0-1000 ft (0-300 m) thick (Osburn and Chapin, 1983b).

Chapin et al. (1978) and Chapin (1989) described the Socorro accommodation zone which cuts across the center

of the Magdalena Mountains (Fig. 2) as a transverse shear zone that acted as a transfer fault connecting en-echelon axes of extension. Chapin (1989) further stated that rifting in the region began around 32.0 Ma, with eruption of the Hells Mesa Tuff and foundering of the Socorro caldera centered in the Magdalena Mountains (Fig. 2). This foundering is the earliest volcanic event linked to the Socorro accommodation zone. Eruption of the Hells Mesa Tuff occurred in a weak tensional-stress field before rapid extension began along the Rio Grande rift at about 29 Ma. In the Magdalena Mountains, several intrusive bodies were emplaced following formation of the Socorro caldera. Kelley et al. (1992) determined a zircon fission-track age of 27.9 ± 1.5 Ma for one of the quartz-monzonite dikes. Monzonitic to granitic stocks in the northern Magdalena Mountains have K/Ar ages of 28 to 31 Ma (Chapin, 1989). $^{40}\text{Ar}/^{39}\text{Ar}$ dating by McIntosh et al. (1991) has shown that in the Magdalena Mountains ash-flow volcanism was voluminous between 32 and 24 Ma; basaltic-andesite volcanism was common between 30 and 24 Ma. Volcanic rocks are sparse during the period from 24 to 18 Ma. Following this volcanic lull, moderately voluminous siliceous lavas began to be erupted near Magdalena. Rhyolite volcanism continued sporadically at several eruptive centers along the Socorro accommodation zone until about 7 Ma. Basaltic volcanism began prior to the rhyolitic eruptions and continued until at about 4 Ma.

The location of vents and domes for the 19 to 7 Ma siliceous volcanism is controlled largely by the Socorro accommodation zone and the caldera-margin ring-fracture zone. At lower-to-middle crustal depths the structure provides paths of low resistance for rising magma, while at upper crustal depths the caldera ring-fracture zones allow magmas relatively easy access to the surface.

Intrusive activity

Intrusions in the Magdalena mining district are either Proterozoic or Tertiary in age. Beyond a passive role, the

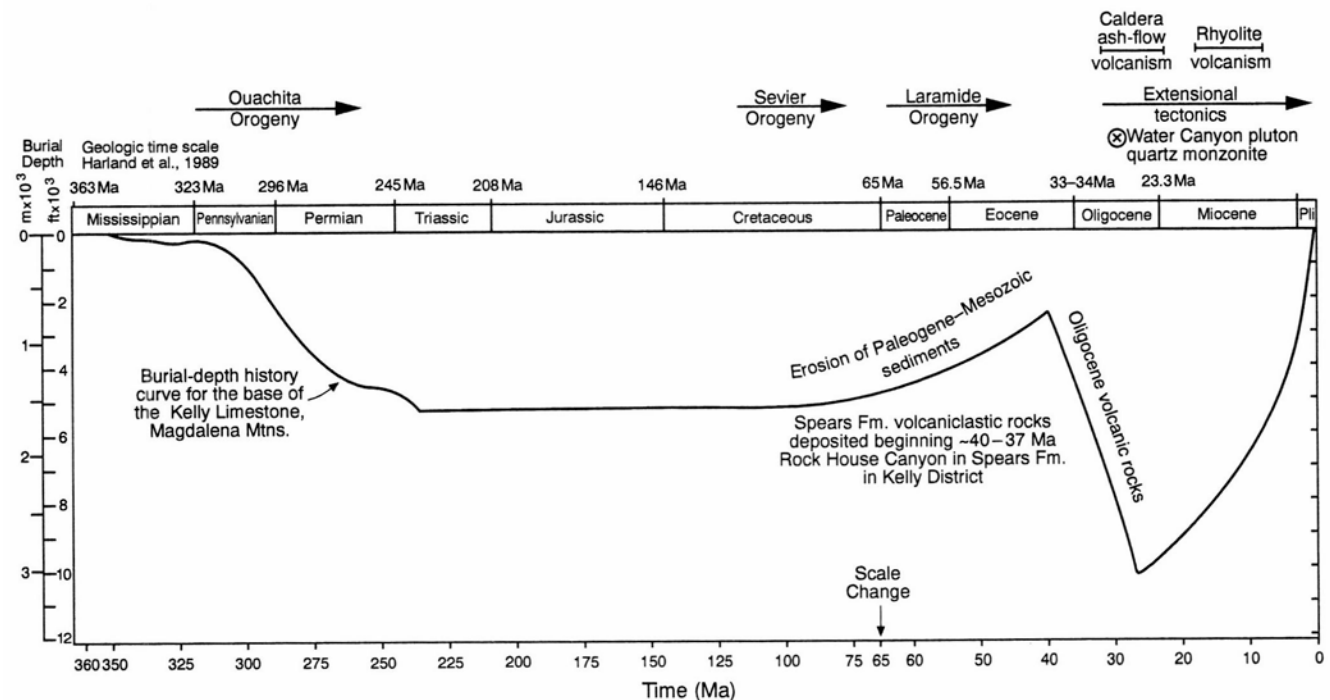


FIGURE 8—Burial history of the Kelly Limestone through time.

Proterozoic intrusions do not seem to have had a direct influence on mineralization. However, in the Linchburg mine and elsewhere they are intensely altered and may have been a source of metals (Titley, 1959). Following Blakestad (1978), the Tertiary intrusions are grouped informally as the Anchor Canyon Granite, latite porphyry of Mistletoe Gulch, latite dikes, Linchburg quartz monzonite, other intrusive rocks, mafic dikes, augite andesite, and white rhyolite dikes.

As discussed below, there is a geochemical relationship between jasperoids and igneous differentiation. Several authors (Blakestad, 1978; Bobrow et al., 1983; Osburn and Chapin, 1983a, b) have reviewed the igneous rocks of the district, but there is still much to be done on their geochemistry and petrology. At this point, only indirect relationships and indirect geochemistry and geothermometry establish a genetic tie of the igneous rocks to jasperization (Figs. 9, 10).

Mineralization

Most previous workers recognized that north-south faults played a very important role in localization of mineralization (Loughlin and Koschman, 1942; Titley, 1959, 1961). Blakestad (1979) further implicated the intersections of faults as important controls of ore. However, the depositional and diagenetic history of Carboniferous sediments played an important role in the stratigraphic location of the Tertiary base-metal replacement deposits and the movement and concentration of the solutions which formed the jasperoids (Figs. 11, 12).

Carboniferous and Tertiary events critical to setting the stage for development of the jasperoids were:

- (1) Deposition of Mississippian carbonates (Kelly Limestone) on the peneplained Proterozoic supracrustal rocks;
- (2) subaerial erosion and karsting for about 21 m.y. which enhanced the porosity of the crinoidal packstones and

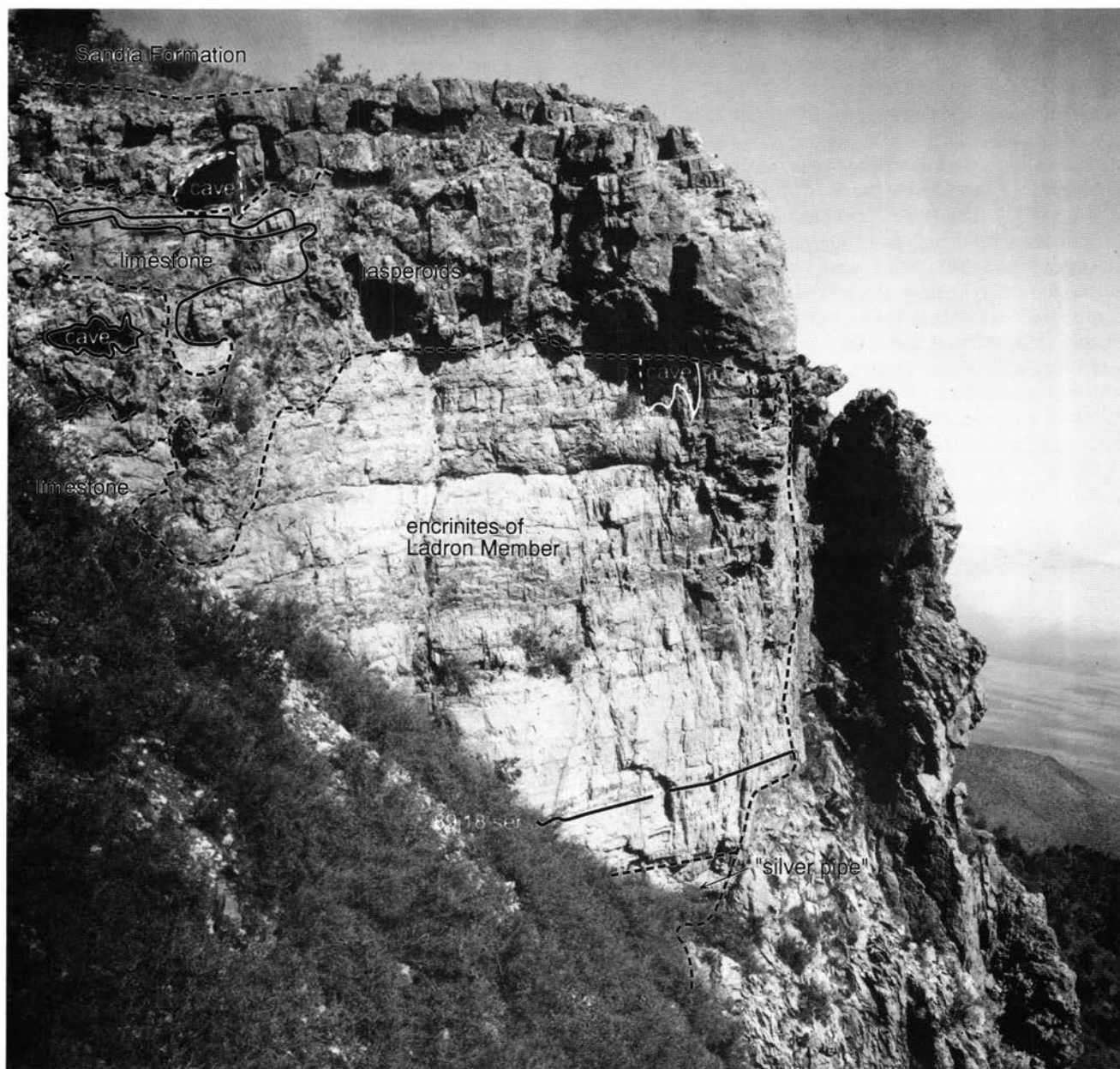


FIGURE 9—Rhyolite dike cutting across the Kelly Limestone, and upper limestone beds of the Ladron Member invaded and replaced by jasperoid. Just east of North Baldy, altitude 9600 ft (2926 m).

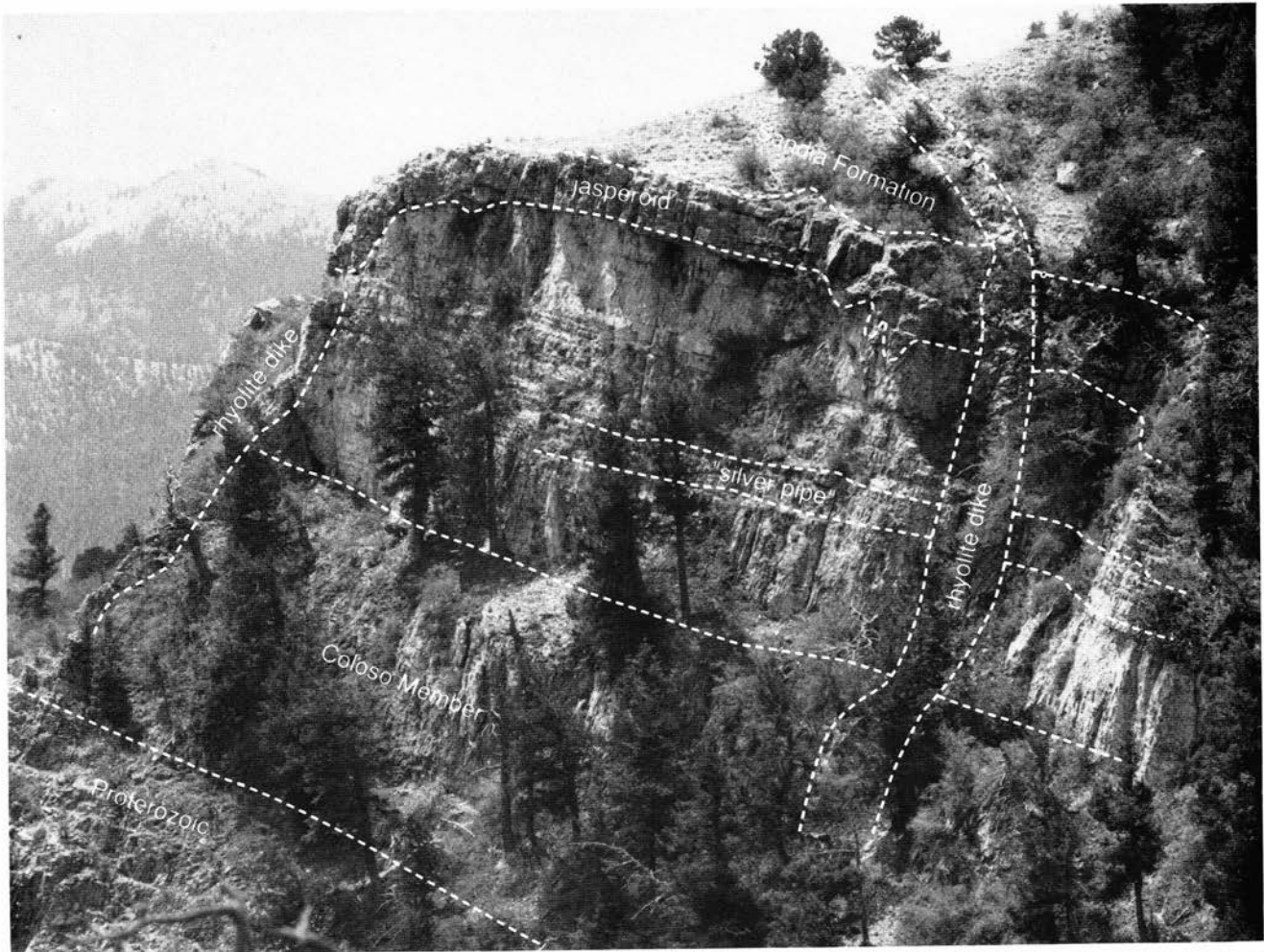


FIGURE 10—Kelly Limestone outcrop, view to the south, at 8600 ft (2621 m), some 1000 ft (305 m) east of North Baldy peak. The porous and karsted zone 14 beds of the Ladron Member have been selectively replaced by gold-bearing jasperoids that form a sharp ledge below the low slope made up by shales and siltstones of the Pennsylvanian Sandia Formation.

grainstones before the deposition of the overlying Pennsylvanian Sandia Formation;

(3) deposition of Lower Pennsylvanian impermeable black-shale seal on top of the Mississippian crinoidal carbonate rocks which formed a seal for upward migrating solutions;

(4) development, in the Oligocene, of the Socorro accommodation zone across the Magdalena Mountains and formation of the Socorro caldera and overlapping subsequent calderas;

(5) emplacement of several intrusive bodies following formation of the Socorro caldera. Fractures, many of which are occupied by rhyolite dikes, guided associated metalliferous hydrothermal fluids through the Proterozoic rocks and into the Mississippian carbonates. The faults and fissures associated with the caldera systems (Figs. 1, 2) were the major pathways.

The lower part of the Sandia Formation, which overlies the encrinites of the Kelly Limestone, is 80 ft (24 m) thick and is composed of black shale, siltstone, quartz sandstone, and thin lime mudstone. This marine section of terrigenous black shales formed a nearly impervious seal for the upward-moving hydrothermal fluids. These fluids upon encountering the black shale and siltstone were then forced

to move laterally within the underlying Kelly karsted and porous crinoidal limestones.

Laughlin and Koschman (1942, p. 104) have shown that the largest replacement deposits of zinc-lead and copper ores, between the Nitt stock and the ghost town of Kelly, have replaced beds in the Kelly Limestone both below and above the "silver pipe" along fissures of northerly and northwesterly trend. Nearly all the production from the mining district has come from replacement deposits in the Kelly Limestone, with smaller deposits of similar ores in adjacent parts of the limestones in the Sandia and Madera Formations.

The jasperoids are often intricately veined and brecciated. They host virtually every ore mineral in the district. However, we observed no jasperoid crosscutting the replacement sulfide deposits. Furthermore, the spacial distribution of the jasperoids is different; it is more prevalent to the east. This leads us to believe that the hydrothermal fluids which formed the jasperoids in the Kelly Limestone may have had timing and origin different from the fluids which deposited the replacement sulfide deposits. The jasperoids are concentrated in the Kelly Limestone above the "silver pipe" and adjacent to, and below, the Sandia Formation basal black shales. Field studies show the



FIGURE 11—Outcrop showing exposure and texture of jasperoid. Crest of range southwest of Jordan Canyon road, altitude 9100 ft (2774 m).

black shales were an impervious seal and forced the upward moving hydrothermal fluids to move laterally and replace the upper part of the Kelly Limestone (Fig. 12).

Jasperization

Definition and formation of jasperoids

Jasperoid was originally defined as "a rock consisting of cryptocrystalline, chalcedonic, or phenocrystalline silica, which has formed by the replacement of some other material, ordinarily calcite or dolomite" (Theodore and Jones, 1992, pp. 10-13, quoting Spurr, 1898). A detailed and useful discussion of physical properties and genesis was given by Lovering (1972), who also evaluated jasperoid as a potential guide to ore in porphyry-copper and carbonate-hosted base-metal replacement districts in the western United States. Lovering (1972) followed Spurr's (1898)

original definition, which defines jasperoids in terms of petrography and genesis, and excludes syngenetic or diagenetic silica rocks such as primary chert and novaculite.

The silica of jasperoid is typically fine-grained to cryptocrystalline. Extremely fine-grained textures and ghost colloform banding commonly observed in finely crystalline quartz of jasperoid suggest that the silica is generally deposited as a colloidal gel and later converted to quartz in such rocks (Lovering, 1972). Rock color may be white, gray, red, brown, or black depending primarily on the oxidation state of the included iron and on the presence of various other hydrothermally induced minerals (Spurr, 1898). Much of Lovering's treatment is directed at volume-for-volume replacement, but open-space deposition is not excluded and is in fact very important in the Magdalena district. The replacement host rock is most commonly

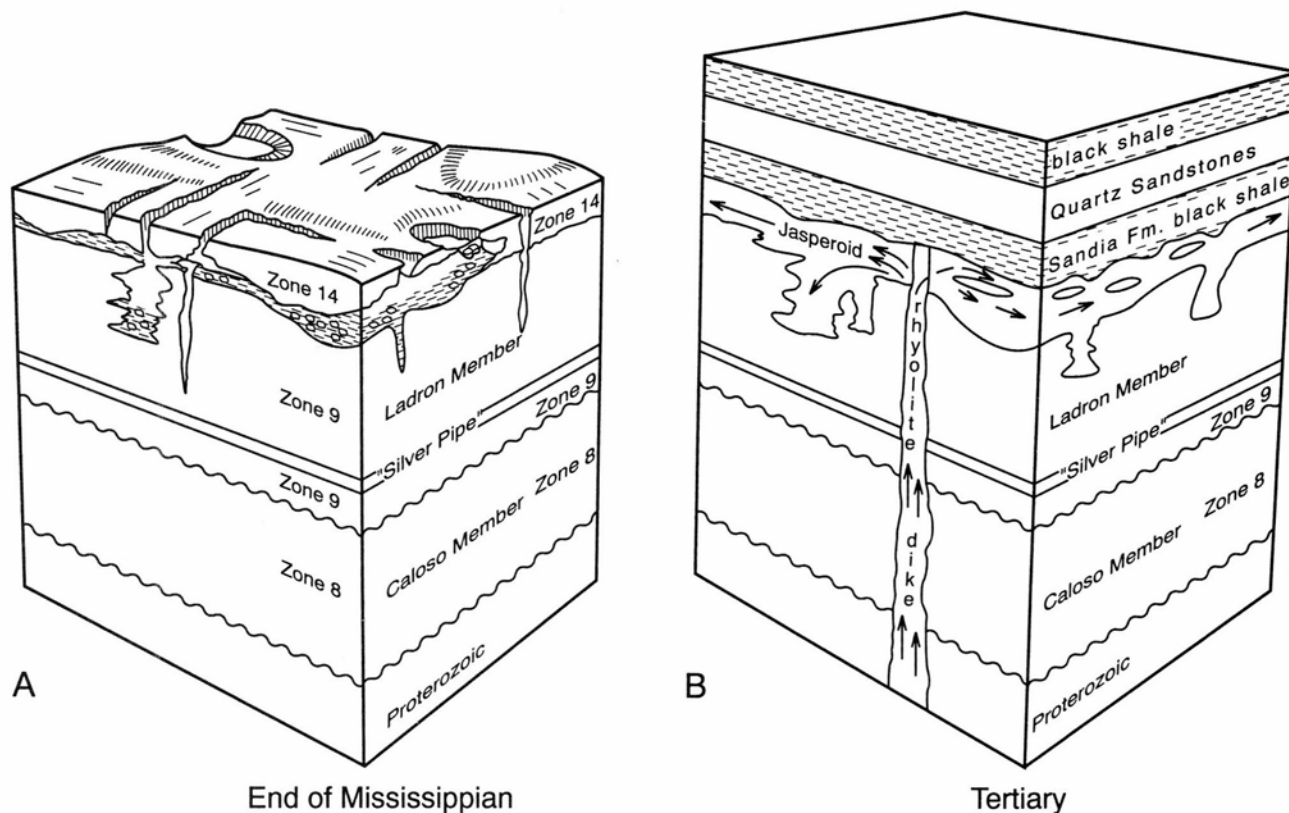


FIGURE 12—Evolution of Kelly Limestone and emplacement of gold-bearing jasperoids. At the end of the Mississippian the Kelly Limestone was subjected to 18 m.y. of subaerial erosion and karsting. In the Cenozoic fractures and faults zones were filled with rhyolite dikes and ascending hydrothermal fluids. The later moved into the karsted and porous Kelly Limestone. The fluids precipitated in the pore spaces and also replaced the limestone with mineralized jasperoids.

limestone or dolomite. Shale, siltstone, and siliceous hypabyssal and extrusive igneous rocks are also susceptible to replacement by silica, but much less so than carbonate and calcareous rocks (Lovering, 1972). Lovering noted that silica may replace carbonate rocks by diffusion of reaction products through a gel layer behind a dissolution front, or by movement of silica-bearing fluid along fractures, or both. He also observed that many jasperoid bodies are localized around structural planes of weakness such as faults, breccia zones, or perhaps bedding planes which served as conduits for silica-bearing fluids. The structurally controlled nature of the feeder zones to such mineralized systems was emphasized strongly by Madrid and Bagby (1988). Many jasperoids are spatially related to granitic intrusions. Thus, enhanced silica contents in rocks resulting from their selective replacement by jasperoids may reflect initially SiO_2 -saturated late-magmatic fluids emanating from a pluton, or they may reflect initially SiO_2 -unsaturated fluids that become SiO_2 -saturated during reaction with wall rock en route to their eventual deposition sites. Silica may originate from siliceous fraction of the host rock elsewhere or may even be due to paleoweathering cycles of the overlying or adjacent rocks. In any case, a silica-saturated or nearly saturated solution is required to reach the site of deposition (Fournier, 1973, 1985).

Lovering (1972) presented a theory of the replacement of limestone by jasperoid. He imagined a hot aqueous solution merely saturated with silica and containing CO_2 , H_2S , and perhaps HCL rising from depth and becoming an acid solution supersaturated with SiO_2 . As long as the pH

remains low, silica will be stabilized as a dispersed colloidal sol. When favorably prepared limestone beds (such as the Kelly Limestone) are encountered, the solutions enter and begin to dissolve the carbonates. Although rising pH would inhibit the replacement process, this effect is diminished by the exsolution of CO_2 and H_2S with declining pressure and formation of bicarbonate. Silica gel coats the replacement surfaces, but armoring is ineffective because the gel is sufficiently permeable to diffusing ions, and volume decrease due to precipitation of quartz allows rapid ingress to the unreplaced limestone.

Volume-for-volume replacement is apparent in many instances in which fossils and other delicate limestone structures are preserved. The silica gel is fragile and easily brecciated after it begins to desiccate, ultimately showing complex paragenesis of jasperization, brecciation, and veining noted by us and others. The paragenesis in the Kelly district indicates that jasperoid precipitated early during mineralization and was contemporaneous with the deposition of barite (see Iovenitti, 1977).

In addition to replacement textures, the Kelly jasperoids display abundant evidence of open-space deposition controlled by karst (see Figs. 6, 9, 11, 12). The frequent, large-scale open spaces in the Kelly Limestone minimize the difficulty of diffusion through incompletely desiccated gel to unreplaced carbonate.

Mineralogy of Kelly Limestone jasperoids

The mineralogy of the Kelly jasperoids reflects the mineralization of the Magdalena mining district, but

includes minerals not described by Laughlin and Koschmann (1942). Some of these, namely apatite, goethite, lepidolite, orthoclase, rutile, and zircon, would have certainly been mentioned by them if the host rocks had been given more attention, but these minerals are usually not of interest in studies of base-metal ore deposits. Others, namely "beckelite," cassiterite, cerianite, fraipontite, gismondine, itoite, plumbiferite, sauconite, stibnite, and zippeite, were revealed to us through x-ray diffraction and scanning electron microscope (SEM) equipped for energy-dispersive x-ray (EDX) analysis. This methodology was unavailable to Laughlin and Koschmann (1942).

Most occurrences of minerals in the Kelly jasperoids are listed in Table 1. The samples listed in the table are 88N-1 through 88N-50 and are the same samples as those collected for the opportunistic-sampling plan described in the geochemistry section below. SEM observations were made on two additional series of jasperoids, 89F30 and 89j09, which were not analyzed for bulk geochemistry. The first series occurs near the crest of the ridge and is a horizontally laminated platy jasperoid. The second occurs near the white rhyolite dike cropping out northeast of North Baldy.

Following the table, the minerals observed in the jasperoids are briefly discussed in alphabetical order. Some of them were observed only by SEM, and of these stibnite was only observed in a series of jasperoids for which there is no bulk geochemistry.

Ten of the samples gave no XRD signal for any mineral but quartz. Six of the samples have no quartz or only moderate amounts and are not jasperoids.

Table 1 also shows the precious-metal content of the randomly collected samples. The mean concentrations of Au and Ag in jasperoids having the more frequently encountered minerals are shown at the right-hand end of the table to give an indication of correlation between precious-metal content and mineralogy. The mean Au concentration in samples with galena and sphalerite is more than twice its mean concentration in all the samples, whereas in hematite-bearing samples it is less than one-third. The mean concentration of Ag, on the other hand, is exceptionally high only in samples with hematite.

Allanite is a calcium rare-earth silicate deduced from the juxtaposition of Ca, Ce, La, and Si of EDX analyses. It occurs in bladed crystals up to 10 μm long (Fig. 14D). "*Beckelite*" ($\text{Ca}_3(\text{Ce},\text{La})_4\text{Si}_3\text{O}_{15}$) is another possibility for this occurrence; it was described by Dana, but has since been abandoned as a legitimate mineral name. Other rare-earth-bearing phases are illustrated in Figs. 14C and E. Ce is associated with Fe in sample 89j09h (Fig. 14C). La and Nd are associated with Pb and P in sample 89f30c (Fig. 14E). La in a Cu, Pb, Zn, Ag sulfide association is shown in Fig. 14E.

Apatite was observed only by SEM. A 10 μm euhedral grain from specimen 19 is illustrated in Fig. 15B. Other phosphate phases are shown in Figs. 15C and D. Apatite with Pb is inferred from the juxtaposition of Ca, Pb, and P in three samples from EDX analysis. Its presence in only three samples in the table is not representative because only six samples (and subsamples of them) were examined by SEM.

Barite is one of the most common gangue minerals in the district and is the accessory mineral most frequently encountered in XRD analysis. It often completely fills open space in the jasperoids. Barite is associated with Mn and P

phases in sample 15 (Fig. 15C). The jasperoids carrying barite have an average Au concentration twice as high as the mean Au for all the samples; their Ag concentration is about equal to the average for all.

Calcite is present in about 20% of the samples. It is a common gangue mineral in the district and is expected in jasperoid replacement of limestones. Calcite in association with quenselite is shown in Fig. 15F. The caries texture defining the calcite-quartz interface in this photograph suggests arrested replacement of carbonate by silica. The concentration of Au in the calcite-bearing jasperoids is 1.5 times higher than the average concentration for the whole sample suite, whereas that of Ag is about three-quarters of that of the whole suite.

Cassiterite was identified only by SEM/EDX. It occurs as minute euhedral crystals in open spaces. As with apatite, its observation in only the few samples examined by SEM is not representative of the whole jasperoid suite. It appears as an euhedral grain displaying a 4 μm hexagonal section in a 10 μm cavity in sample 89J09E (Fig. 13C). This occurrence is unusual because, to our knowledge, hexagonal tin minerals containing no other elements but oxygen are unknown in nature. The *Handbook of Chemistry and Physics* (71st edition) lists hexagonal and rhombohedral forms for cassiterite, but we have not been able to find a reference to that information (even through the editor of the Handbook). However, cassiterite is ditetragonal, and twinning can occur as sixlings with 110 as the composition plane. This habit is reported by Taylor (1979, p. 421) and is probably the simplest explanation of the hexagonal form we observed. A more remote possibility is pseudomorphous replacement of quartz. This habit is also reported by Taylor (1979, p. 416). Cassiterite is generally considered a high-temperature mineral found in the subvolcanic environment.

Cerianite was reported by XRD in two samples. The lower limit of detectability for rare-earth minerals by XRD is not good, and their disclosure by EDX indicates that they may be more widespread in the jasperoids than is indicated here.

Cerussite is reported by XRD in six samples; however, one of the samples, #22, contains only moderate quartz and is not exclusively a jasperoid. The cerussite-bearing samples have a mean Au concentration 1.9 times higher than the mean of the whole suite, and a mean Ag concentration is 1.6 times higher. Note that the high-cerussite sample #22 has an abnormally low Au concentration and is very high in goethite and hematite.

Chalcopyrite and *pyrite* are only rarely observed in the Magdalena jasperoids. Their paragenesis was troublesome to Laughlin and Koschmann (1942) because of limited occurrence at the base of the Kelly Limestone, where they seem to preferentially replace more siliceous host rocks. See detailed discussion below under *pyrite*.

Fluorite is uncommon in the Magdalena jasperoids except for vug occurrences along the crest of the range above Jordan Canyon. In the one XRD occurrence it is associated with the two Pb minerals, galena and cerussite. Its one SEM/EDX occurrence is doubtful. In view of the abundance of barite in the jasperoids and the common association of fluorite with barite in the Magdalena mining district, the rarity of fluorite in the jasperoids is surprising.

Fraipontite is a very rare mineral occurring at the Ambrosia mine in association with goethite and sauconite (a Zn smectite). Fraipontite is a Zn—Al silicate listed with hemi-

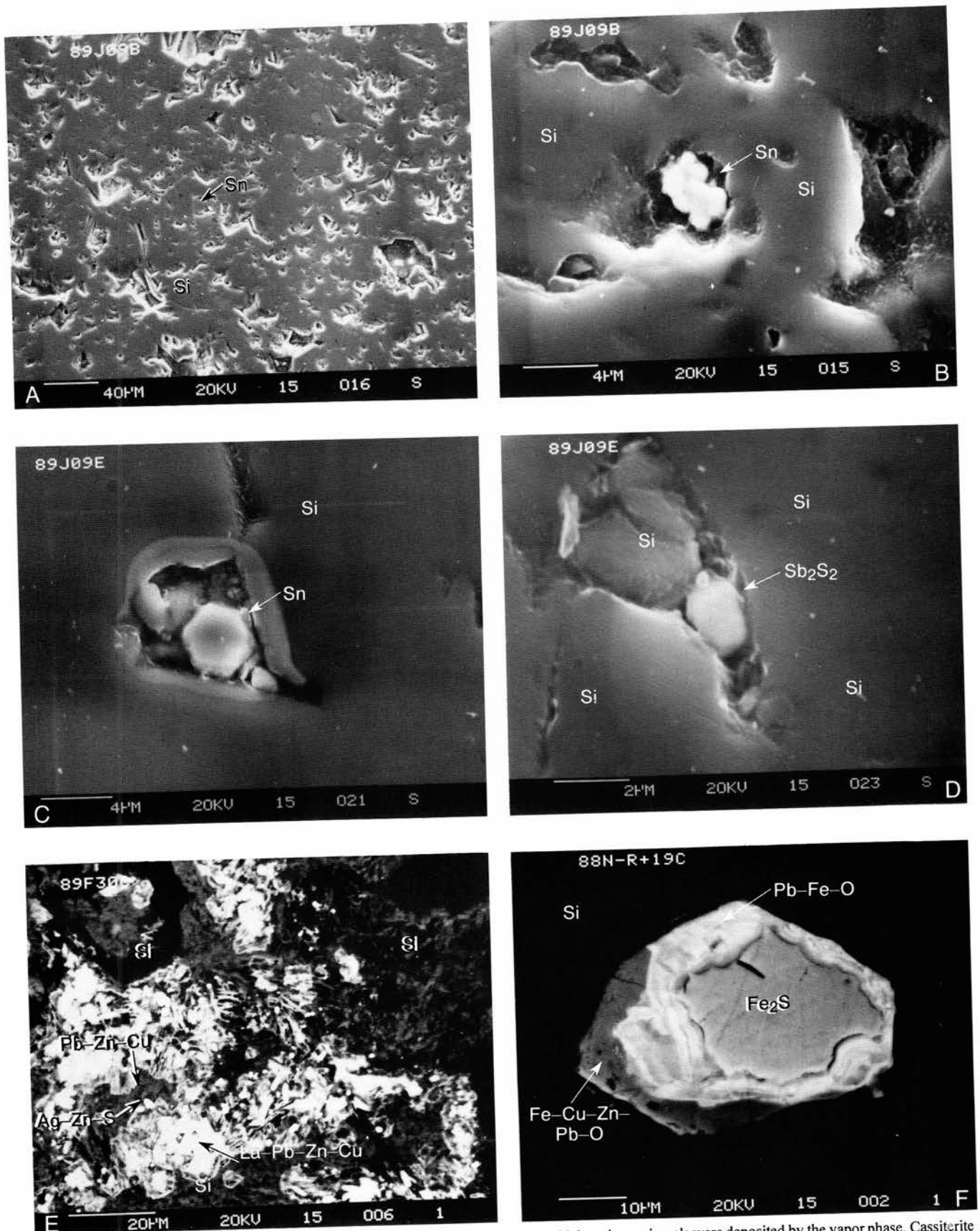


FIGURE 13—All SEM. A. Jasperoid showing abundant small cavities and pores in which various minerals were deposited by the vapor phase. Cassiterite (SnO_2) crystals shown enlarged in B. Also present in this specimen are barite, sphalerite, galena, Mn-Pb, iron oxide, lead phosphate in apatite. Cassiterite grain which partially fills a cavity in the jasperoid. 89J09B. B. Cluster of cassiterite crystals in vug cavity, formed by vapor phase after formation of jasperoid. 89J09B. C. Hexagonal crystal of cassiterite in jasperoid cavity. 89J09E. D. Rare crystal of stibnite (Sb_2S_2) in small jasperoid cavity. 89J09E. E. Complexly zoned aggregate filling vug in the jasperoid. 89F30C. F. Complexly zoned aggregate filling vug in the jasperoid. Center is a pyrite crystal followed by oxide banding of Pb-Fe and outer layer of mixed oxides of Fe, Cu, Zn, and Pb. Mn-Pb and Fe-Pb minerals identified. The Fe-Pb mineral displays growth rings and an iron-oxide rind with a euhedral-grain boundary. The Mn-Pb mineral may be quenselite $2\text{PbOMn}_2\text{O}_3\cdot\text{H}_2\text{O}$. The Pb-Fe may be the mineral plumboferrite (PbFe_2O_7). An SSQ analysis shows that the molecular % is Fe > Pb but not 4:1. An Sn mineral, sphalerite, galena, and a Cu-Ni mineral were also identified. All the minerals were in jasperoid pores. 88N-R-19C.

TABLE 1—Mineralogy of Magdalena mining district jasperoids.

MINERAL	No.	1	2	3	4	5	6	7	8	9	10	11	12	13	14	15	16	17	18	19	20	21	22	23	24	25	26
Alumite (Ce,Ca) ₂ (Al,Fe) ₂ (SiO ₄) ₂ (OH)	1																										
Apatite* (Ca,Pb) ₅ (PO ₄) ₃ (F,OH)	3								+																		
Barite BaSO ₄	11	+						m	m	+										t+							
Calcite CaCO ₃	9	+	m					m					M							+?	t						
Caastierite* SnO ₂	3	+							+																		
Cerianite CeO ₂	2		t																								t
Cerussite PbCO ₃	6						t													t		M					t
Chalcopyrite CuFeS ₂	1																										
Chlorochlore (Mg,Fe) ₂ Al(Si,Al) ₂ (OH) ₂	2			t																							
Fluorite CaF ₂	2						t																				
Fraipontite Zn ₂ Al ₂ (Si ₂ O ₇) ₂ ·11H ₂ O(?)	1																										
Galena PbS	8	+					t		+																		M
Gismondine Ca ₃ Al ₂ (Si ₂ O ₇) ₂ (OH)	3	t							t																		
Goeschite Fe-O(OH)	7								+				M									m	M				
Hedenbergite Ca(Fe,Mn)Si ₂ O ₆	1																										
Hematite Fe ₂ O ₃	5	t											t														
Hemimorphite Zn ₄ Si ₂ (OH) ₂ ·H ₂ O	4			t					m	m																	
Iloite Pb ₂ Ge(SO ₄) ₂ (OH) ₂	1																										
Jarosite KFe ₃ (SO ₄) ₂ (OH) ₆	1																										
Lepidolite K(Li,Al) ₃ (Si,Al) ₃ (OH) ₂ (F,OH) ₂	3	t					t																				
Orthoclase KAlSi ₃ O ₈	1																										
Plumbogjarosite PbFe ₂ (SO ₄) ₂ (OH) ₂	2																	+									
Plumbiferite* PbFe ₂ O ₇	2																										
Pyrite FeS ₂	1																										
Quartz SiO ₂	47	M	M	M	M	M	M	M	M	M	M	M	M	M	M	M	M	M	M	M	M	M	M	M	M	M	M
Quenselite* PbMnO ₂ (OH)	2	+																									
Rutile* TiO ₂	1																										
Sauconite Na ₃₋₄ Zn ₂ (Si,Al) ₂ (OH) ₂ ·4H ₂ O	1																										
Smithsonite ZnCO ₃	3																										
Sphalerite ZnS	5									+																	m
Zipperite (Mg) Mg ₂ (UO ₂)(SO ₄)(OH) ₂	1																										
Zircon* ZrSiO ₄	1																				+						

Notes: *; obs only with microprobe; M: > 33%; m: 10-33%; t: < 10%; +: microprobe

Au (ppb X 0.1)

Ag (ppm)

	10	5	30	0.4	10	90	70	100	130	40	20	5	40	0.6	30	20	20	30	140	20	10	28	1.2	1.6	40	0.2
	10	15	5	1.5	30	10	30	15	20	20	15	3	7	10	7	2	15	20	30	2	20	20	10	20	70	3

TABLE 1—(continued)

Mineral	27	28	29	30	31	32	33	34	35	36	37	38	39	40	41	42	43	44	45	46	47	48	49	50	MEANS Au Ag
Alumite (Ce,Ca) ₂ (Al,Fe) ₂ (SiO ₄) ₂ (OH) ₂																									
Apatite* (Ca,Pb) ₅ (PO ₄) ₃ (F,OH)													+												
Barite BaSO ₄				t						t									t						54.3 20.8
Calcite CaCO ₃		m								m					M										42.2 16.4
Castierite* SnO ₂																									
Cerianite CeO ₂																									
Cerussite PbCO ₃																					m				51.1 36.7
Chalcocite CuFeS ₂																									
Clinocllore (Mg,Fe) ₂ Al ₂ (Si,Al) ₂ O ₁₀ (OH) ₂																									
Fluorite CaF ₂																									
Fraspionite Zn ₂ Al ₂ (SiO ₄) ₂ ·11H ₂ O?																							M		63.1 26.9
Galena PbS							M						m+												
Gismondine CaAl ₂ (Si ₂ O ₇) ₂ (H ₂ O)																									
Goethite FeO(OH)																							m		32.0 15.2
Hedenbergite Ca(Fe,Mn)Si ₂ O ₆																									
Hematite Fe ₂ O ₃										t															7.3 60.6
Hemimorphite Zn ₅ (Si ₂ O ₇) ₂ (OH) ₂ ·H ₂ O																									50.1 13.8
Itoite Pb ₂ Ge(SO ₄) ₂ (OH) ₂																									
Jarosite KFe ₃ (SO ₄) ₂ (OH) ₆																									
Lepidolite K(Li,Al) ₃ (Si,Al) ₃ O ₁₀ (F,OH) ₂																									
Orthoclase KAlSi ₃ O ₈																									
Plumbogjarosite PbFe ₂ (SO ₄) ₂ (OH) ₆																									
Plumboferriite* PbFe ₂ O ₇																									
Pyrite FeS ₂																									
Quartz SiO ₂	M	M	M	M	M	M	M	M	M	M	M	M	M	M	M	M	M	M	M	M	M	M	M	M	
Quenselite* PbMnO ₂ (OH)																									
Rutile* TiO ₂																									
Sauconite Na ₂ Zn ₂ (Si,Al) ₂ O ₇ (OH) ₂ ·4H ₂ O																M									
Smithsonite ZnCO ₃																									
Sphalerite ZnS																									
Zippelite (MC) Mg ₂ (UO ₂) ₂ (SO ₄) ₂ (OH) ₂																									66.0 33.0
Zircon* ZrSiO ₄																									

Notes: *; obs. only with microprobe; M: > 33%; m: 10-33%; t: < 10%; +: microprobe

	20	25	28	29	30	31	32	33	34	35	36	37	38	39	40	41	42	43	44	45	46	47	48	49	50	MEANS
Au (ppbX 0.1)	0.2	25	0.2	0.2	0.2	0.2	0.2	0.2	0.2	0.2	0.2	0.2	0.2	0.2	0.2	0.2	0.2	0.2	0.2	0.2	0.2	0.2	0.2	0.2	0.2	27.4
Ag (ppm)	20	20	10	10	50	7	15	30	30	70	15	20	2	30	5	50	20	15	1.5	10	10	70	10	1.5	200	22.3

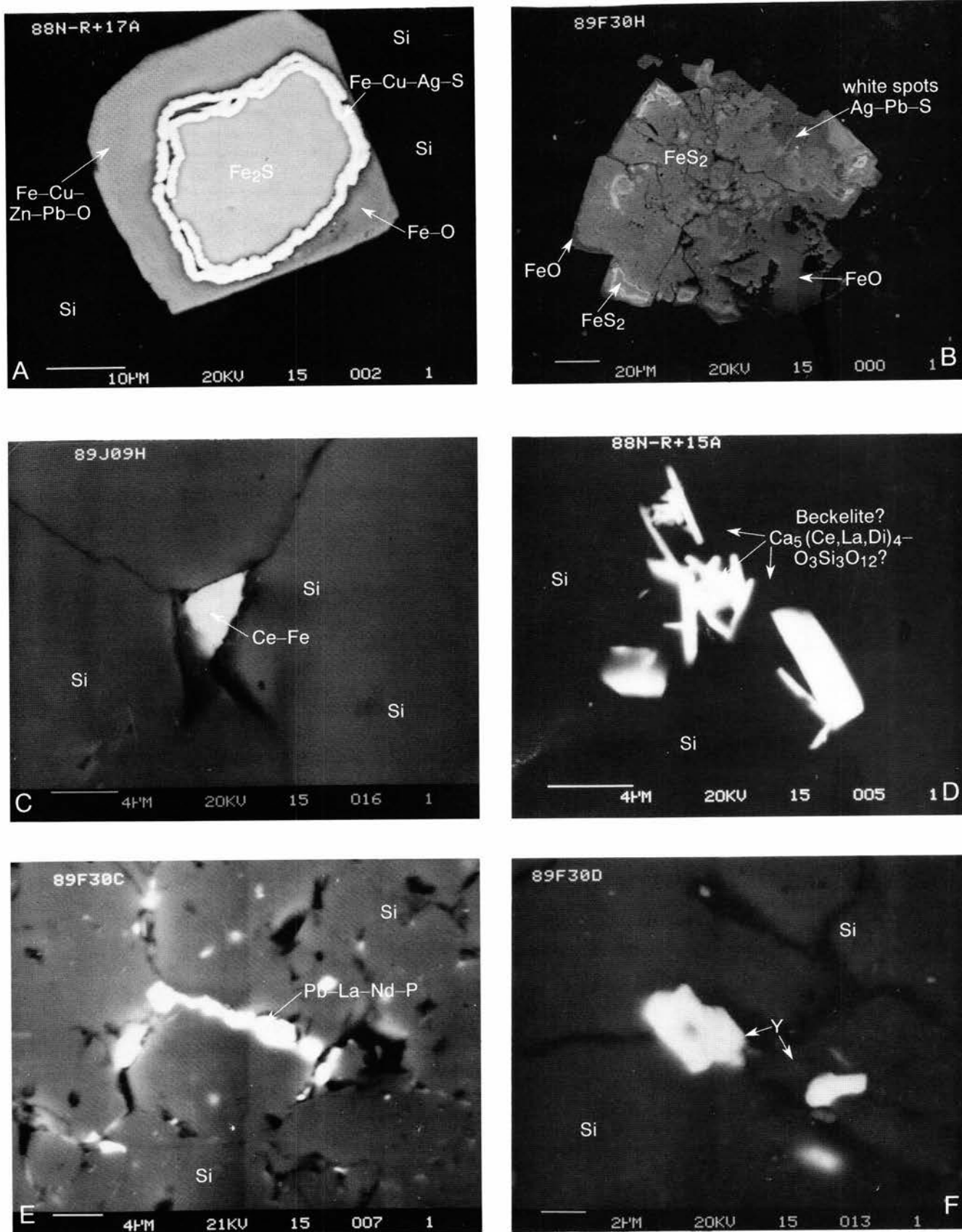


FIGURE 14—All SEM. A, Complex void filling in jasperoid. Center of filling is pyrite followed by a band of Fe, Cu, Ag, and S. Outer layer is composed of Fe, Cu, Zn, and Pb oxides. Silver is present in association with pyrite and the Fe-Cu-Zn-Pb mineral in a reaction rim. 88N-R+ 17A. B, Complex pyrite crystal in the jasperoid, with areas of Pb, Ag, and S. 89F30H. C, Rare-earth mineral composed of Ce, Fe in vug within the jasperoid. 89J09H. D, Rare-earth mineral, possibly allanite, $\text{Ca}_5(\text{Ce,La,Di})_4\text{O}_3\text{Si}_3\text{O}_{12}$, filling cavities in jasperoid. 88N-R+15A. E, Rare-earth mineral composed in part of Pb, La, Nd, and P, which was deposited in a jasperoid vug. 89F30C. F, Rare-earth mineral composed of yttrium (Y) and silica, found in a small jasperoid vug. 89F30D.

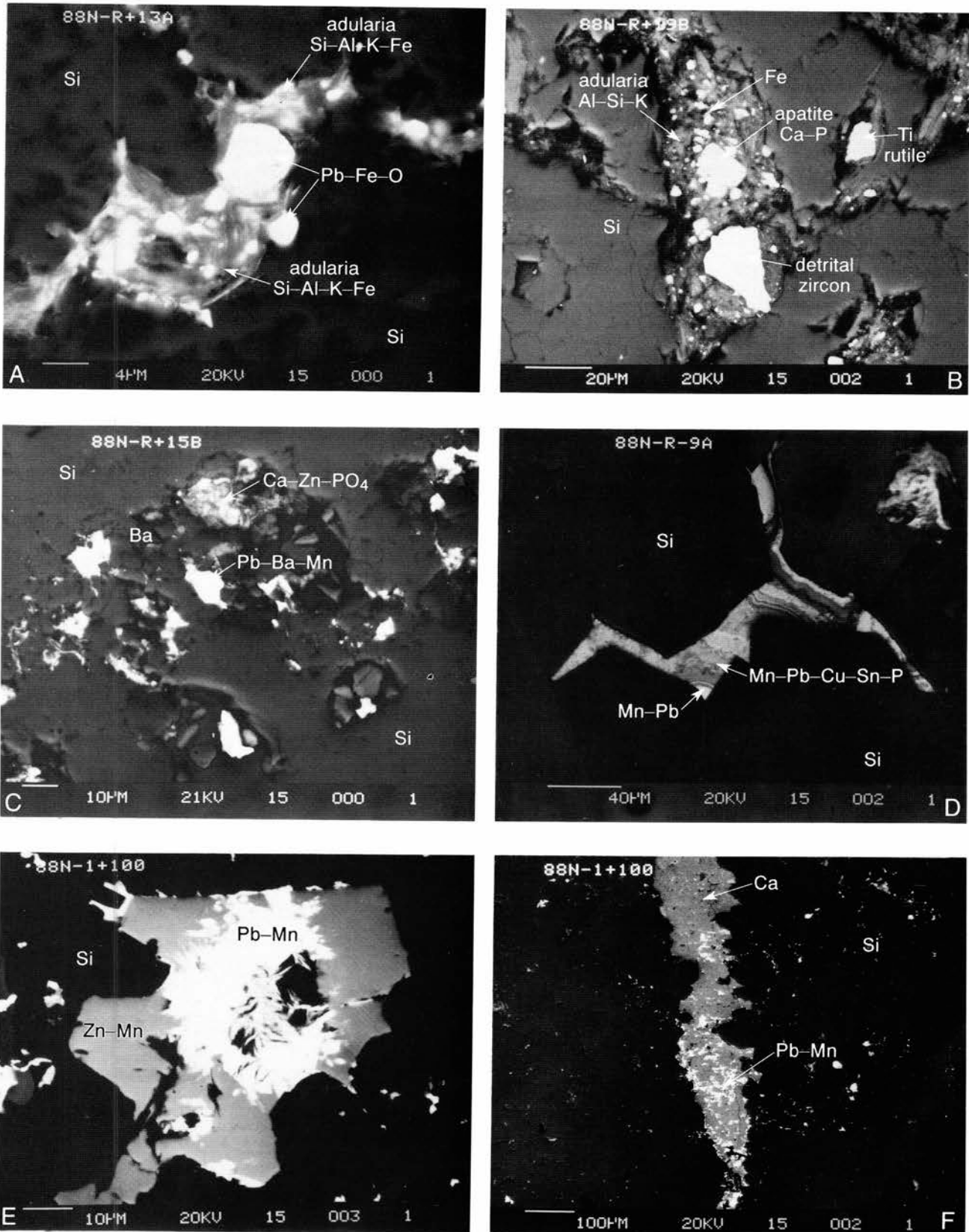


FIGURE 15—All SEM. A, Crystals of adularia and an oxide of Pb and Fe filling a cavity in jasperoid. Pb phosphate minerals were also identified. 88N-R-13A. B, Cavity in jasperoid with angular grains of zircon, rutile, and apatite, all of which may be detrital. Clay minerals or adularia are also present. Also identified were barite, cassiterite, iron oxides, and a La-Ce rare-earth mineral. 88N-R-19B. C, Barite mixed with a Ca, Zn, PO₄ mineral. Adjacent to this is a Mn, Ba, Pb mineral. Associated with these minerals are light earth Y-silicates and heavy rare-earth silicates of Ce and La; their crystals are very small, only 1–2 µm. 88N-R-15B. D, Mn, Pb and Mn, Pb, Cu, Zn, P minerals filling a pore in jasperoid. The minerals show banding as a result of changing chemistry of the hydrothermal fluids. Also present in this specimen is an euhedral grain of cassiterite and one Ni mineral. 88N-R-9A. E, F, A late-phase calcite vein cutting through jasperoid. The calcite represents a later stage of mineralization than the jasperoid. Within the calcite vein is the Mn-Pb mineral quenselite. Photomicrograph shows the quenselite to be intergrown with an Mn-Zn mineral. A spectrum obtained from the Mn-Zn mineral has almost the same amount of carbon as a spectrum from the jasperoid matrix. The Mn-Zn mineral is probably not a carbonate because microanalysis spectra show no increase in carbon. It may be an oxide. Galena and barite were also identified. 88N-1+100.

morphite by Dana. The International Committee for Diffraction Data (ICDD) shows two fraipontite cards, 14-366 and 34-0782. The chemical formula given in Table 1 is from Fleischer (1975). The ICDD cards give $(\text{Zn}, \text{Al}, \text{Cu})_3(\text{Si}, \text{Al})_2\text{O}_5(\text{OH})_4$. The first lists it as monoclinic and the second as orthorhombic. We have been able to recognize the mineral only by XRD.

Galena was recognized in eight jasperoid samples by XRD and SEM. The mean concentration of Au in galena-bearing jasperoids is 2.3 times the mean of all the jasperoids. The mean Ag concentration in samples with galena is essentially equal to the mean of all the jasperoids.

Gismondine, a zeolite, occurs in only three of the jasperoids. It is generally considered to be a product of low-temperature alteration of feldspar, but that may not apply in these rocks.

Goethite occurs in seven samples, three of which show it only in SEM/EDX analysis where it could only be reported as an iron oxide. We include those reports with goethite because they are in an alteration association, as opposed to hematite that is usually present as specularite in the district. However, as discussed below under *Interpretation of jasperoid geochemistry*, hematite is the stable iron-oxide phase with pyrite under conditions of silicification of limestone by replacement. Jasperoids bearing goethite have a mean Au concentration about equal to the mean for all the jasperoids, and a mean Ag concentration of 0.67 for all the jasperoids.

Hedenbergite occurs in only one jasperoid sample which was collected from the Linchburg mine dump. Contact metamorphism has been described in the Linchburg workings by Titley (1959).

Hematite was observed by XRD in five jasperoids. These samples have a mean Au concentration of only 0.25 the mean for all the jasperoids. Ag, on the other hand, has a mean concentration 2.7 times higher than that for all the jasperoids.

Hemimorphite was recognized by XRD in four of the jasperoids. Au is relatively high and Ag relatively low in these samples, having means of 1.8 and 0.6, respectively, of the means for all the jasperoids.

Itoite, a rare hydrous Pb/Ge sulphate, was recognized in trace concentrations by XRD in only one sample, where it is associated with Pb mineralization along a shear zone. The formula given in Table 1 is from Fleischer (1975), but ICDD card 12-0641 gives it as $\text{Pb}(\text{S}, \text{Ge})(\text{O}, \text{OH})_4$. The notes on that card indicate that itoite may be a germanium anglesite. Ge was one of the elements tested for in the geochemical examination of these jasperoids, but was not detectable at the 10 ppm level in any of the samples.

Jarosite was found only in one sample, where it is a major constituent in association with goethite. This sample is not a jasperoid but rather a soft clay-like material from the Ambrosia mine.

Lepidolite was detected at trace levels by XRD in two reddish to maroon shales (1 and 12) above the Kelly Limestone and one red jasperoid breccia (5), also at the top of the Kelly Limestone.

Orthoclase was observed by XRD in only one specimen, a sample of jasperoid taken from a prospect pit in Kelly Gulch. We resampled the locality in an effort to find adularia for Ar/Ar geochronology, but in vain. *Adularia*, also KAISi_3O_8 , is illustrated in association with Pb and Fe oxides in Fig. 15A. It is also associated with apatite, rutile, and zircon in Fig. 15B.

Plumboferrite has been detected by SEM examination in one jasperoid sample (19). It occurs with growth layers replacing pyrite (Fig. 13F). Caries texture suggests that it replaces pyrite.

Plumbojarosite occurs in two specimens, 17 and 47. One determination is by SEM and one by XRD. The sample determined by XRD is from the jasperoid at the Ambrosia mine.

Pyrite was observed in polished thinsections and by SEM, but it is rare in the jasperoids. In sample 19 it is associated with plumbojarosite, as described above. Its paragenesis with Ag and the principal ore elements is clearly shown in Fig. 14A, where an oxidized pyrite cube contains a core of unaltered pyrite mantled by an Fe—Cu—Ag sulfide. The euhedral form of the oxidized grain and the irregular inner zone suggest that Cu and Ag diffused into the outer Cu-, Pb-, Zn-bearing goethite/hematite alteration of pyrite and precipitated as sulfides at the oxide—pyrite interface where S was available. A similar relationship with Pb and Ag sulfides mantling unaltered pyrite cores is illustrated in Fig. 14B. These relationships are consistent with Laughlin and Koschmann's (1942) report of the paragenesis of early pyrite upon which later base-metal sulfides grow.

Pyrite was observed in two polished thinsections of sample 89j09c which was collected 2.1 m (7 ft) west of the white rhyolite dike east of North Baldy. The thermal evolution of this dike is discussed under *Geothermometry*. The pyrite in this sample is almost thoroughly altered to iron oxide. The size of the largest pseudomorph was 100 μm . The largest continuous pyrite grain was 70 μm and possessed a 5 μm rim of iron oxide. This particular grain shows caries texture in its scalloped pyrite—iron oxide contact. The scallops are deeper at the triple point contacts with the enclosing jasperoid, suggesting that this alteration was partly controlled by fluids present after crystallization of the jasperoid.

Four pyrite grains from sample 89j09c were analysed for $\delta^{34}\text{S}$ by secondary ion microprobe spectroscopy (SIMS). The SIMS analyses were performed by Graham Layne at the UNM/SNL Ion Microprobe Facility, a joint operation of the Institute of Meteoritics, University of New Mexico, and Sandia National Laboratories. The four values of $\delta^{34}\text{S}$ relative to Canyon Diablo troilite were -7.7 , -10.7 , -9.7 , and -6.8 per mil. The analytical error on each determination was ± 0.4 per mil.

Quartz is the essential mineral of jasperoid and occurs in virtually every conceivable texture in grain sizes from $1\mu\text{m}$ to over 1 cm. Porosity is generally high, with open spaces of a few microns to several centimeters. A typical example of micropore space occurs in sample 89j09b (Fig. 13A). This configuration of pore space is more characteristic of shrinkage during desiccation of silica gel than subsequent fracturing due to deformation. The arrow points to a cavity containing micrometric cassiterite grains shown enlarged in Fig. 13B. Angular open space defined by quartz crystal faces is filled with a banded Cu, Pb, Zn, Mn, P mineralogy in Fig. 15D. Angular open space is almost completely filled with Zn—Mn and Pb—Mn minerals in Fig. 15E.

Quenselite was recognized only by SEM/EDX examination in two jasperoids, 1 and 19. It appears as bladed crystals in open space in Fig. 15E, and is associated with calcite in Fig. 15F.

Rutile was observed only in specimen 19, by SEM. Its shape and environment suggest detrital origin, as shown in Fig. 15B.

Sauconite is a Zn smectite. It was observed by XRD in sample 42, collected from light-gray shales at the base of the Caloso Member of the Kelly Limestone. This sample shows no Zn anomaly, so sauconite may be misidentified on the diffractogram. However, sauconite definitely occurs as snow-white nodules in red, earthy terra rosa at the Ambrosia mine. Sauconite has been most recently reported by Rivière et al. (1985) in material from karstic caves of central Tunisia. In the Magdalena mining district it is probably a principal constituent of the "tallow clay" described by Laughlin and Koschmann (1942).

Smithsonite is recognizable in three samples as trace and major XRD occurrences. At the sample 43 location it is megascopically associated with chalcopyrite, sphalerite, galena, and pyrite, but these minerals are not present in the sample collected. In sample 44, from the same locality, it occurs in an otherwise unmineralized chert.

Sphalerite occurs in five samples and is commonly associated with other Cu-, Pb-, Zn-mineralization. In samples 9 and 19 it is observed only by SEM. The mean Au concentration in the sphalerite-bearing samples is 2.4 times the mean for all the samples, and the mean for Ag is 1.5 times the mean of all the samples.

Stibnite (Sb_2S_3) was only observed in one sample, and that in the 89j09 series. It was collected close to the white rhyolite dike cropping out northeast of North Baldy; its identification is based on elemental composition and nearly euhedral shape (Fig. 13D).

Thalenite ($Y_2Si_2O_7$) is a possible occurrence illustrated in Fig. 14F. The EDX spectrum of this phase shows only Y and Si present.

Zippelite (hydrous uranium sulfate) was identified as a trace occurrence by XRD only in jasperoid sample 44. *Zircon* was observed by SEM only in sample 19. Its shape and manner of occurrence suggest detrital origin (Fig. 16B).

Geochemistry of Kelly Limestone jasperoids

Sampling for jasperoid geochemistry followed an opportunistic strategy and a systematic strategy. In the first, samples were collected from the vicinity of mineralized outcrops and mine and exploration cuts as well as along roads and trails where good jasperoid outcrops could be found. In the second strategy, samples were collected at uniform intervals along two widely separated vertical sections on jasperoid cliff faces. Sample locations are given in Appendix 3 and Tables 8 and 9.

Opportunistic sampling

Fifty samples of jasperoid were collected during the 1988 field season and were analyzed for 35 elements by optical emission spectroscopy at the U.S. Geological Survey Branch of Geochemistry, Lakewood, Colorado, under the direction of D. E. Detra. Each sample was cleaned of matrix, soil, and vegetation and reduced to about 250 grams. Ca, Fe, Mg, Ti, Ag, Ba, Be, Co, Cr, Cu, Ga, Mn, Mo, Ni, Pb, Sc, Sr, V, Y, Zr, As, Bi, Cd, Sb, and Zn were the only elements consistently measurable at significant levels in the jasperoids; they are statistically summarized in Table 2. Means and estimated standard deviations are computed assuming normal distributions. Although log-normal distribution may more accurately estimate the population, the abundance data are apparently arithmetic means. Furthermore, many analyses are reported as below the limit of detection; the normal mean can include zeros, but the log-normal cannot. Seven samples with Ca concen-

trations higher than 0.7 wt% were deleted from the original list to minimize the effects of contamination by carbonate rocks hosting the jasperoids.

The following elements were measurable in very few samples. P was determined in three samples at the 0.2 wt% level. La was determined at 70 and 100 ppm in two samples. W was determined in one sample at 100 ppm and another with high Ca at 150 ppm. Although Sn gave no signal in the spectrographic analyses, minute cassiterite grains were observed in cavities of some jasperoids.

Au was determined by atomic-absorption spectrometry in the same laboratories under the direction of R. M. O'Leary and is included in Table 2. It was below the limit of detectability (0.002 ppm) in only two samples.

Means, estimated standard deviations (e.s.d.), and analytical ranges of 43 samples are listed in Table 2; also listed are the ratios of mean concentration to crustal abundance,

TABLE 2—Summary statistics of 43 jasperoid samples.

	Wt. %			
	Ca	Fe	Mg	Ti
mean	0.18	3.65	0.15	0.06
e.s.d.	0.15	4.82	0.19	0.06
maximum	0.7	20	0.7	0.3
minimum	0.015	0.15	0.02	0.01
mean/crust	0.044	0.65	0.065	0.10

	ppm				
	Ag	Ba	Be	Co	Cr
mean	23.4	2650	2.4	18.4	22.6
e.s.d.	33.4	2160	2.2	46.6	26.4
maximum	200	5000	15	300	150
minimum	1.5	100	1	0	10
mean/crust	330	6.2	0.86	0.74	0.23

	Cu	Ga	Mn	Mo	Ni
	mean	2030	7.07	1350	39.6
e.s.d.	4240	4.81	1540	56.2	24.6
maximum	15000	30	5000	300	100
minimum	30	5	150	5	0
mean/crust	37	0.47	1.4	26	0.24

	Pb	Sc	Sr	V	Y
	mean	6820	3.83	379	35.8
e.s.d.	7790	5.01	674	31.5	17.3
maximum	20000	20	3000	150	70
minimum	100	0	0	10	10
mean/crust	546	0.17	1.0	0.27	0.79

	Zr	As	Bi	Cd	Sb
	mean	44.9	27.9	80.2	56.3
e.s.d.	57.7	77.5	493	138	45.7
maximum	300	500	3200	710	170
minimum	10	0	0	0.4	0
mean/crust	0.27	15	470	280	110

	Zn	Au
	mean	7100
e.s.d.	8740	0.45
maximum	26000	2.1
minimum	140	2.1
mean/crust	100	>5

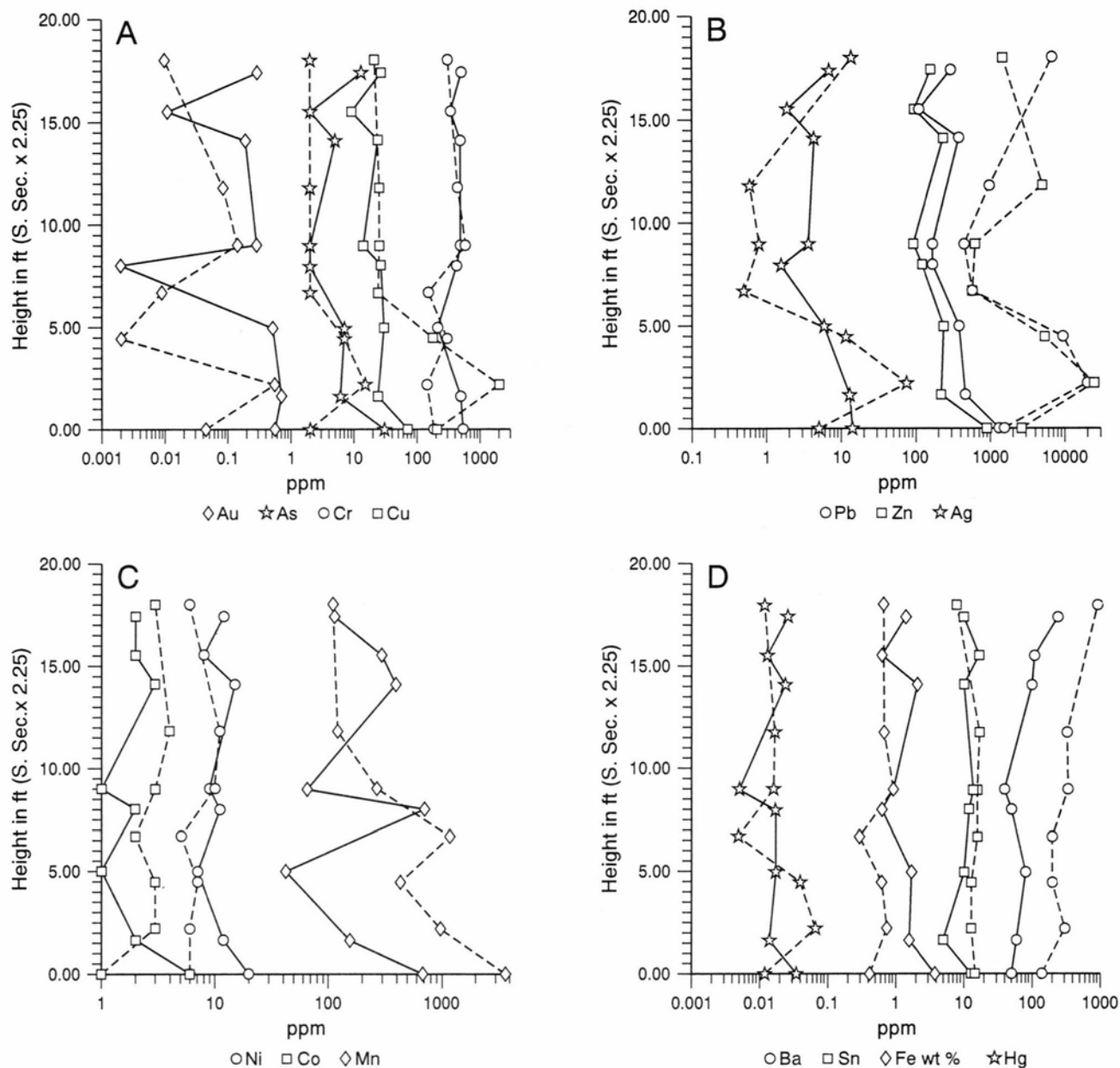


FIGURE 16—Element variation in two jasperoid outcrop sections.

with ratios greater than 1.0 highlighted. The crustal-abundance data used to construct the ratios can be found in Krauskopf (1967, p. 639). The correlation coefficients of all pairs of analytes with coefficients **1.071** are shown in boldface in Table 3.

We adopt the comparison of jasperoid geochemistry with crustal abundances in order to have a point of reference for the origin of the Magdalena jasperoids, which occur in close proximity to older igneous rocks. Insofar as the igneous activity is derived from crustal melting, crustal abundances allow the null hypothesis that the jasperoid geochemistry is no different from that expected for the evolution of late-stage igneous fluids to hydrothermal fluids. Thus, the elements determined in the jasperoids are considered in Table 2 from the standpoint of depletion and concentration relative to magmatic differentiation. Of course, other kinds of fluids can also precipitate microcrystalline silica. Except for burial metamorphism, fluids due to regional metamorphism during jasperoid precipita-

tion probably were not available. Formation fluids were probably available, but we have no data on their likely compositions. Siemers (1973) reported extensive propylitization of Abo Formation shales north of our field area. Propylitization can release substantial amounts of silica, but at this time we have no quantitative measure of its effect on the development of the Kelly jasperoids.

Smith's (1963) *Physical Geochemistry* is our principal source of depletion and concentration data used in the discussion below. It should be consulted for further detail. Ca, Fe, Mg, Ti, Be, Co, Cr, Ga, Ni, Sc, V, Y, and Zr have mean/crust ratios less than 1.0. For the most part, these elements are removed from igneous melts by precipitation of ferromagnesian minerals at an early stage of igneous differentiation. Fe, Be, and Y, however, can concentrate in late-stage fluids, and their ratios, along with Co, are closer to 1.0 than to 0.1. Ga is geochemically similar to Al. It can substitute in the quartz structure more than any other of the elements determined here.

TABLE 3—Correlation coefficient table of selected elements.

	Fe	Mg	Ti	Ba	Co	Cr	Cu	Ni	Sc	Sr	V	Y	Zr	Cd	Zn
Fe	1.000														
Mg	0.331	1.000													
Ti	0.272	0.581	1.000												
Ba	-0.736	-0.164	-0.175	1.000											
Co	0.555	0.556	0.349	-0.359	1.000										
Cr	0.352	0.613	0.768	-0.232	0.319	1.000									
Cu	0.467	0.100	-0.153	-0.446	0.269	-0.153	1.000								
Ni	0.380	0.651	0.343	-0.163	0.702	0.301	0.073	1.000							
Sc	0.536	0.718	0.596	-0.334	0.482	0.594	0.200	0.542	1.000						
Sr	-0.555	-0.078	0.007	0.788	-0.234	-0.017	-0.380	-0.099	-0.195	1.000					
V	0.283	0.714	0.703	-0.138	0.439	0.721	-0.041	0.446	0.689	0.107	1.000				
Y	0.412	0.638	0.441	-0.290	0.551	0.416	0.081	0.728	0.616	-0.148	0.528	1.000			
Zr	0.131	0.532	0.829	-0.094	0.338	0.676	-0.260	0.305	0.433	0.011	0.514	0.344	1.000		
Cd	0.607	0.100	-0.130	-0.574	0.457	-0.093	0.733	0.271	0.155	-0.530	-0.093	0.222	-0.162	1.000	
Zn	0.578	0.272	-0.048	-0.555	0.528	-0.055	0.660	0.340	0.294	-0.546	0.024	0.334	-0.083	0.899	1.00

Fe is positively correlated with every element except Ba and Sr (see Table 3). It has greater than 0.5 correlation coefficients with Sc, Co, Cd, and Zn. Its correlation with Ba and Sr is -0.6 and -0.7 , respectively. Correlation of Fe with Ba is the strongest negative correlation in the jasperoids. Co is easily accommodated in the pyrite structure, and Fe and Cd are easily taken into the sphalerite structure. Sc is trivalent and strongly oxyphile, and is expected to follow Fe in oxide minerals.

Mg concentration in the jasperoids is slightly greater than that of Ca, but its weight fraction in the carbonate rocks replaced by jasperoids is expected to be less than half of Ca's. It has correlation coefficients >0.5 with Ti, Co, Cr, Ni, Sc, V, Y, and Zr. The Mg correlation coefficients of >0.7 with Sc and V are among the highest in the jasperoids. Its high concentration reflects Mg's hydrophilic character (Smith, 1963, p. 387) and, like Ca, its tendency to concentrate in late-stage hydrothermal fluids. The association of Mg with the other elements mentioned (except Co and Ni) is consistent with their oxyphile character. Mg is about 1000 times as abundant as Co and Ni in the crust, whereas it is only about 100 times as abundant in the jasperoids. Ba, Cu, Mn, Sr, Mo, As, and Au have mean/crust ratios from 1.0 to 40. Mn and Sr have mean concentrations similar to crustal abundances. Both are extracted from the melt by ferromagnesian minerals during igneous differentiation, but not as strongly as Fe. Mn, like Sr, is partitioned into the aqueous differentiate. Ba and Sr have correlation coefficients of 0.8 in the Magdalena jasperoids and both are negatively correlated with other elements, having correlation coefficients $> |0.5|$. The Sr mean corresponds to the maximum of 9 mole % of celestite molecule found in naturally occurring barites, as reported by Haynor (1968). The higher mole ratios of Sr/Ba are substantially greater than those likely to be found in naturally occurring barites. Celestite has not been reported from the district, but it may have been overlooked because its optical properties are similar to that of barite. Concentrations of Cu and Mo enriched in the jasperoids are 37 and 26 times higher than in the crust. Both are strongly chalcophile elements concentrated in late-stage magmatic fluids. Au has a mean/crust ratio of >5 and about the same order of magnitude as As. Au has no strong correlation coefficients with any other element in the jasperoids, but is weakly correlated with chalcophile elements Ag, Cu, Mo, and Pb, with correlation coefficients of 0.22, 0.29, 0.31, and 0.46, respectively. It is not correlated with As.

Ag, Pb, Bi, Cd, Sb, and Zn have mean/crust ratios from 100 to 546. All are chalcophile elements and tend to be concentrated in late-stage magmatic fluids. The ratios for Bi, Sb, and As (472, 108, and 15, respectively) parallel their tendency to precipitate in hydrothermal veins from higher to lower temperature, or earlier to later as pointed out by Smith (1963, p. 425). Cd and Zn have the highest correlation coefficient (0.90) observed in the Magdalena jasperoids.

Systematic sampling of two outcrops

Two jasperoid sections in the upper part of the Kelly Limestone were systematically sampled. The northern section is located at the head of Jordan Canyon and the southern section is located 2 mi (3.2 km) south near North Baldy (Fig. 9). The north section is 18 ft (5.4 m) thick and was sampled at approximately 2.4 ft (0.73 m) intervals. The south section is 8 ft (2.4 m) thick and was sampled at 1 ft (0.31 m) intervals.

The physical aspects of the two sections are different. The rock of the north section is a pink to maroon vuggy jasperoid with inclusions of limestone and sedimentary chert. Open space in the lower part of the section is filled with a poorly consolidated, soft, red terra rossa containing ochre layers and laminated with clay and silt. Barite filling subvertical fractures is conspicuous in the north section. The jasperoid of the south section is white at the top and banded gray and white at the bottom, near its contact with limestone. It is more massive than the north-section jasperoid, but also contains limestone inclusions.

Galena and malachite are conspicuous in the south section, whereas barite is not. A white rhyolite dike is in sharp contact with the jasperoid of the south section (Fig. 9). This exposure did not provide paragenetic relationships.

Fifteen jasperoid samples from the two sections as well as a sample of terra rossa and silicified "terra rossa" from the north section, and terra rosa-like material from the Ambrosia mine 1.7 mi (2.7 km) north of the north section, were collected for trace-element analysis. Terra rossa from the Kelly Limestone and shale from a Pennsylvanian channel fill in the Kelly Limestone were also collected near each other in the Ladron Mountains, 20.2 mi (32.5 km) north of Magdalena. These two groups of samples were analyzed by Bondar—Clegg analytical laboratory in Sparks, Nevada. Au was determined by fire assay with a lower limit of detection (LLD) of 5 ppb. Ag, Cu, **Pb**, Zn, Ni, Co, As, Fe, Mn, and Cr were determined by inductively coupled plasma

atomic absorption. Hg was determined by cold-vapor atomic absorption, and Ba and Sn by x-ray fluorescence. Bi, Sb, and W were also determined, but their concentrations were too low to show meaningful variations in the sections.

Variation in the chemistry with stratigraphic position in the north and south Magdalena jasperoid sections is shown in Figs. 16A—D. To facilitate comparison, the shorter south section has been graphically stretched by a factor of 2.25 to equal the north section. In these figures, the north-section data points are connected with solid lines and the south-section data points with dashed lines. Concentrations have been plotted on a logarithmic scale to accommodate their large range.

For the most part, the geochemical character of the two sections is similar. The ranges of the elements are similar, and Au, Cr, As, Ag, Ni, Hg, Fe, Sn, and Mn have similar vertical variation in the two sections. On the other hand, Cu, Pb, Zn, Co, and Ba differ from section to section.

Fig. 16B shows that the concentrations of the two chalcophile elements, Pb and Zn vary together in the two sections but their concentrations are several hundred ppm higher in the south section. Fig. 16A shows Cu varying with As in the the two sections, but their concentrations differ in the two sections. Fig. 16C shows Ni and Co varying together in the two sections, with Co concentrations higher in the south section. Mn has a similar vertical variation in the two sections, but concentrations are higher in the lower part of the southern section. Fig. 16D shows that the vertical variation of Sn, Fe, and Hg in the south section is similar to that in the north section. Ba, on the other hand, is a few hundred ppm higher in the south section.

Figs. 17A—E are log-log scatter diagrams showing correlations among several pairs of elements. Fig. 17A shows that the Ni—Co correlation is the same for all the samples. The concentrations of these elements in the terra rossas are about the same as their average concentrations in the opportunistic samples, and in the north- and south-section jasperoids they are lower than in the terra rossas. In turn, their concentrations in the terra rossas actually are somewhat lower than their averages in the Earth's crust.

Fig. 17B shows the correlation of Cu with Pb in the south and north sections and in the terra rossas. The mean of Cu in the opportunistic sampling is two orders of magnitude higher than in the systematic sampling. Note that in the opportunistic sampling Cu varied between 30 and 15000 ppm. The scatter diagram for Zn vs. Pb is very similar to Fig. 17B.

In the Cu—Pb correlation, the dike, the jasperoids, and the Kelly Limestone terra rossas all fall in the same correlation pattern. The compositions of the Ladron Mountain terra rossas, however, are unrelated to the Kelly district Cu—Pb correlation. The same relationships exist for Zn vs. Pb.

Fe and Cr are lithophile elements but, unlike Ni and Co, they are correlated only in the jasperoids and not in the terra rossas. Fig. 17C shows that Fe is clearly enriched in the terra rossas, as expected. The concentration of Cr in the systematically sampled jasperoids is an order of magnitude lower than in those opportunistically sampled. Cr is expected to be concentrated in the terra rossas, because Cr_2O_3 behaves like Fe_2O_3 , but in the Kelly Limestone its concentration is apparently nil, and its concentration in the

jasperoids reflects more the composition of the jasperoid fluids.

The correlation of Ag with Pb is shown in Fig. 17D. Both Ag and Pb are chalcophile elements and are expected to be correlated. Ag commonly occurs in galena which is one of the most common ore minerals in the Magdalena mining district. The variation of Ag vs. Pb shows two parallel trends, with a higher Ag in the north section and with a lower Ag in the south section. The Ambrosia mine terra rossa is not included in the Ag—Pb jasperoid correlations; it has the same order of Pb concentration, but Ag is below its level of determination. The two Ladron Mountain samples appear to be correlated with the jasperoids, but they also have Ag below level of determination.

The relationship of Ag to Au is shown in Fig. 17E. Au is a lithophile element and is not expected to show a strong correlation with Ag unless the two precipitate together. Two north-section and two south-section samples are high in Ag and exceptionally low in Au. The Ambrosia mine terra rossa and the Ladron Mountain terra rossa are below limits of detectability. They are plotted at a point which is the average of their LLDs and zero.

The correlations of pairs of other elements illustrated in Fig. 16 are substantially poorer than those shown in Fig. 17. Ba is surprising in this regard when compared to Pb, for it is ubiquitous in this district and other Pb—Zn districts. As is below the limit of detectability in most of the samples.

Interpretation of jasperoid geochemistry

The minor- and trace-element concentrations in the jasperoids can only indirectly model the composition of a source fluid. The fluid almost certainly contained a component of the dissolved carbonates replaced by the jasperoid; however, Mg/Ca is too high to reflect only carbonate compositions even if dolomite were an important rock type in the district. Most workers agree that the microcrystalline quartz of a jasperoid crystallizes from an amorphous form of silica which began as a gel (see Lovering, 1972). The source fluid is partitioned into a silica gel according to poorly understood rules (see Henisch, 1988, p. 27), but one expects that the elemental ratios in a gel would monitor the composition of a fluid more closely than minerals precipitating directly from it. Quartz tolerates few impurities, so the composition of the jasperoids primarily reflects the non-quartz component of intergranular, veinlet, and druse mineralogy. We see the trace elements of the gel being progressively concentrated interstitially to crystalline silica as the gel dehydrates and crystallizes. No doubt a portion of the gel's trace-element load was lost in the initial dehydration fluid, but the opal—CT precursor to quartz can tolerate far more impurities than quartz. Those trace elements were probably immobilized to some degree in the opal—CT structure and swept into the intergranular volume when the precursor inverted to the quartz structure.

Of the elements determined during the opportunistic sampling of the jasperoids, the mean/crust ratios of only Be and Y are inconsistent with the igneous differentiation concentration/depletion model. Ca, Fe, Mg, Ti, Co, Cr, Ni, Sc, V, Cu, Mo, Ag, Pb, Bi, Cd, Sb, Zn, and Mn are consistent with it. The other five elements, Ba, Zr, As, Ga, and Sr, are not diagnostic. On the basis of the trace-element geochemistry of these samples, the null hypothesis cannot

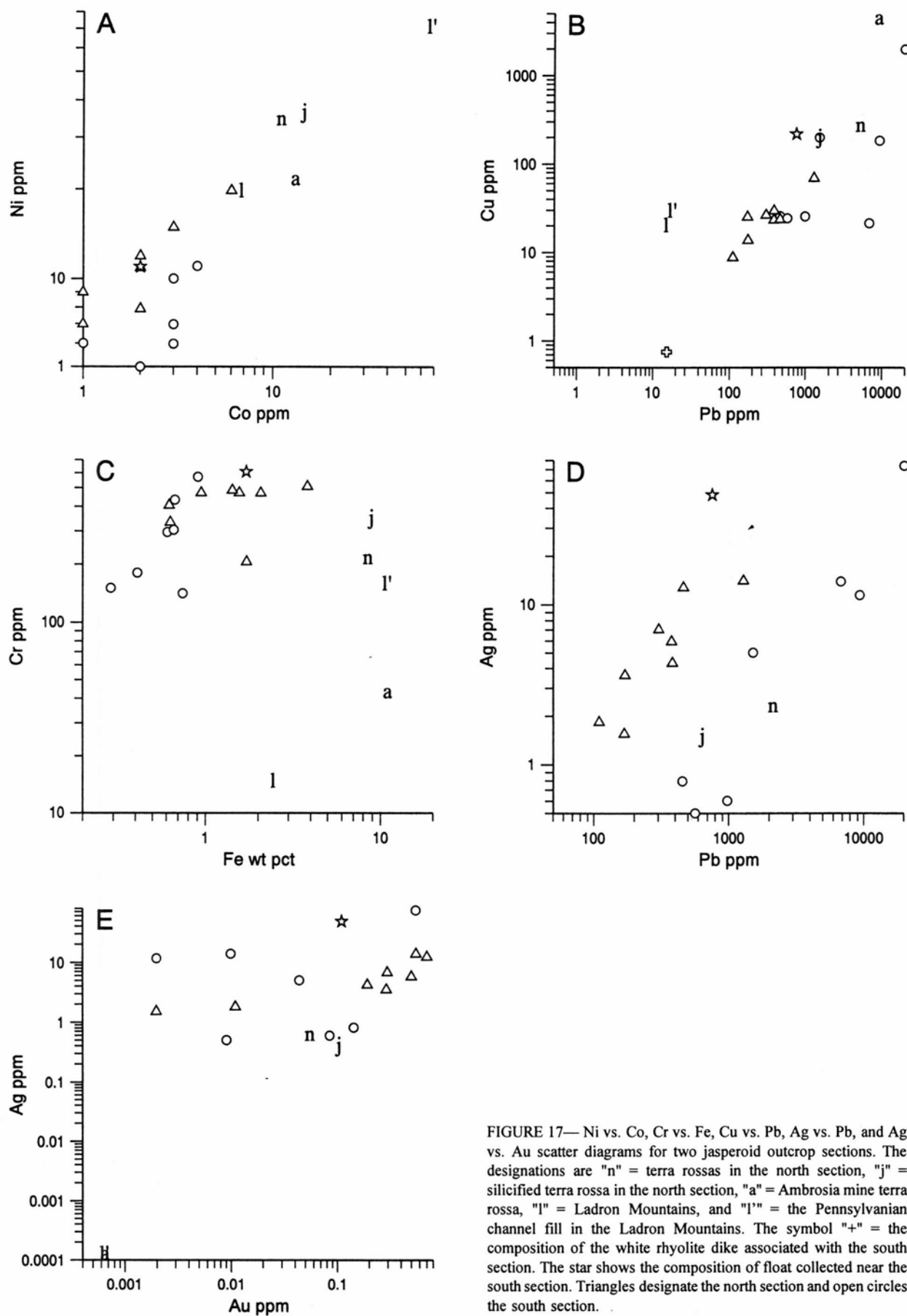


FIGURE 17—Ni vs. Co, Cr vs. Fe, Cu vs. Pb, Ag vs. Pb, and Ag vs. Au scatter diagrams for two jasperoid outcrop sections. The designations are "n" = terra rossas in the north section, "j" = silicified terra rossa in the north section, "a" = Ambrosia mine terra rossa, "l" = Ladron Mountains, and "l'" = the Pennsylvanian channel fill in the Ladron Mountains. The symbol "+" = the composition of the white rhyolite dike associated with the south section. The star shows the composition of float collected near the south section. Triangles designate the north section and open circles the south section.

be rejected and the affinity of the jasperoids to igneous processes appears to be strong; however, the trace-element geochemistry of these samples is only one line of evidence.

In the above description of opportunistic geochemical sampling we compare the jasperoid geochemistry to concentration and depletion of elements due to igneous differentiation. Systematic sampling of the two jasperoid sections provides further insight.

The general similarity of elemental distribution in the two sections strongly suggests that the jasperoids at the two localities were deposited during one event. The uniformity from bottom to top of the two sections shows that there was little geochemical evolution during the jasperoid deposition. Au, Ag, and Mn show some conspicuous excursions from uniformity that are similar in both sections.

Although the geochemical sampling is not adequate to firmly establish the reality of these variations, the association of Au and Ag with mineralogy is instructive. The strongest Au enhancement in the opportunistically sampled jasperoids is associated, in decreasing order, with sphalerite, galena, barite, cerussite, and hemimorphite. Ag is strongly concentrated in jasperoids containing hematite. Au is weakest with hematite, and Ag is weakest with hemimorphite.

Au, then, seems to be closely associated with base-metal deposition. Ag, on the other hand, shows no strong association with the base metals, but its association with hematite suggests a higher temperature regime. Laughlin and Koschmann (1942) presented evidence suggesting that pyrite was early in the paragenetic sequence and that base metals precipitated on it. SEM evidence presented above under *Pyrite* in the mineralogy section confirms this.

A possible explanation for the correlation of Ag with hematite, as stated above under *Mineralogy of the jasperoids*, is that a significant amount of Ag was introduced with silica during jasperization. As oxidation of Mississippian pyrite progressed, Ag along with Cu combined with liberated sulfur and precipitated at the pyrite—hematite interface as illustrated in Fig. 14A.

Pb, Zn, Cu, and Ba behave differently from the other elements determined in the two systematically sampled sections. Pb, Zn, and Cu are highly correlated with each other, but the concentrations of each in each section are different. Ba does not correlate convincingly with other elements identified in the sections and differs from section to section. We argued above that the similarity in behavior of other elements in the two sections and the uniformity in their concentrations from bottom to top suggest that the jasperoids were deposited during a single event. However, the differences in Pb, Zn, and Cu between the two sections suggest that they were introduced into the jasperoids following silicification of the Kelly Limestone. The large base-metal mines on the western slopes of the Magdalena Range show relatively little jasperization. Perhaps early jasperization that exploited karst and reduced porosity forced subsequent base-metal mineralization to the west.

The position of the Ladron Mountain samples in the Cu, Zn, and Pb correlations shows that in the Magdalena district these elements are strongly enriched at ratios different from those found in a remote Mississippian terra rossa or a Pennsylvanian shale. The Kelly Limestone terra rossas, however, lie on the Cu—Pb and Zn—Pb trends. The concentrations of these elements in the white rhyolite dike also lie on this trend. We suspect that the concentrations of

these elements in the Kelly jasperoids and terra rossas are related to emplacement of this dike and, by implication, other white rhyolite dikes in the district. However, we cannot discount the possibility that the dikes and jasperoids were affected by the same hydrothermal fluids, but from another source, even though we found no conspicuous sulfide mineralization in the dike.

The strong correlations of Pb—Zn—Cu found in the systematic samples are not found in the opportunistic samples, although Zn—Cu are moderately correlated at 0.66 (Table 3). The Ba—Fe correlation of the opportunistic samples does not appear in the systematic samples. Our only explanation for this is that more of the opportunistic sampling occurred close to areas of strong mineralization and the correlations are modified by mineralogical and paragenetic complexity. We mentioned above that Ag seems to have two different correlations with Pb in the systematically sampled sections. The one with higher Ag concentrations is in the north section. The south section has an Ag—Pb relationship more like the terra rossas, (excluding the sample of terra rossa enriched in Pb, from the Ambrosia mine to the north). Furthermore, Ag and Pb are uncorrelated in the opportunistically sampled jasperoids. These relationships are difficult to accommodate in a single hypothesis, but the southern section, being farther away from the main massive Pb—Zn mineralization of the district, seems to reflect more the Ag—Pb ratio of the terra rossas. The lack of correlation of Ag with Pb and Zn mineralogy mentioned above suggests that at least some Ag and Cu were introduced with the jasperoids during earlier, higher-temperature mineralization. In this regard, the relationships described above under *Pyrite* in the section on jasperoid mineralogy are pertinent.

Ni and Co correlate well in both the opportunistic and systematic samples. Although the concentration of Co is less than mean crustal concentrations as would be expected in an igneous differentiation model which has it extracted in early ferro-magnesian phases, its concentration is 30 times higher than Mason and Moore (1982) reported for average carbonate rock, and is consistent with a residual soil such as terra rossa.

Both Ni and Co are siderophile elements, and, although they are more mobile than Fe, they are also concentrated in the terra rossas and the Pennsylvanian channel-filling shale of the Ladron Mountains relative to their concentrations in the Kelly jasperoids. We have no geochemical data on the Kelly Limestone, but the Ni—Co ratios in the terra rossas are probably like those in the limestones from which they were derived. Because their ratios in the terra rossas are essentially the same as in the jasperoids, we suspect that the geochemistry of the jasperoids reflects at least to this degree the geochemistry of the terra rossas and indirectly the limestones. The same argument cannot be made for the other element pairs in Fig. 17, because their concentrations or ratios in the Ladron samples are very different. In brief, the concentrations of the siderophile elements in the terra rossas seem to be due to residual-soil-forming processes. The jasperoid, having powerful replacing properties, inherited the Ni—Co ratio of the terra rossas, and by implication of the limestones.

Au and Ag have similar patterns in both north and south sections, indicating that they were introduced with silicification, but some Au must have been introduced with Pb and Zn as evidenced by the mineralogy.

Cr is strongly correlated with Ti and V but not with Fe in

the opportunistically sampled jasperoids. This follows from its oxyphile character and suggests that it was introduced with silicification. In the systematically sampled jasperoids Cr is somewhat correlated with Fe, but this is clearly independent of the terra rossas. This is also consistent with its introduction during silicification.

The correlation of Pb and Zn in the same jasperoid sections suggests that they have similar origins and were introduced together; however, their concentrations in the two sections differ and suggest that they were introduced into them differently. Cu, on the other hand, has about the same concentration in both sections. Cu and Pb have better correlation in the north section than in the south, and the concentrations of both are higher in the north section than they are in the south.

The simplest explanation of the base-metal concentrations in the light of the uniform behavior of the other elements in the two sections is that the base metals were introduced after silicification, but an important amount of Cu was introduced during silicification as can be seen in upper part of the south section (Fig. 16A).

Ba also shows non-uniform concentrations from section to section, which suggests that it too was introduced subsequent to silicification. Iovenitti (1977) presented a paragenesis based on crosscutting relationships, which shows that all of the galena and most of the barite were introduced after deposition of microcrystalline quartz (silicification). He demonstrated, however, that at least one stage of barite introduction was contemporaneous with microcrystalline-quartz silicification. Laughlin and Koschmann (1942) placed barite at the margins of galena and sphalerite veins.

The limited number of ^{634}S determinations we described under *Pyrite* in the mineralogy section have a mean of -8.7 with a range of 3.9. The mean lies midway between the mode of igneous and sedimentary sulfides summarized by Ohmoto and Rye (1979, p. 510), and these isotope data by themselves thus neither support nor undermine the null hypothesis (igneous kinship). It is possible that the pyrite is derived from the replaced limestone and present as a relict phase. It is almost always euhedral and accompanied by iron oxide, probably hematite. The grains we measured were truly disseminated in the jasperoid indicating that they witnessed jasperization.

Hemley and Meyers (1967, p. 220) showed that at 250°C the equilibrium phase boundary for coexistence of pyrite and hematite extends from about pH 6.5 to 3. At this temperature, pH neutrality in an aqueous solution saturated with α -quartz is about 5.2 (Smith, 1963), and at 400°C it descends to 4.7. The pH of the hydrothermal solution that dissolved and silicified the Kelly Limestone must have been on the order of 4 to 5, and with falling temperature and constant pH the solution would have become relatively more acid. If during limestone dissolution and replacement the partial pressure of oxygen diminished more slowly than sulfur, then conditions were favorable for oxidation of pyrite to hematite and incorporation of oxidized Kelly Limestone pyrite into the jasperoid.

In conclusion, all workers in the district have found that jasperoid is frequently intersected by base-metal-bearing veins whereas the reverse is not known to occur, and they therefore deduce that jasperization preceded base-metal mineralization. The geochemistry is consistent with these physical observations. Furthermore, the geochemical signature of the jasperoids is similar to that of fluids

expected to form from late-stage igneous differentiation. However, the geochemistry, mineralogy, and spatial relations of the jasperoids are only consistent with that hypothesis and do not rule out possible precipitation from fluids of meteoric origin.

Geothermometry

Conodont color-alteration index (CAI) and silica-crystallite-size geothermometry were used to determine the maximum temperatures witnessed by the limestones, cherts, and jasperoids in our area of study. The CAI studies were done by Repetski and the silica-crystallite-size studies were done by Renault. Details of the CAI data are given in Appendix 2.

The silica crystallite-size method is not well known, and is therefore discussed in detail in Appendix 1. In brief, silica minerals crystallizing from silica gel grow as imperfect crystals containing domains bounded by dislocations. The domains are called crystallites and with increasing temperature the imperfections move and the sizes of the domains increase. The mean crystallite size can be easily determined from the breadth of x-ray diffraction lines; when calibrated against temperature, the crystallite size of microcrystalline silica is a geothermometer which, like the conodont alteration index, records the maximum temperature the crystallites have seen.

Thermal effect of a dike intrusion on Kelly Limestone chert

The influence of temperature on the crystallite size of the microcrystalline-quartz component of Mississippian chert was observed in a suite of samples collected as a function of distance from a white rhyolite-dike contact in the Magdalena mining district (Fig. 18 and frontispiece). Samples of chert were collected 200 m northeast of North Baldy in sec. 17, T3S, R3W. The chert is beautifully exposed, and we were able to sample away from the dike contact at 30 cm intervals along a single sedimentary horizon about 1 m above the "silver pipe."

The white rhyolite dike is similar to others that abound to the south and are the youngest intrusions in the Magdalena Mountains. They are Tertiary in age, but have not been radiometrically dated. See Krewedl (1974) for petrographic details. The dike near North Baldy is about 6 m thick at the level of sampling. Twenty-five meters above this level it is closely associated with a massive gray/white subhorizontal jasperoid zone where it diminishes in thickness to about 2 m, but the contact relationships are not observable. The dike has suffered strong alteration but can be identified as a rhyolite porphyry with quartz and alkali-feldspar phenocrysts set in a felted groundmass now completely trans-

TABLE 4—Summary of conodont CAI data.

Sample # minimum	CAI minimum	T°C	N	Remarks
88N-1+4	5	300	1	Near 89f30b
88N-1+95	4, 6	200, 350	21	
89N-W1+1	4, 6½	200, 440	2	
89N-W3T	6½, 7	440, 490	2	
89N-R11	4	190	52	
89N-15	4	190	44	
89N-R16	4	190	9	
91J23C	4½, 7	200, 490		

formed to sericite and some chlorite. The dike is characterized by millimeter-scale bands of microcrystalline quartz parallel to its contacts. The bands are tortuously contorted even at the microscopic scale and are clearly not due to emplacement in fractures or well defined shears. Texturally, they are a primary component of the dike, displaying flow structure due to its emplacement.

Fig. 18 shows the variation in silica-crystallite temperature away from the dike. There is a clear decrease in temperature with distance, and we have fit a linear regression line to the variation of temperature with reciprocal distance from the dike center in Fig. 19 as per Turcott and Schubert (1982, eq. 4-165). The standard error of the fit is 3.5°C. At three standard errors, the 99.7% confidence interval in the fit is $\pm 10.5^\circ\text{C}$.

Several data points have been excluded from the linear fit. The four points in the middle of Fig. 19 depart more than 18 standard errors from the fitted line. The rightmost data set is anomalously low and has also been excluded from the fit. Its deviations are, respectively, 10.4, 16.0, and 18.9 standard errors below the regression line. These three measurements are rejected because the sample was close to the contact and displayed distinctive silica-replacement texture with limestone, and because we could not exclude the possibility of late secondary silicification. Evidence developed below suggests that the dike served as a conduit for solutions responsible for jasperization.

The regression equation gives the ambient temperature at the time of intrusion as 197°C. This is very close to the minimum ambient temperature of 190°C obtained by one of us (Repetski) with the CAI method. The equation gives the temperature of the intrusive contact as 347°C. If this is the average of ambient and intrusion temperatures, then the dike was intruded at 497°C, which is about 225° below the liquidus of a water-saturated granodiorite at 1 Kbar (see Burnham, 1967, p. 69). Even considering that the dike was rhyolitic in composition and would have had a lower liquidus than granodiorite, the crystallite-size temperatures seem too low for a magma to have been present at the

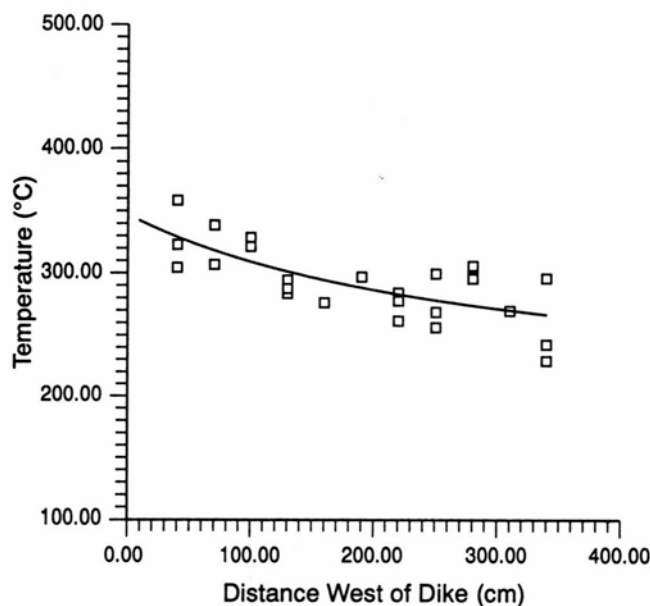


FIGURE 18—Variation of [212] crystallite temperature in sedimentary chert as a function of distance from white rhyolite dike contact.

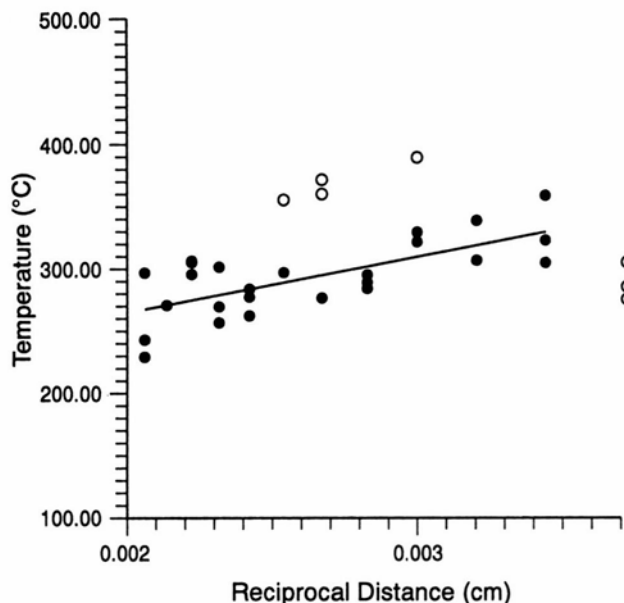


FIGURE 19—Variation of [212] crystallite temperature in Kelly Limestone cherts as a function of reciprocal distance from center of white rhyolite dike. Equation of least squares fit is $T = 4.5E+04(1/x) + 197$.

sampled level of intrusion in the absence of strong mineralizers such as F^+ and Bo^{++} , neither of which is significantly concentrated in the dike at the level of sampling. It is more likely that the intrusion was more of a hydrothermal mush than a water-saturated magma.

The simple theory we have used to explain the temperature decline with distance from the dike expects the temperature measurements to be normal to the plane of the dike contact. In fact, the line of traverse intersects the plane of the dike at approximately 15° below normal, so the temperature decline with distance is gentler than the simple theory expects; consequently, the temperature of 197°C remote from the dike is overestimated by the equation. It should be noted, however, that the Magdalena Range subsurface contains numerous plutons, and it is reasonable to assume elevated ambient temperatures at the time of intrusion of the white rhyolite dikes.

The three anomalously low silica-crystallite temperatures 10 cm from the contact suggest that the chert there has been contaminated by silica introduced subsequent to dike emplacement. This interpretation is supported by the limestone replacement textures as well as by temperatures determined for chalcedonic bands in the dike and for the lower part of a silicification zone spatially associated with the dike. See samples 89j18b and 90120a under the following discussion of jasperoid temperatures.

The heat content of the contact at 347°C can be determined from the slope of the regression equation. Using a cgs thermal diffusivity of 1.054.10, specific heat of 0.204, and a density of 2.5 (Kappelmeyer and Haenel, 1974), the heat content is $9.5 \cdot 10^4 \text{ cal cm}^{-2}$. This is about half of what would be expected from a basaltic intrusion as calculated by Turcotte and Schubert (1982).

Two subsamples of chalcedonic silica (90f20a1 and a2) from the dike at its contact give crystallite-size temperatures of 303 and 302°C. Since the texture of the chalcedonic bands implies that they solidified with the dike, and the maximum contact temperature was 347°C, the paleo-temperature of these subsamples indicates that either (1)

their recrystallization was arrested by the falling thermal regime of the dike, or (2) their recrystallization was much slower and records a later thermal pulse.

Solving for time in the temperature-distribution equation of Turcotte and Schubert (1982, eq. 4-163) gives 49 days as the time required for the contact to rise to its maximum temperature and another 167 days to fall to 302°C, the paleotemperature of the chalcedonic bands in the dike. The fitted temperature of the set of chert samples 130 cm from the contact (430 cm from the dike center) is 302°C, and the time for the limestone to rise to this temperature was 100 days. McKenzie and Melling (1974) showed that anatase crystallites reached their maximum sizes after only 90 minutes at 500°C. The required time for microcrystalline quartz to reach its maximum crystallite size at 302°C is not known, but it seems likely that several days would be sufficient.

If the chalcedonic bands crystallized as rapidly as the sedimentary chert recrystallized, the intersection of their crystallization and the contact's cooling at 216 days implies that they began to crystallize at most 100 days before this time or at least 116 days after the dike's emplacement. However, because reactions run faster at high temperatures, the chalcedonic bands would crystallize more rapidly in a temperature regime falling from higher temperatures than the cherts would recrystallize in a rising regime, so the crystallization of the bands may have been more rapid.

The above analysis does not eliminate the opposing hypothesis that the chalcedonic bands in the dike recrystallized at a much later time in a rising thermal regime. This hypothesis is more complicated and requires that the silica gel from which the bands crystallized remained stable for more than 216 days and was then heated by another intrusive event. Although the white rhyolite dikes are considered by all workers in the Magdalena district to be the last intrusions emplaced, Blakestad (1978) reported that recent exploration had revealed a shallow, unexposed intrusion beneath North Baldy peak, whose age relationship to the dikes is unknown.

Silica-crystallite analysis of other cherts and jasperoids

Silica-crystallite temperatures of other Mississippian cherts in the Kelly district are given in Table 5 and those of jasperoids are given in Table 6. Most of the data in the tables are averages of two or more subsamples taken from a single hand specimen; however, 89j09b—i is an average of 16 determinations on eight hand specimens.

The silica-crystallite temperatures of other cherts vary from 276 to 330°C. The two samples with the largest errors, 89f30f and 89i30i, are closely associated with mineralization, and more than one generation of silica may have been analyzed. Iovenitti (1977) studied fluid inclusions in barites of the district and found two temperature populations of 235°C and 285°C (uncorrected for pressure). The association of barite with sample 89f30i is thus consistent with the silica-crystallite-size temperature measured by us.

Two samples, 89f30b and 89h23c, have temperatures substantially higher than other cherts. Although higher temperatures were measured close to the white rhyolite dike northeast of North Baldy, 89f30b is not close to an exposed intrusion. It is, however, below massively silicified Kelly Limestone which gives a temperature of 329°C in sample

TABLE 5—Silica geothermometry of Kelly Limestone cherts.

Sample	T°C±σ	N	Elev. (ft)	Location
89f30b	305±7	2	9020	Immediately above "silver pipe," Jordan Canyon Rd.
89f30f	282±16	2	9200	450 m S of previous sample. Immediately above laminated jasperoid of 89f30c,d,e.
89f30g	276±3	2	9100	Ridge above 89f30f, limestone float.
89h23c	330±10	3	8200	SE side of road in Chihuahua Gulch.
89f30i	277±12	4	8300	Head of Mistletoe Gulch. Barite-coated chert nodule in karst deposits.

89i30a. Sample 89h23c with 330°C has the highest temperature of the cherts in this group. It is about 76 m northeast of one of the dikes in the latite-porphry complex of Mistletoe Gulch and about 30 m southwest of an important normal fault.

The growth of quartz crystallites records the maximum temperature they experienced. Insofar as both jasperoid and sedimentary chert began as silica gels, both should respond to thermal effects in the same way. However, as a product of mineralization, jasperoid often displays a very complex paragenesis which may include more than one episode of replacement, brecciation, and veining. This frequently occurs on a millimeter-scale, and excluding veinlet quartz

TABLE 6—Silica geothermometry of Kelly Limestone jasperoids.

Sample	T°C±σ	N	Elev. (ft)	Location
89f30c	303±16	2	9200	See 89f30f in Table 8. Top layer of laminated vuggy jasperoid.
89f30d	332±33	2	9200	As 89f30c. Middle layer of laminated vuggy jasperoid.
89f30e	315	1	9200	As 89f30c. Bottom layer of laminated vuggy jasperoid.
89j18a	266±7	3	9570	200 m NW of North Baldy. Upper part of banded silicification zone.
89j18b	313±15	2	9560	As 89j18a. Lower part.
89j09a	341±75	3	9440	Prospect 290 m SE of North Baldy. Chalcedony bands in white rhyolite dike.
89j09b-i	355±39	16	9450	As 89j09a. Jasperoids extending west of white rhyolite dike.
89f30h	358±14	3	9160	Prospect at saddle 2200 m N of North Baldy. Silicified and mineralized limestone.
89f30a	329±33	4	9000	1 m below top of Kelly Limestone, Jordan Canyon Rd. Massively silicified limestone.

from microcrystalline quartz crystallized from a silica gel is difficult. For this reason the ranges in silica-crystallite temperatures recorded in Table 9 are much broader than those for the cherts in Table 5.

In general the jasperoids have higher silica-crystallite temperatures than the cherts, because they occupy the channels that guided the hydrothermal fluids which imported much of the heat. Cherts sufficiently remote from those channels record only maximum ambient temperatures.

Two suites of jasperoids, 89f30c—e and 89j18a—b, are samples of subhorizontally banded silicified rock. Both have higher temperatures at the bottom of each banded jasperoid unit than at the top. The middle sample of the first suite, 89f30d (332°C), has the highest temperature.

If the banded jasperoids formed by replacement of limestone along bedding planes as is usually expected, it is reasonable to assume that the central zone, being the plane of initial ingress, would have the higher temperatures, provided crystallization rates were rapid enough. Subsequent replacement of horizons above and below would be expected to display lower temperatures as the replacing solutions lost their physical—chemical effectiveness and the replacement episode waned. However, access to the outer zones would have to be through the already crystallized inner zone. Lovering (1972) thought that shrinkage of silica gel would provide avenues of access to unreplaced limestone. Although the sample populations are too small to statistically verify differences in the means, the differences are in the right directions.

Sample 89j09a gives the paleotemperature of silica bands within the altered white rhyolite dike. The actual distance from the contact is unknown, but it is not very close to it. This temperature is 341°C; it is virtually the same as the estimated contact temperature of the dike, but of course the interior temperature of the dike would be much higher at the time of intrusion. As discussed above, sample 90f20a from the dike contact has a paleotemperature of 302°C. The silica-crystallite size temperatures indicate that crystallization reached its maximum at about 160° below the intrusion temperature. The thermal diffusivity of limestone is 0.007 cm²sec⁻¹ (Carslaw and Jaeger, 1959, p. 497). The heat flow calculated from the regression equation then is 0.007 × 45000 = 300 J/cm².

Sample suite 89j09b—i consists of eight jasperoid samples collected over a distance of 64 m east of the white rhyolite dike discussed above in connection with sedimentary cherts. The jasperoids displayed no systematic variation in temperature away from the dike. Although the mean temperature is 25°C higher than the temperature recorded for silica banding in the dike, the errors are too large to differentiate between the two.

Sample 89f30h at 362°C has a relatively small error. It is from a highly silicified prospect. The sample has a complex paragenesis with pink and greenish jasperoid cut by two generations of drusy-quartz veinlets. Galena and pyrite are disseminated in the jasperoid and flakes of free gold occur on the first-generation quartz veinlet selvages.

Sample 89f30a contains pink lamellae of a silicified bryozoan-echinoderm grainstone. It is a complex of several subsamples: a1 (414°C) is a silicified mudstone showing fine bedding; a2 (378°C) is lilac-colored microcrystalline silica; a4 (300°C) and a5 (338°C) are yellowish microcrystalline silica; and a6 (305°C) appears to be a silicified mud.

Summary of geothermometry study

The Magdalena district cherts and jasperoids display two temperature ranges. The mean and e.s.d. of silica-crystallite temperatures of the cherts is 293°C ± 52.8, and the mean and e.s.d. of the jasperoid temperatures is 348°C ± 52.4. The *t* test gives the difference in the means as 4.59 times the standard error of the difference, so we take the jasperoid and chert means as significantly different. However, it is clear from the white rhyolite and chert study and the variation in temperatures of the layered jasperoids that strong temperature gradients existed in the Kelly rocks. For this reason, local temperature differences are important. The crystallite-size temperatures and the conodont alteration indices strongly suggest that background temperatures were between 190 and 223°C prior to mineralization. Impregnation of the white rhyolite dike with microcrystalline silica at 344°C suggests to us that fractured dikes served as conduits of silica-rich solutions that replaced the Kelly Limestone. Others have implicated the white rhyolite dikes (and the shear zones they follow) in the mineralization of the Magdalena district (see Blakestad, 1978). The mean of 344 and 223°C is 284°C, which is very close to the temperature measured in the chert 10 cm from the dike contact that we take to be contaminated by silicification subsequent to the intrusion.

Elsewhere in the layered jasperoids temperatures ranged from 334°C in the center layers to 262 and 290°C in the upper layers, and 305 and 315°C in the lower layers. The silica deposited in these layers appears to be of the same origin as the silica which deposited as lamellae in the dike. The thorough alteration of the dike suggests solutions similar to those that replaced the limestones.

The uniformly high paleotemperature of jasperoids in the vicinity of the dike when compared with the declining paleotemperature of cherts moving away from the dike shows that the two types of microcrystalline silica responded to two different kinds of heat transport. The cherts responded to heat diffusing out from the dike, whereas the jasperoids responded to heat advected along the channels in which they deposited. The similarity of jasperoid paleotemperatures and dike chalcedony implicates the dikes in silica transport.

Mere spatial association of silicification with an igneous intrusion is insufficient evidence for its magmatic origin. However, as described in the geochemical section of this report, the trace-element composition of the jasperoids is strongly suggestive of this origin. It appears very likely that igneous activity thermally prepared the Magdalena district for extensive silica replacement by raising the temperature of the susceptible horizons to the middle mesothermal range. Solutions of lower hypothermal temperatures were then able to gain broad access to the Kelly Limestone via karst open space and replace portions of the limestone without losing heat to the wallrocks too rapidly. Cassiterite, galena, possibly pyrite, and to a lesser extent other sulfides precipitated along with the jasperoid, but only sparse native gold precipitated later in the drusy-quartz veinlets. Some pyrite in the jasperoid was inherited from the replaced carbonate rock.

Summary and conclusions

The Kelly Limestone in the study area consists of the lower Caloso Member (zone 8, Tournaisian) and the upper

Ladron Member (zones 9, Tournaisian, and 14, Viséan). The Caloso Member rests unconformably on Proterozoic igneous and metamorphic rocks and is separated from the Ladron Member by a short hiatus. A cryptic unconformity accounts for the absence of zones 10 through 13, Tournaisian. This unconformity may represent 12-15 m.y., during which the lower part of the Ladron Member was subjected to vadose and phreatic cementation and porosity reduction.

Karst developed in the upper beds of the Kelly Limestone prior to deposition of the Pennsylvanian sediments. Karsting extended down from the paleoerosion surface to, and rarely into, the more thoroughly cemented Caloso Member. The relatively high degree of cementation in the lower parts of the Kelly Limestone resulted in less solution activity.

The initial goal of this study was to evaluate the Kelly jasperoid as a potential disseminated-gold resource. In that regard our results are disappointing, the gold content is not likely to average more than 0.08 oz/ton in the 1.7×10^6 metric tons of jasperoid exposed in the Magdalena Mountains. However, a number of relationships have emerged during the course of the study which bear on the origin of mineralization in the Magdalena district.

Both limestone replacement and open-space filling of karst solution cavities were important in jasperoid emplacement. The emplacement occurred as a single event with replacement following karst filling. The geochemistry and mineralogy of the jasperoids suggest that silicification of the limestones was closely associated with igneous activity.

The jasperoids have inherited some of the chemistry of the limestones they replaced and at least their pyrite mineralogy, but they also bear an important igneous signature. This signature is reflected in the tendency of the jasperoids to display higher than crustal abundances of elements which are concentrated in hydrothermal fluids derived from differentiated crustal melts, and less than crustal abundances of elements depleted during differentiation of those magmas. The presence of minute crystals of cassiterite in jasperoid vugs further suggests their igneous provenance. The distribution of Pb and Zn concentrations in the jasperoids indicates that these metals were mainly introduced subsequent to jasperization of the Kelly Limestone.

Geothermometry by conodont color-alteration index and by silica-crystallite size shows that the background temperature prior to mineralization had reached between 190 and 223°C. The mean temperatures of the cherts and jasperoids are 293 and 348°C, respectively, and are significantly different. The temperature data imply that heat was imported by the silicification event, and the field relationships indicate that silica-rich fluids were conducted into the karsted carbonate rocks of the Kelly Limestone by dikes that filled fractures. The fluids were prevented from reaching higher in the section by an impermeable seal of Pennsylvanian black shales and siltstones.

Acknowledgments

This work has been supported by the New Mexico Bureau of Mines & Mineral Resources (NMBMMR) and the U.S. Geological Survey. Special thanks are due to Dr. Frank E. Kottowski, former director of the NMBMMR, under whom this research was initiated and who gave us invaluable financial and intellectual support. Dr. Charles E. Chapin, Director of the NMBMMR, has continued that support. Dr. Miles L. Silberman examined with us the jasperoid out-

crops in the Magdalena Mountains and greatly helped us in understanding the geochemistry of these rocks. We are also grateful for the excellent sample preparation by Frank Craig who did much of the x-ray diffraction work. We gratefully acknowledge the thorough and helpful manuscript reviews by Charles Chapin, Ted Theodore, and Miles Silverman.

APPENDIX 1

Theory and calibration of silica-crystallite geothermometer

Variation in breadth of x-ray diffraction profiles of microcrystalline quartz has been noted intermittently in the literature since Hathaway (1972) drew attention to the resolution of 212 reflections in the diffractograms of deep-ocean-floor silica. Murata and Norman (1977) defined a crystallinity index based on the resolution of this peak and published an extensive list of determinations for microcrystalline quartz of various origins. Renault and Iovenitti (1978), Renault (1979, 1980), and Blankenburg and Freiberg (1981) showed that crystallite size can be related to the maximum paleotemperature of microcrystalline silica. Iovenitti and Renault (1977), Harrover et al. (1982), and Cook (1986) applied resolution measurements and silica-crystallite temperatures to mining districts known to have experienced thermal events.

A natural crystal is imperfect and composed of coherently diffracting, mutually misoriented domains. These domains impart a mosaic structure (Henry et al., 1960) to it and are often called crystallites (Wood, 1939), mosaic blocks (Azaroff, 1963), or subgrains (Smallman, 1970). In the context of cold work-hardening of metals, Wm. Bragg (Richards, 1970) understood the crystallite dimension to be the size of the strain field around a single dislocation. Wood (1939) and Wood et al. (1949) understood it to be a discrete subgrain. Azaroff (1963) noted that its size "...indicates the extent of the coherent regions in a crystal but does not directly disclose the nature of the imperfections that disrupt the crystal's coherency."

Smallman (1970, p. 253) gave perhaps the clearest description of a crystallite: "The 'mosaic' may be regarded as an assembly of crystallites, or sub-grains, bounded by dislocation walls in such a way that each crystallite is slightly misoriented from its neighboring crystallite. Since only one dislocation is required to misorient one crystallite from another, the structure is a network ... and the dislocation density is given by VP where $/$ is the linear dimension of a crystallite". The crystallite (i.e. domain) dimensions in quartz grains range from a few tens to several thousand Angstroms. The mosaic structure is three-dimensional and not unlike the structure of foam in the head on a beer. For mosaic quartz grains with an average crystallite size of 1000 Å, the average dislocation density is 10^{10} .

The term "crystallite" is used in other senses, for example embryonic crystals (Johansen, 1939, p. 12) and micron-sized grains in a polycrystalline aggregate. The sense in which we use the term in this report is as a mosaic block and should not be confused with the usage for micrometric grains observed in optical and scanning-electron microscopy.

The mosaic structure of crystalline materials contributes to the several components of x-ray diffraction line broadening. The broadening component due only to the crystal is

called pure diffraction broadening and increases both with decreasing crystallite size and with increasing internal strain. The profile of the x-ray diffraction line also contains broadening components due to mechanical aspects of the diffractometer (Klug and Alexander, 1974).

The various components of total broadening are separated analytically by x-ray line profile deconvolution. Several methods of deconvolution are available including the graphical method of Jones (1938), the Lagrangian method of Weideman et al. (1987), the Fourier transform methods of Warren and Averbach (1950) and Mitra and Misra (1967), and the variance methods of Wilson (1962) and McGehee and Renault (1972).

When internal strain is small enough to be neglected, the relationship between apparent crystallite size and pure diffraction broadening is described by the Scherrer equation

$$D_{hkl} = \frac{K\lambda}{\beta \cos \theta}$$

where λ is the wavelength of x-radiation, θ is the Bragg angle, β is the pure diffraction line broadening, and K is the shape constant which accounts for crystallites being non-spherical. D_{hkl} is the mean diameter of crystallites in the $[hkl]$ direction, i.e. normal to the diffracting planes. We use $K = 1.0$, emphasizing that D_{hkl} is only an apparent diameter.

Insofar as crystallites are like discrete subgrains, their growth is analogous to grain growth during annealing. Both are driven by strongly temperature-dependent processes which seek to minimize surface free energy. Grain growth, however, is more complex than crystallite growth, because the intergranular surfaces are more complex. The intergranular surface is often populated by a variety of soluble and insoluble phases, and adjacent grains are usually highly misoriented with respect to each other. The movement of intergranular boundaries can be retarded or "pinned" against insoluble solid phases, or movement can be accelerated by solvent or catalytic phases. Under many geological circumstances, the intergranular surface is relatively permeable. Crystallite growth, on the other hand, progresses mainly due to the healing of dislocations and the alignment of adjacent lattice planes. The precipitation of insoluble phases within dislocations occurring in mixed crystals mediates their evolution, and these are sometimes seen as decorated dislocations. However, the diffusion of hydrothermal fluids through the quartz crystal is expected to be very slow in comparison with the diffusion of intergranular fluids. Kronenberg et al. (1986) were unable to diffuse molecular water into natural quartz crystals. Although they found that hydrogen was taken up and formed hydroxyl groups, the solubility of hydrogen in quartz was found to be independent of both temperature and pressure. These authors account for the differences in their results and the pioneering work of Griggs and Blacic (1964, 1964) by suggesting that micro-cracking and crack-assisted diffusion of water influenced the reported weakening of quartz.

The form of the temperature dependence of both grain growth and crystallite growth follows the Arrhenius equation

$$\text{rate} = C \cdot \exp(-E/RT)$$

where C is a constant containing the lattice vibration frequency, E is the activation energy, T is absolute temperature, and R is the thermodynamic gas constant.

The basic-rate equation applied to crystallite growth by Shewman (1964) is

$$\frac{dD}{dt} = \frac{A}{D^n} \exp(-E/RT) \quad (1)$$

where D is the crystallite diameter, t is time, A is a probability function related to the tendency of an atom to escape from its lattice site, and E is the activation energy of recrystallization. The exponent, n , can vary depending upon the manner in which recrystallization occurs. For volume diffusion and vapor transport at constant pressure $n = 3$. For surface diffusion $n = 4$. Note that the rate of crystallite growth is strongly dependent not only on temperature but also on the size of crystallites. This means that at constant temperature growth rate diminishes rapidly as crystallite diameter increases. Idzikowski (1977) showed experimentally and theoretically that growth rate must approach zero after only a few hours at constant temperature.

If, following Shewman, equation (1) is integrated as a definite integral, then, because time (t) is effectively a constant, $D^{n+1} - D_0^{n+1} = kt \exp(-E/RT)$. We stipulate that the silica whose crystallite size we measure grew from a silica gel, so the initial diameter, D_0 , is effectively zero. Sweeping the constants together,

$$D^{n+1} = K \exp(E/RT) \quad (2)$$

Other workers, especially Nichols (1966) and MacKenzie and Melling (1974), have applied the Arrhenius equation to crystallite growth and recrystallization with success; however, there has not been enough experimental work done on the recrystallization of silica to know whether D in fact increases as a function of volume diffusion, vapor transport, or surface diffusion. It is almost certainly a combination of these mechanisms, and the exponent in equation (2) has a value between 4 and 5. It is probably closer to 5, because the recrystallization proceeds by annihilation of the dislocation walls defining crystallite boundaries which would function like exceedingly close intergranular surfaces. MacKenzie and Melling (1974) found that the exponent was 5 for growth of anatase crystallites at temperatures from 500 to 900°C.

The application of silica recrystallization to paleotemperature determination requires that the starting materials have very small crystallite size, the chemical composition is uniform, and that heating times are long enough for equilibrium to obtain. The initial crystallite size has to be small to make the difference of the limits of integration in equation (1) as close to the crystallite size as possible. The chemical composition needs to be uniform so that crystal chemistry does not have more influence on crystallite size than temperature. Heating times have to be long so that equilibrium is attained. These conditions are easily met by sedimentary chert and other forms of microcrystalline silica such as agate, chalcedony, and jasperoid which crystallize from silica gels that ultimately become quartz.

The crystallite size measured is a volume-weighted average of the grains mounted on the x-ray diffractometer. Herein lies the main difficulty with the method. Parts of the sample that contain only one generation of silica must be selected for XRD analysis. A chert sample, for instance, may contain detrital quartz and vein quartz which could

bias the analysis toward larger crystallite sizes, or late opal which could bias it toward smaller sizes.

Fortunately, the small size and random orientation of microcrystalline quartz grains obviates prolonged grinding. As a consequence, detrital, drusy, and vein quartz contaminating the sample mount will be coarse-grained. The contaminant, being in low concentration but large grain size, will tend to cause the intensity of the various quartz reflections to depart from their expected values. We use this effect to detect the presence of contamination by measuring the crystallite size at both the 212 and 104 reflections.

Figs. 20 and 21 are scatter diagrams of the [212]/[104] crystallite-size ratios for Kelly cherts and jasperoids with least squares best-fit lines. The ratio of the d-spacings of the 212 and 104 planes is 1.07. The figures show that the

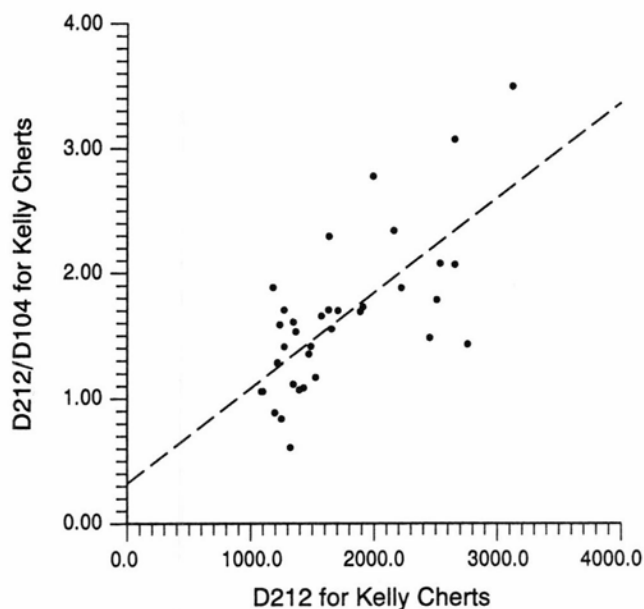


FIGURE 20—Variation of [212]/[104] silica crystallite size in Kelly Limestone cherts.

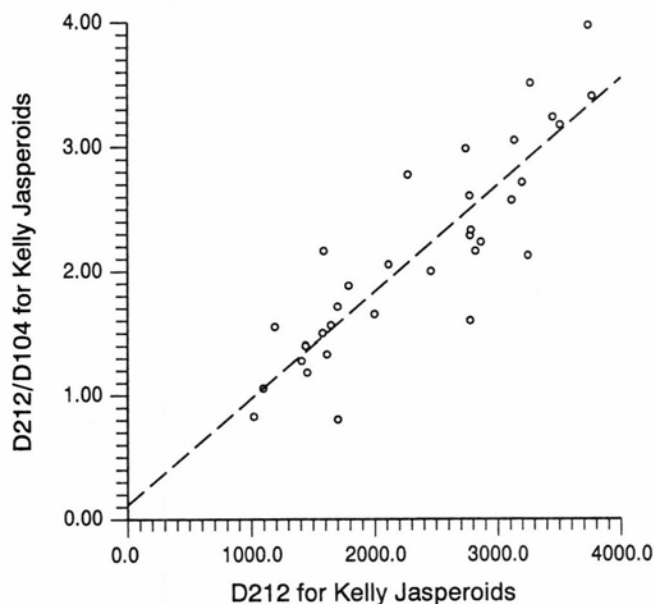


FIGURE 21—Variation of [212]/[104] silica crystallite size in Kelly Limestone jasperoids.

ratio of [212]/[104] crystallite sizes departs conspicuously from the ratio of the d-spacings. The departure increases with [212] crystallite size. The dislocation densities are clearly lower in the [212] than in the [104] direction, which makes the [212] crystallite size a more sensitive geothermometer than the [104] size.

Tables 7 and 8 show the [212] and [104] crystallite sizes we measured for Kelly jasperoids and cherts. The few rogue values are easily recognized by their [212]/[104] ratios greater than 5.0. When they are rejected, the mean [212]/[104] for the Kelly jasperoids is 2.0 with an estimated standard deviation of 1.0. For the Kelly cherts the statistics are 1.6 and 0.6, respectively.

Calibration

Early work on the calibration of silica-crystallite size vs. temperature is given in Renault (1980), and the method we use at present is substantially the same. Sample preparation and x-ray diffractometer resolution are particularly important.

As mentioned above, samples mounted on the diffractometer must exclude silica of different generations, because x-ray crystallite sizes determined by x-ray diffraction are averages. For this reason, it is important to be able to evaluate the mineral paragenesis and select areas which

TABLE 7—Temperature and size data for Kelly jasperoids. Numerals following a sample number, e.g. 1 in 89f30a1, are sub-samples. Rejected data are offset.

Sample #	T°C	[212] Å	[104] Å	[212] [104]
89f30a1	404.5	3452	1063	3.246
89f30a2	372.6	2786	1193	2.336
89f30a3	865.3	19945.6	2052.7	9.7
89f30a4	300.7	1576	1051	1.500
89f30a5	335.6	2113	1026	2.059
89f30a6	305.7	1646	1051	1.567
89f30c2	291.7	1453	1226	1.185
89f30d1	309.3	1700	2102	0.809
89f30d2	355.4	2459	1226	2.006
89f30e1	808.0	17399.3	1379.2	12.6
89f30e2	315.4	1791	949	1.887
89j09a1	395.3	3251	1522	2.136
89j09a2	255.6	1018	1226	0.831
89j09a3	372.1	2776	1209	2.296
89j09c1	374.3	2820	1298	2.172
89j09c2	372.1	2776	1731	1.604
89j09c3	503.8	6006.2	1176.9	5.1
89j09d1	370.6	2747	919	2.988
89j09d2	389.9	3136	1026	3.055
89j09d3	418.6	3770	1103	3.417
89j09e1	376.6	2866	1279	2.240
89j09e2	262.9	1098	1038	1.058
89j09e3	372.1	2776	1063	2.610
89j09f1	393.0	3202	1177	2.721
89j09f2	417.5	3743	939	3.986
89j09f3	288.5	1410	1103	1.278
89j09g1	290.7	1439	1026	1.402
89j09g2	328.6	1998	1209	1.653
89j09g3	389.0	3118	1209	2.578
89j09h1	396.2	3271	929	3.520
89j09i1	344.9	2272	818	2.777
89j09i2	407.1	3509	1103	3.180
89j18a1	301.5	1587	730	2.175
89j18a3	271.0	1192	768	1.553
89j18b2	303.2	1611	1209	1.332
89j18b3	309.4	1701	992	1.715
MEAN	316.4	2168.3	1042.1	2.0
S.D.	105.8	1022.6	399.5	1.0

TABLE 8—Temperature and size data for Kelly cherts.

Sample #	T°C	[212] Å	[104] Å	$\frac{[212]}{[104]}$
89f30b1	309.9	1708	1003	1.702
89f30b2	300.7	1576	949	1.661
89f30f1	293.4	1476	1090	1.354
89f30f2	270.2	1183	626	1.889
89f30g1	277.9	1275	748	1.704
89f30g2	273.4	1221	949	1.286
89f30h1	366.0	2658	1279	2.078
89f30h2	342.1	2223	1177	1.889
89f30h3	366.0	2658	865	3.072
89f30i1	282.0	1325	2153	0.616
89f30i2	271.4	1196	1337	0.894
89f30i3	263.4	1104	1038	1.063
89f30i4	290.0	1429	1317	1.085
89j18c1	275.1	1240	781	1.588
89j18c2	305.1	1638	712	2.301
89j18c3	285.3	1368	892	1.535
89j18d1	358.3	2513	1400	1.795
89j18d2	323.0	1909	1103	1.730
89j18d3	304.6	1631	956	1.706
89j18e2	338.4	2161	921	2.346
89j18e3	306.7	1661	1066	1.558
89j18f1	389.4	3127	892	3.507
89j18f2	321.7	1888	1114	1.695
89j18f3	328.4	1995	718	2.779
89j18g1	294.4	1489	1051	1.417
89j18g2	287.7	1399	1299	1.077
89j18g3	283.8	1349	1205	1.120
89j18h1	276.3	1255	1485	0.845
89j18h2	796.0	16874	1587	10.6
89j18h3	371.4	2763	1920	1.439

contain only one generation of the silica that crystallized from a gel. As only the highest temperature of microcrystalline quartz is recorded, early low-temperature episodes of crystallite growth are not detectable. However, lower paleotemperatures in a later thermal regime are recorded, because the earlier high thermal regime has decayed.

The x-ray diffractometer must be properly aligned to give maximum resolution. In addition, we use 0.5° slits as opposed to the normally used 1° slits. We do this to improve resolution even though intensities are halved, because the broadening of the microcrystalline silica is compared with a standard quartz that is expected to be broadened only by equipment effects. The standard must not have significant pure diffraction broadening, otherwise excessive breadth will be deducted from the sample's diffraction profile and yield an erroneously large crystallite sizes.

For the present study, samples were prepared by slabbing to thickness of approximately 6 mm. Three or more sites in each sample were selected to be free of veinlet or drusy quartz by examination under binocular microscope. Cores 3 mm in diameter were extracted from each site by means of an ultrasonic disc cutter manufactured by GATAN, Inc. The cores were crushed and hand-picked to further reduce the possibility of contamination by vein quartz and other impurities.

The purified samples were prepared for x-ray diffraction by light grinding under acetone, followed by decantation to remove the <1 gm fraction and mounting on a thin strip of double-stick tape attached to a microscope slide.

The x-ray diffraction patterns were obtained from a Rigaku horizontal diffractometer with a Cu target long fine

focus x-ray tube operating at 40 kV and 25 mA. 0.5° divergence slits and 0.15 mm scatter slits were used together with a graphite exit-beam monochromator. Data were collected at 0.01° 2θ steps and 40 sec/step over the 100, 212, and 104 reflections.

As discussed above, there are some systematic differences between the [100], [212], and [104] crystallite sizes, so only the [212] crystallite-size temperatures are given in this report. The pure diffraction broadening of the 212 reflection was obtained by Ka, and Ka, resolution method (Renault and Iovenitti, 1978) with a very well crystallized quartz standard from Mondredon Labessonier, France. Crystallite sizes obtained by this method compare favorably with crystallite sizes obtained using the fourier and variance deconvolution methods (see Renault and Iovenitti, 1978).

The calibration data are given in Table 9 and plotted as an Arrhenius diagram in Fig. 22 which shows their ranges. Three sets of calibration-data temperatures have been retained from Renault and Iovenitti (1979) and are shown in italics in Table 9. The temperature data of Hein (1978) and our data from opal C—T heating are plotted in Fig. 22, but do not contribute to the calibration curve fit. New temperature data and crystallite-size data are shown in normal type. With one exception, the calibration data are on sedimentary chert; the data from which the Iovenitti temperatures are taken is on jasperoid. Table 9 shows the ranges of temperature and size data available for each occurrence.

The temperature data of Budding and Broadhead (1977) and Ewing and Thompson (1977) are from the KCM #1 Forest Federal Well in southwestern New Mexico. This petroleum test extended down through a Permian—Pennsylvanian limestone—shale sequence and terminated in an igneous—metamorphic complex. Samples of chert were separated from the well cuttings by hand-picking under a binocular microscope. X-ray diffractograms were obtained from the purified chert using the methods described above. Chert was not available from the interval measured by Budding and Broadhead (2010 ft), so we used silica from the nearest chert-bearing intervals above and below (1970

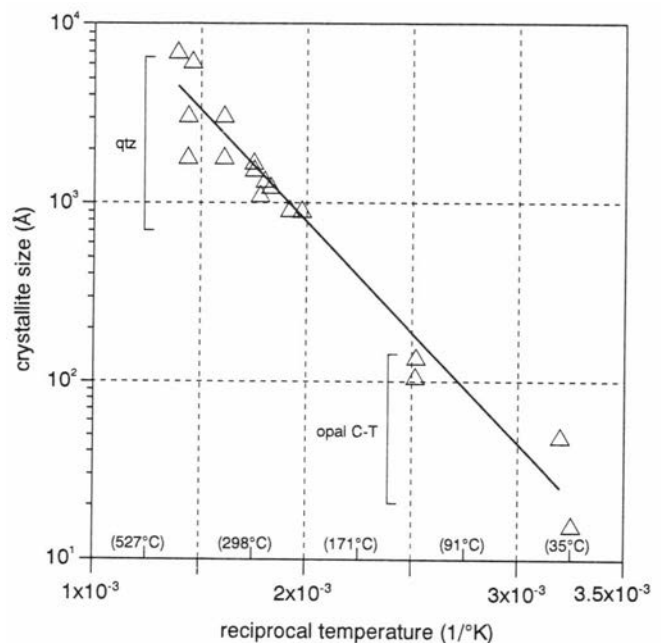


FIGURE 22—Calibration curve of silica crystallite size to temperature.

TABLE 9—Calibration data.

Temperature method and source	T°C	Crystallite size (Å)
Metamorphic equilibrium	410	6383
Budding and Broadhead (1977)	450	7013
Novaculite textures	350	3106
Keller et al. (1985)	425	3106
Metamorphic equilibrium	350	1844
Hoersch (1981)	425	1844
CAI	300	1708
This study	300	1556
Fluid inclusions	275	1250
Giraud et al. (1982)		
H' carbon maturation	250	932
Ewing and Thompson (1977)	290	1129
Fluid inclusions	235	926
Iovenitti (1977)	285	1360
Opal CT heating	125	106
This study	125	140
Opal CT oxygen isotope	35	16
Hein et al. (1978)	40	50

and 2040 ft). Well cuttings suffer from up-hole contamination, and we found low-temperature chalcedony in the 2040 ft sample. This material had an anomalously small crystallite size and was discarded. Budding and Broadhead (1977) determined the temperature from microscopic examination of the calcite—tremolite association in the cuttings.

The Keller et al. (1985) temperatures and their ranges are based on evaluation of novaculite textures. These in turn are referenced to the metamorphic assemblages from Skye, Scotland, observed by Hoersch (1981). We determined the silica crystallite sizes on material kindly provided by Keller.

The CAI temperature was determined by one of us (Repetski) on material we collected from Mississippian limestones of the Kelly mining district.

The Iovenitti (1977) temperatures are from fluid inclusions in barite from the Kelly mining district. The barite is contemporaneous with jasperoids from which the crystallite-size measurements were taken. The temperatures may underestimate the maximum jasperoid temperature, because vacuoles in fluid inclusions often form in a falling-temperature regime.

The opal C—T temperatures are from siliceous Quaternary hot-spring sinter collected by us at San Diego Mountain, New Mexico (Seager et al., 1971). This deposit has never been buried and is unlikely to have exceeded 50°C. We heated this material for eight days at 125°C in a muffle furnace and observed slight narrowing of the 100 cristobalite peak. This data set does not contribute to the calibration curve, but is presented to illustrate the compatibility of the measurements.

The Ewing and Thompson (1977) temperatures were based on hydrocarbon maturity. They estimated 270°C as the maximum paleotemperature of the upper part of the drill hole. We estimate the error in this measurement as ± 1.0 LOM (level of maturity) and 50% of the estimated

heating time (1 m.y.). The range in crystallite size is given as its error.

The opal C—T temperature of Hein et al. (1978) is based on oxygen-isotope and XRD data. We simply measured the breadth of the illustrated diffraction peaks, because the sample material is no longer available. This data set, like the hot-spring data, is not used to fit the calibration curve, but is presented to show the compatibility of opal C—T crystallite sizes with the quartz.

The calibration data given in Table 9 are plotted as an Arrhenius diagram in Fig. 22. The form of the calibration is found by taking the log of both sides of equation (2)

$$\ln D = \frac{K}{n+1} + \frac{-E}{(n+1)R} \cdot \frac{1}{T} \quad (3)$$

whereupon it is straightforward to calculate the activation energy of recrystallization from the slope of the calibration curve.

Although the curve fit is based only on the measurement of quartz-crystallite sizes, opal C—T sample sets lie on the calibration curve. This suggests that the responses of opal C—T crystallites and quartz crystallites to temperature follow the same law. For this reason, the variation in chert- and jasperoid-crystallite size versus temperature is conveniently called the silica-crystallite geothermometer as opposed to simply the quartz-crystallite geothermometer. The calibration equation of the new data is practically identical to the equation determined by Renault (1979), which included the Hein et al. (1978) data set.

From equation (3), the activation energy of crystallite growth can be determined from the slope of $D_{[2121]}$ vs. $1/T$ on the Arrhenius calibration curve. Solving for E in

$$\frac{-E}{(n+1)R} = -2.70 \cdot 10^3$$

gives 21.4 Kcal/°K/mole for volume diffusion and 26.8 Kcal/°K/mole for surface diffusion. These two values bracket the activation energy of 23.2 Kcal/°K/mole determined by Ernst and Calvert (1969) for the conversion of opal C—T to quartz.

APPENDIX 2

Conodont descriptions

Nine samples from the Magdalena Mountains were examined for conodonts to date the sampled parts of the Kelly Limestone and to see what geothermal data the conodonts could contribute related to the ore-depositing fluids that passed through these host rocks.

Seven of the samples produced conodonts, six definitely Mississippian and one constrained only to Late Devonian through Mississippian. The color alteration of the conodonts is consistent with a background host-rock heating of at least about 190°C, but with an overprint of much hotter fluids passing through and both raising the color alteration index of the conodont elements and having a corrosive effect on their surfaces (Figs. 23-25). Details of the individual samples follow.

Sample 88N-1+4 [USGS fossil locality 30883-PC]. Kelly Limestone from beside jeep trail that heads eastward into Jordan Canyon, SW1/4NW1/4 sec. 5 T3S R3W, at approx. 300 m SE of hilltop '9174', lat. 34°04'43"N, long. 107°10'56"W. Magdalena 71/2 min. quad., Socorro County,

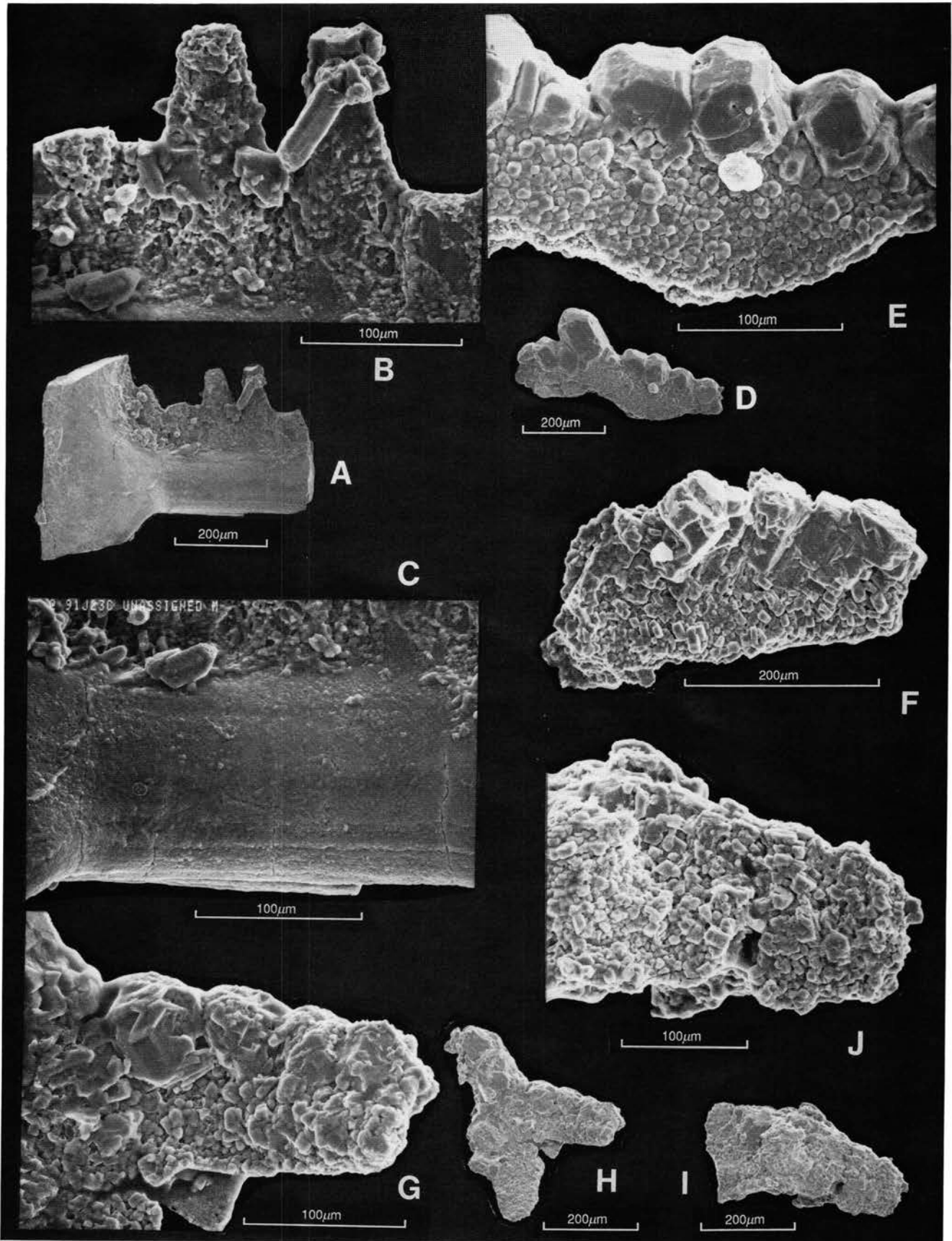


FIGURE 23—SEM photomicrographs of conodont elements from top bed of Kelly Limestone near jasperoid replacement and a weakly altered and mineralized area. Sample 91J23C from head of Mistetoe Gulch on west side of Magdalena Mountains, USGS fossil locality 31272-PC. A–C, Unassigned makelliform (M) elements, inner lateral view, USNM 481993. CAI = 4½; element surface fairly smooth, with some mineral overgrowth concentrated in an area of denticles (A, largest overgrowth crystals are quartz), and with slight etching/corrosion concentrated where conodont growth lamellae terminate in basal region (C). D, E, Unassigned Pb element, lateral view, USNM 481994. CAI = 6½ to 7; basal (lower) edge strongly corroded; entire element overgrown by apatite crystals, with largest crystals aligned along upper edges syntaxially over denticles. F, Indeterminate bar fragment, USNM 481995. CAI = 6½ to 7. G, H, *Hindeodus* sp. indet., inner lateral view of M element, USNM 481996. CAI = 6½ to 7. I, J, *Gnathodus* cf. *G. texanus* Roundy; lateral view of Pa element, USNM 481997. CAI = 6½ to 7.

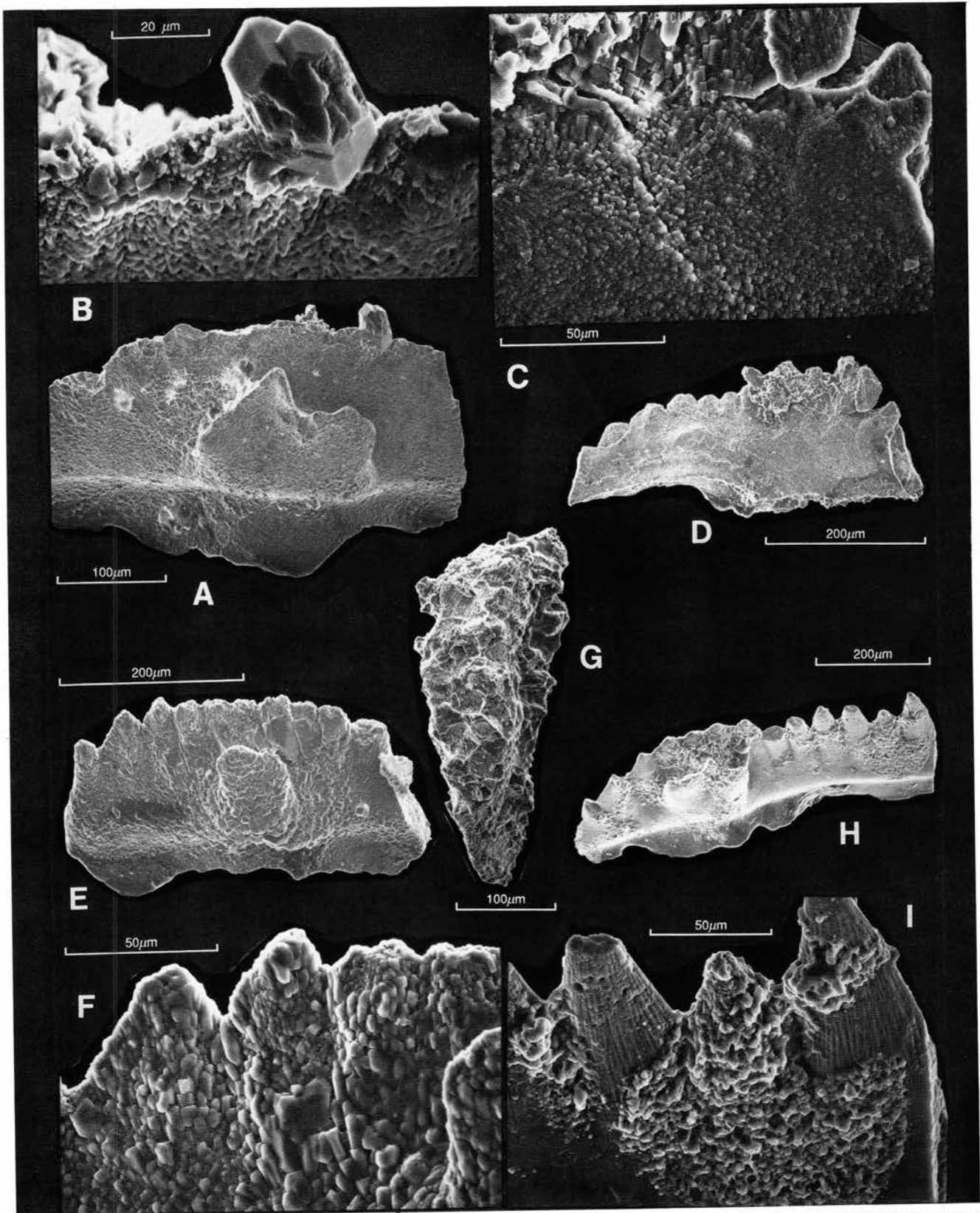


FIGURE 24—SEM photomicrographs of conodonts from Kelly Limestone at Waldo mine (A, B, E–I) and east side of crest of Magdalena Mountains, east of Kelly (C, D). A, B, *Gnathodus texanus* Roundy, upper oblique lateral view, sample 89N–W3T, Waldo mine; USGS fossil locality 30886–PC, USNM 481998. CAI = $6\frac{1}{2}$ to 7. Specimen strongly corroded. C, D, *Gnathodus typicus* Cooper Morphotype 2→*Gnathodus texanus* Roundy transitional form, lateral view of Pa element, sample 88N–1+95; USGS locality 30884–PC, USNM 481999. CAI = 6. Element etched and corroded along margins and denticles; lateral surfaces (C) show incipient apatite overgrowths, with overgrowth orientation controlled by conodont-element crystallite orientation. E, F, *Gnathodus texanus* Roundy, upper oblique lateral view of Pa element, sample 89N–W3T, Waldo mine; USGS locality 30886–PC, USNM 482000. CAI = $6\frac{1}{2}$ to 7. Element strongly corroded and overgrown syntaxially by apatite. G, *Cavusgnathus* sp., upper view of Pa element fragment, sample 89N–W1+1, Waldo mine; USGS locality 30885–PC, USNM 482001. CAI = $6\frac{1}{2}$. Element strongly etched and corroded. H, I, *Gnathodus texanus* Roundy, upper oblique lateral view of Pa element, sample 89N–W1+1, Waldo mine; USGS locality 30885–PC, USNM 482002. CAI = 4. Lower margins and denticles show some breakage, but corrosion is limited to minor effects on upper parts of denticles (I), where outer edges of apatite crystallite bundles have been exposed. Minor overgrowth is by non-syntaxial apatite and quartz.

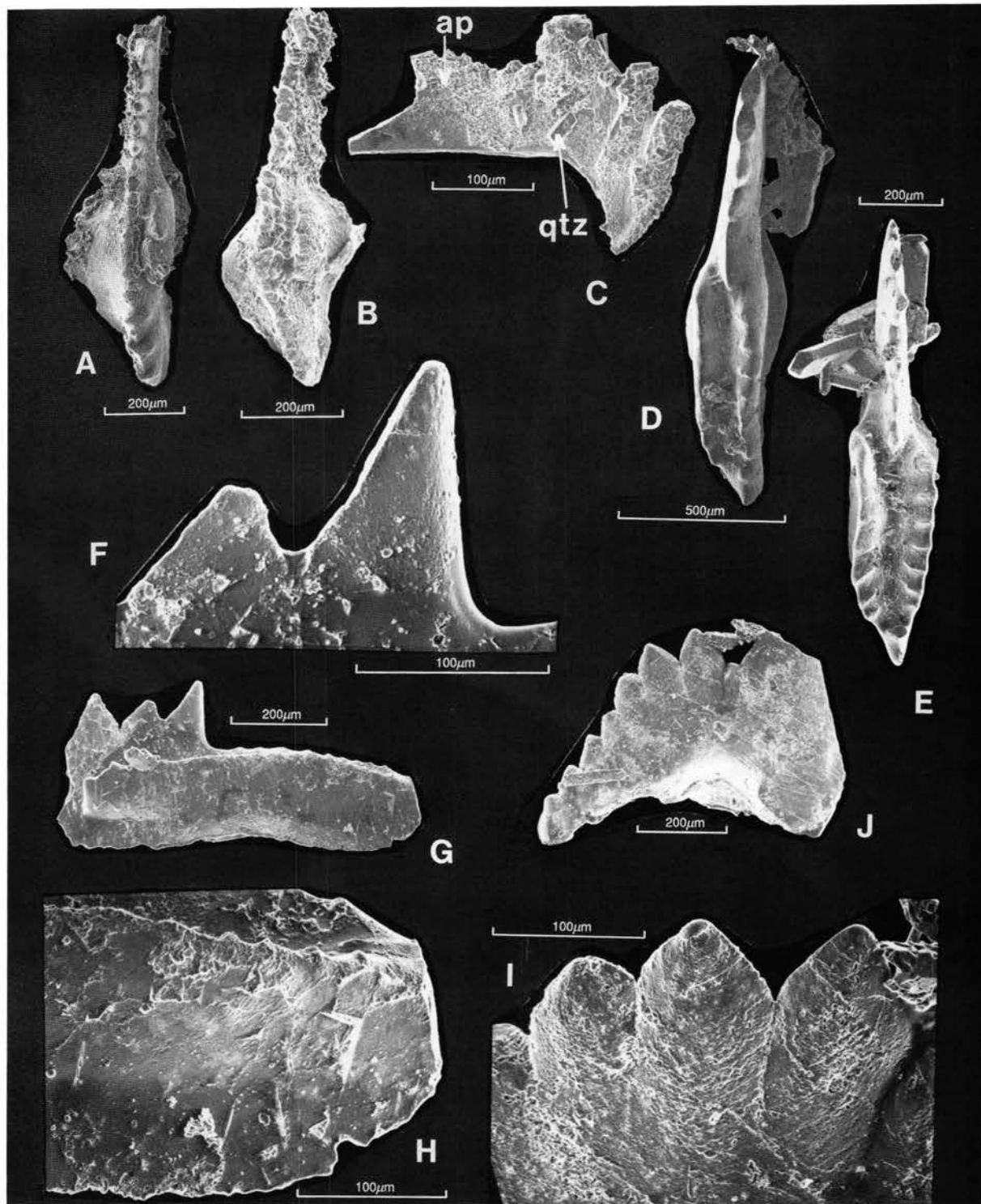


FIGURE 25—SEM photomicrographs of conodonts from Kelly Limestone near crest of Magdalena Mountains. **A**, *Gnathodus typicus* Cooper Morphotype 2→*Gnathodus texanus* Roundy transitional form, upper view of a Pa element, sample 88N-1+95; USGS locality 30884-PC, USNM 482003. CAI = 4. Specimen shows some minor adventitious overgrowth, but no significant corrosion or syntaxial overgrowths. **B**, *Gnathodus typicus* Cooper Morphotype 2→*Gnathodus texanus* Roundy transitional form, upper view of a Pa element, sample 88N-1+95; USGS locality 30884-PC, USNM 482004. CAI = 6. Specimen from same sample as A, but in addition to elevated CAI value shows also some corrosion and overgrowth by syntaxial apatite and adventitious quartz. **C**, Unassigned Sb element, inner lateral view, sample 88N-1=95; USGS locality 30884-PC, USNM 482005. CAI = 6. Another element from the same sample as A and B; specimen somewhat corroded, shows both syntaxial and epitaxial overgrowth of apatite (Ap) and quartz (Qtz). **D**, *Cloghergnathus globenskii* Austin and Mitchell, upper view of Pa element, sample 89N-R11; USGS locality 30887-PC, USNM 482006. CAI = 4. Surface chiefly smooth, with minor adventitious quartz overgrowths. **E**, *Taphrognathus varians* Branson and Mehl, upper view of Pa element, sample 89N-R11; USGS locality 30887-PC, USNM 482007. CAI = 4. Prominent overgrowths are quartz. **F-H**, *Cavusgnathus unicornis* Youngquist and Miller, inner lateral view (G) of Pa element, and enlargements of portions of denticle row (F) and posterior end of element (H), sample 89N-R11; USGS locality 30887-PC, USNM 482008. CAI = 4. Surfaces chiefly smooth, with only minor etching and pitting mainly on blade denticles (F). H shows some minor surface overgrowths, probably clay minerals or authigenetic feldspar, between now-vanished rhombohedral crystals, probably diagenetic dolomite that grew adjacent to element. **I, J**, *Hindeodus scitulus* (Hinde); lateral view (J) of a Pa element and upper oblique view of enlargement of a part of denticle row (I); sample 89R-R11; USGS locality 30887-PC, USNM 482009. CAI = 4. Surface generally smooth, except for some etching found chiefly on denticles.

New Mexico. Collector: A. K. Armstrong. Sample was 44.4 kg and was processed for conodonts; 200 g of coarse (>20 mesh) insoluble residue remained (discarded). The microfauna included only one *Kladognathus* sp. ramiform (Sc) element and one conical fish-tooth fragment. Based on the presence of *Kladognathus*, the age is Late Devonian (Famennian) through Mississippian. The CAI = 5, indicating that this conodont element experienced heating of at least 300°C (caution is called for because this is a minimum based on a single specimen). The conodont as well as the fish tooth show some surface corrosion.

Sample no. 88N-1+15 ft [no USGS fossil locality assigned]. Kelly Limestone, same locality as previous sample. A 4.5 kg sample processed; 150 g of coarse residue remained (discarded), no microfossils recovered.

Sample no. 88N-1+95 ft [USGS fossil locality no. 30884-PC]. Kelly Limestone, same locality as above. A 4.0 kg sample processed; 500 g of coarse residue remained (discarded). Microfauna included only *Gnathodus typicus* Cooper Morphotype 2 *G. texanus* Roundy transitional form, 21 Pa elements; two indeterminate cavusgnathid Pa elements (broken); one unassigned M element; and one unassigned Sb element. Based on the species of *Gnathodus* that we think is transitional between *G. typicus* Morphotype 2 and *G. texanus* the age is Mississippian, late Osagean or Meramecian. The taxa present also indicate shallow biofacies. CAI = 4 and 6. CAI of 4 indicates more than 200°C and CAI of 6 indicates more than 350°C. All elements have moderately corroded surfaces.

Sample 89N—W1+1 [USGS fossil locality 30885-PC]. Kelly Limestone, Waldo mine approx. 850 m south of Baxter Peak at end of jeep trail, NW1/4NW1/4SE1/4 sec. 35 T2S R4W, lat. 34°05'31"N, long. 107°12'31"W, Magdalena 7/2 min. quad., Socorro County, New Mexico. Collector: A. K. Armstrong.

A 3.0 kg sample processed; 250 g of coarse residue remained (discarded). The following conodonts were found: *Gnathodus texanus* Roundy, one Pa element, and an indeterminate cavusgnathoid, one fragmentary Pa element. The age is Mississippian, late Osagean to early Chesterian. Biofacies is shallow and/or nearshore. CAI: one element has a CAI of 4 (at least 200°C); it also has a gray patina and a rather smooth surface. The other element has a CAI of 11/2 (at least about 440°C) and a corroded surface texture. The range of CAI's and differences in surface textures indicate probable hydrothermal effects.

Sample no. 89N—W2+5 [no USGS fossil locality number assigned]. Kelly Limestone from Waldo mine, locality and collection details same as for previous sample. A 3.1 kg sample processed; 500 g of coarse residue remained (discarded). No conodonts or other fossils recovered.

Sample no. 89N—W3T [USGS fossil locality no. 30886-PC]. Kelly Limestone from Waldo mine, locality and collection details same as for previous two samples. A 3.6 kg sample processed; 2.2 kg of coarse residue remained (discarded). The following conodonts were found: *Gnathodus texanus* Roundy, five Pa elements; and *Cavusgnathus* sp., one fragmentary Pa element. The age is Mississippian, late Osagean to early Chesterian. Biofacies is shallow marine. CAI = 6 1/2 and 7, indicating temperatures of at least 440 to 490°C. The element edges are lighter than the main bodies, which is consistent with passage of hydrothermal fluids through these rocks.

Sample 89N—R11 [USGS fossil locality no. 30887-PC]. Kelly Limestone approximately at spot marked as elevation

9149 ft, about 20 m E of jeep trail along crest of Magdalena Mountains, NE1/4NE1/4 sec. 7 T3S R3W, lat. 34°04'12"N, long. 107°11'05"W, Magdalena 71/2 min. quad., Socorro County, New Mexico. Collector: A. K. Armstrong. A 7.2 kg sample processed; 120 g of coarse fraction remained (discarded). Conodonts include the following: *Cavusgnathus altus* Harris and Hollingsworth, 22 Pa elements; 3 *C. unicornis* Youngquist and Miller, three Pa elements; *Cloghergnathus globenskii* Austin and Mitchell, 15 Pa elements; *Gnathodus texanus* Roundy, two Pa elements; *Hindeodus scitulus* (Hinde), four Pa elements; *Hindeodus* sp., four Pa elements; *Lochriea commutatus* (Branson and Mehl), one Pa element; *Taphrognathus varians* Branson and Mehl, one Pa element. Unassigned elements: 2 Pb, 21 M, 11 Sa, 3 Sb, 16 Sc + about 230 indeterminate fragments. The age is Mississippian, latest Osagean to middle Meramecian. Biofacies is shallow. CAI = 4 (at least 190°C). These specimens are moderately well preserved except for breakage and some being possibly abraded. Some have edges that are barely "grayed," but that could be from acid preparation. The surfaces are not corroded; a few elements have acicular quartz crystals grown off their surfaces.

Sample 89N-15 [USGS fossil locality no. 30888-PC]. Kelly Limestone from E side of jeep trail along crest of Magdalena Mountains at approx. 700 m N of North Baldy, NE1/4NW1/4NW1/4 sec. 17 T3S R3W, lat. 34°03'25"N, long. 107°10'46"W, Magdalena 71/2 min. quad.; Socorro County, New Mexico. Collector: A. K. Armstrong. A 5.9 kg sample processed; 260 g of coarse residue remained (discarded). Conodonts found include: *Cavusgnathus unicornis* Youngquist and Miller, two Pa elements; *Hindeodus scitulus* (Hinde), 10 Pa elements, two Pb elements; 27 Sa—Sc elements; *Hindeodus* sp., three Pa elements. Unassigned ramiform elements: 2 M, 3 Sb + 63 indeterminate fragments. The age is Mississippian, late early Meramecian to earliest Chesterian. Biofacies is shallow marine. CAI = 4 (minimum about 190°C); elements have a gray patina and their surfaces are somewhat corroded.

Sample 89N—R16 [USGS fossil locality no. 30889-PC]. Kelly Limestone at about 80 m E of jeep trail along crest of Magdalena Mountains, elev. approx. 9275 ft, SW1/41'1W1/4SW1/4 sec. 8 T3S R3W, lat. 34°03'40"N, long. 107°10'55"W, Magdalena 71/2 min. quad., Socorro County, New Mexico. Collector: A. K. Armstrong. A 4.8 kg sample processed; 650 g of coarse residue remained (discarded). Conodonts found include: *Cavusgnathus unicornis* Youngquist and Miller, one Pa element; *Gnathodus texanus* Roundy, six Pa elements; *Hindeodus scitulus* (Hinde), one Pa element; *Taphrognathus varians* Branson and Mehl, one Pa element; and 33 indeterminate fragments. The age is Mississippian, middle to late Meramecian. Biofacies is shallow marine. CAI = 4 (minimum 190°C). These elements show evidence of hydrothermal alteration. They have a gray patina and are "grayed-out" along edges, denticles, etc.; otherwise, they still have mostly shiny surfaces, with no corrosion apparent.

APPENDIX 3 Sample locations

Samples collected by Armstrong

Index map of sample locations is Fig. 26.

1, 2, and 89J09A—J. North Baldy Prospect. The prospect pits are located some 1000 ft (305 m) southeast of North

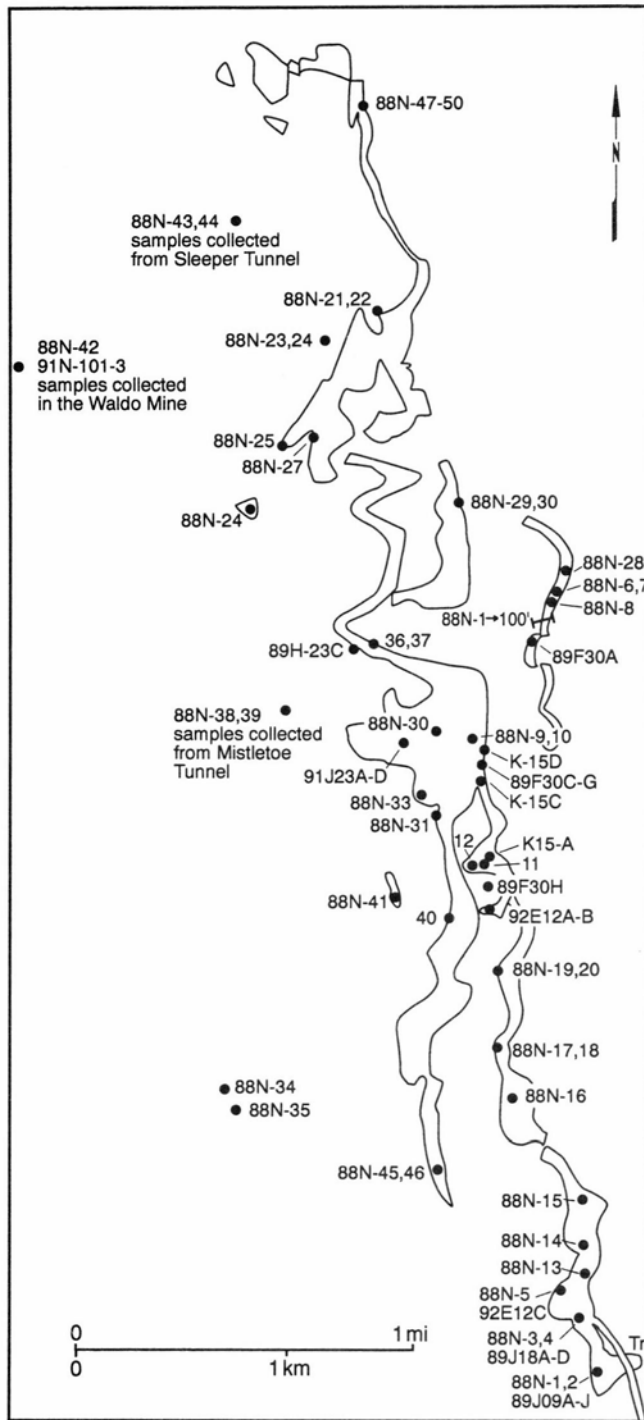


FIGURE 26—Map showing location of specimens collected for geochemical, SEM, and petrologic study. Map base is the 1:24000 USGS, Magdalena, New Mexico, provisional edition, 1985.

Baldy Peak. Samples were collected on a bulldozer outface. Sample 1 is from a highly altered, hematitic red shale between a rhyolite dike and Kelly encrinities. Sample 2 is from highly mineralized Kelly Limestone between two flow-banded rhyolite dikes. Associated minerals are galena, chalcocopyrite, pyrite, and barite.

3, 4, and 89J18A—Q. About 500 ft (152 m) due northeast of North Baldy Peak, on east side of range crest, adjacent to crest road. See text photograph, Fig. 9, for detailed locations. Sample 3 is from upper 10 ft (3 m) of silicified Kelly Limestone at top of section, adjacent to a rhyolite

dike. Sample 4 is from altered green siltstones of the Sandia Formation resting directly on silicified Kelly Limestone.

5. Shallow prospect pit about 800 ft (244 m) northeast of North Baldy Peak, on west side of range-crest road. Specimen is a hematite-stained jasperoid breccia with red clay from near the top of Kelly Limestone.

6. Small prospect pit at head of Jordan Canyon on east side of range just below crest. The prospect pit was dug into the lower part of the Caloso Member of the Kelly Limestone. No apparent sign of a fault. Abundant barite filling a 10 ft (3 m) wide solution cavity. Minor amounts of galena, chalcocopyrite, fluorite.

7. Prospect tunnel about 100 ft (31 m) south of the "silver pipe" dolomitic marker beds in the encrinities of Kelly Limestone.

9, 10. East side at the range crest, adjacent to the road on the north—south ridge of the range. Sample 9 is from near the top of the silicified Kelly Limestone. Sample had copper stains, barite and fluorite crystals in vugs. Sample 10 is from soft, brown, hematitic clay—shale some 30 ft (9 m) below the Kelly Limestone (jasperoid) contact with the Sandia Formation.

11, 12. Top of ridge on east side to crest, east end of west access road beginning at old church in town of Kelly. Prospect trench is on crest of range at the south head of Jordan Canyon. Samples are from an east—west-oriented deep prospect trench. Sample 11 from altered hematitic red clay filling a solution cavity within Kelly Limestone.

12. Hematitic shale to siltstone filling a solution cavity in the Kelly Limestone. Samples collected in maroon to yellow brown shales at the top of Kelly Limestone.

13. Some 1350 ft (412 m) due north of North Baldy Peak on a east side of the ridge road. Jasperoid sample is from near the top of silicified Kelly Limestone and contains galena crystals.

14. Sample collected 500 ft (152 m) north of sample 13, from a shallow prospect pit on east side of road. The specimen is limonite and jasperoid from near the top of Kelly Limestone.

15, 16. Jasperoid samples collected 2500 ft (762 m) north of North Baldy Peak on east side of ridge, just before steep grade of ridge road. Jasper replacement bed is some 25-30 ft (7.6-9.1 m) thick and contains large barite crystals and hematite pseudomorphs after pyrite. Sample 15 collected in the lower half of the jasperoids, and sample 16 is from the top of section.

17, 18. Specimens were collected on the east face just below crest of the range. Sample 17 taken in a 50 ft (15 m) tunnel at the contact of Kelly Limestone carbonates and the replacement jasperoids. The mineralization is along a small, 2-3 ft (0.6-1 m) wide vertical shear zone. Associated minerals are smithsonite, malachite, azurite, and fluorite. Sample 17 is from the shear zone. Specimen 18 is from the top of the jasperoids below contact with the Sandia Formation.

19, 20. Jasperoid samples were collected near the crest of the range, on the east side. Sample 19 is from base of mineralized jasperoids with galena, malachite, and barite. Sample 20 from the top of the section.

21, 22. Stonewall tunnels, specimens collected from mine tunnel. Sample 21 is from a 2-4 ft (0.6-1.2 m) thick jasper zone at top of Kelly Limestone. Specimen has hematite pseudomorphs after pyrite and malachite stains. Sample 22

is dark-brown to black hematitic rock with malachite and azurite copper staining. See Loughlin and Koschmann (1942, pl. 2) for map location of Stonewall mine.

23, 24. Tip Top tunnel, specimens were collected from the mine dump. Specimen 23 is altered, crinoidal limestone, dark brown and hematitic. Specimen 24 is jasper replacement of Kelly Limestone, and has malachite and azurite stains and pyrite. See Loughlin and Koschmann (1942, pl. 2) for map location of Tip Top mine.

25. Grand Tower shaft. Specimen was collected from mine dump, but is from the upper third of Kelly Limestone. It is mineralized limestone with galena, chalcopyrite, and pyrite. See Loughlin and Koschmann (1942, pl. 2) for map location of Grand Tower shaft.

26. East of Kelly mine on south side of Kelly Gulch, within a small fault zone. Kelly Limestone is brecciated, silicified, and faulted against Proterozoic greenstones. Sample is a jasperoid and contains abundant barite crystals.

27. North side of Kelly Gulch, about 1000 ft (305 m) north of Germany mine, on north side of canyon. The jasperoid specimen was collected from a prospect pit dug in upper part of Kelly Limestone. See Loughlin and Koschmann (1942, pl. 2) for map location of Germany mine.

28. Jasperoid specimen, top of Kelly Limestone, just below contact with Sandia Formation. Specimen is mineralized with abundant barite and copper stains. The location is on the crest of the range, facing east, at the end of a bulldozed roadcut made for a drill rig at 9100 ft elevation.

29, 30. Jasperoid specimens from a massive bed 25-30 ft (7.6-9.1 m) thick at top of Kelly Limestone. They were collected on the east face of ridge at the crest of range, about 1 mi (1.6 km) east of Kelly mine. Specimen 29 is from the lower 5 ft (1.5 m) of the jasperoid. Specimen 30 is from the upper 2 ft (0.6 m) of the unit and contains 1-2 inch (2.5-5.1 cm) cubes of hematite pseudomorphs after pyrite embedded in the jasper, and large crystals of barite.

31, 32, 33. Jasperoid specimens collected on a short bulldozed drill-pad road on the west side of the range at an elevation of 9040 ft. Sample 31 taken at contact with Sandia Formation. Specimen 32 collected 10 ft (3 m) below Sandia contact. Large 1-2 inch (2.5-5 cm) hematite pseudomorphs after pyrite and abundant galena crystals embedded in the jasper. Sample 33 is hematitic, clay-rich jasper from the base of the jasperoids, above the contact with encrinites.

34. Jasperoid selected from the Linchburg mine dump. Specimen appears to be from the Kelly Limestone. See Loughlin and Koschmann (1942, pl. 2) for map location of Linchburg mine.

35. Silicified rock taken from the "old Linchburg mine shaft" dump. Specimen appears to be mineralized jasperoid from the Kelly Limestone. The collecting site is about 300 ft (91 m) south and east of the previous location.

36, 37. Specimen 36 was collected at the base of a massive 20 ft thick jasperoid bed. It was hematite-stained, mineralized, and associated with a fault breccia. Specimen 37 was collected away from the mineralized fault zone and near the top of the jasperoid. The jasperoid is overlain by a quartz-pebble conglomerate of the Sandia Formation. The specimen is from the south side of Mistletoe Gulch at an elevation of 8020 ft.

38, 39. Jasperoid samples collected from the lower 5 ft (1.5 m) of massive, 40 ft (12 m) thick chert adjacent to a

fault zone. Sample 39 is mineralized jasperoid with chalcopyrite, galena, and pyrite; it was collected from 3 ft (1 m) below Sandia Formation contact.

40. Jasperoid sample taken from the upper 4 ft of bedded chert, just below green shales of Sandia Formation. Collecting locality is on west side of range at elevation of 9240 ft, on a drill-pad road cut into dip slope of silicified Kelly Limestone.

41. Jasperoid sample collected from near the top of silicified Kelly Limestone, just below Sandia Formation contact. Above the Enterprise tunnel, elevation 8650 ft. See Loughlin and Koschmann (1942, pl. 2) for map location of Enterprise mine.

42. Shales, light gray to white. Base of Caloso Member, Kelly Limestone. Waldo mine, main level. See Loughlin and Koschmann (1942, pls. 32-33) for detailed sections and maps of the Waldo mine.

43, 44. Kelly Limestone jasperoids. Sample 43 has silica replaced with chalcopyrite, sphalerite, galena, and pyrite. Sample 44 is an unmineralized jasperoid specimen. Both samples taken from dump in front of Sleeper tunnel. See Loughlin and Koschmann (1942, pl. 2) for map location of Sleeper tunnel.

45, 46. Jasperoids. Sample 45 is from top of Kelly Limestone silicified zone which is some 40 ft (12 m) thick; it has large hematite pseudomorphs after pyrite and blades of barite. Sample 46 is from basal 10 ft of silicified zone; pyrite molds abundant.

47-50. Ambrosia mine. Sample 47 is a jasperoid collected from top of Kelly Limestone on crest of ridge. Sample 48 collected from a small prospect pit in the upper 3-4 ft (1-1.2 m) of silicified Kelly Limestone; has malachite and azurite copper stains. Sample 49 is from a small pit at south end on the west side of crest; has soft, white silicification with copper stains. Sample 50 appears to be a pre-Pennsylvanian altered, mineralized, terra-rossa soil. It ranges from yellow to maroon to black. Sample collected from major pits along crest of range. See Loughlin and Koschmann (1942, pl. 2) for map location of Ambrosia mine.

91N—W1. Some 92 inches above the Proterozoic gneiss, lime mudstone, intertidal, horizons at which first cherts were found. Caloso Member. Waldo Mine.

91N—W2. Near or adjacent to massive sulfide ore body; collected just above "silver pipe" zone of miners, Ladron Member. Carbonates highly altered and mineralized. Waldo mine.

91N—W3. Collected about 10 ft from previous sample, but from non-mineralized dolomitic lime mudstone recrystallized by heat. High subtidal to low supratidal, abundant microbial mats. Waldo mine.

Samples collected by Renault

89f30a. Elev. 9000 ft, 1 m below top of Kelly Limestone, Jordan Canyon **Rd.** Massively silicified limestone. Jasperoid.

89f30b. Elev. 9020 ft, immediately above Silver Pipe, Jordan Canyon **Rd.** Chert.

89f30c. Elev. 9200 ft, see 89f30f in Table 8. Top layer of laminated vuggy jasperoid. Jasperoid.

89f30d. Elev. 9200 ft, as 89f30c, middle layer of laminated vuggy jasperoid. Jasperoid.

89f30e. Elev. 9200 ft, as 89f30c, bottom layer of laminated vuggy jasperoid. Jasperoid.

89f30f. Elev. 9200 ft, 450 m S of previous sample. Immediately above laminated jasperoid of 89130c, d, e. Chert.

89f30g. Elev. 9100 ft, ridge above 89f30f. Chert in limestone float.

89f30h. Elev. 9160 ft, prospect at saddle 2200 m N of North Baldy. Jasperoid in silicified and mineralized limestone in fault.

89f30i. Elev. 9300 ft, head of Mistletoe Gulch. Chert, barite-oated nodule in karst deposit.

89f30j. Elev. 8300 ft, as 89f30i. Terra rossa.

89h23c. Elev. 8200 ft, SE side of road in Chihuahua Gulch. Chert.

89j18a. Elev. 9570 ft, 200 m NW of North Baldy. Jasperoid, upper part of banded silicified zone.

89j09a. Elev. 9440 ft, prospect 290 m SE of North Baldy Peak. White rhyolite with microcrystalline bands.

89j09b. Elev. 9450 ft, as 89j09a, 1.5 m W of white rhyolite dike. Jasperoids, upper part of banded siliceous zone.

89j18a. Elev. 9560 ft, cliff NE of North Baldy Peak. Jasperoid; gray with vuggy white bands.

89j18b. Elev. 9550 ft, as 89j18a, lower part. Jasperoid.

89j18c. Elev. 9500 ft, base of cliff; 3.3 m traverse through N. Cherts west of rhyolite dike.

89k11 a. Elev. 9160 ft, Armstrong's sites 11 and 12. Jasperoid and altered mudstone.

89k15a. Elev. 9180 ft, 200 m N of Armstrong's site 11. Terra rossa associated with jasperoid and barite + quartz lined cavities.

90f20a. Elev. 9450 ft, See 89j09b—i. White rhyolite dike.

APPENDIX 4 Chemical Analyses

Table 10—Geochemical analyses

Field#	Lab#	Lat.	Long.	Ca %	Fe %	Mg %	Ti %	Ag ppm	Ba ppm	Be ppm	Co ppm	Cr ppm	Cu ppm	Ga ppm	Mn ppm	Mo ppm	Ni ppm
88N-01	D-317304	340300	1071045	0.2	5	0.15	0.015	10.0	2000	3	300	10	700	5	5000	200	100
88N-03	D-317306	340309	1071048	0.2	1	0.2	0.07	5.0	1000	1	10	15	50	5	700	15	20
88N-04	D-317307	340309	1071048	0.2	5	0.7	0.15	1.5	500	1.5	50	100	30	10	700	5	70
88N-05	D-317308	340310	1071050	0.07	3	0.15	0.2	30.0	150	2	10	70	50	10	150	7	15
88N-06	D-317309	340455	1071052	0.5	0	0.02	0.015	10.0	5000	1.5	0	10	700	5	150	15	5
88N-08	D-317311	340453	1071054	0.2	0	0.07	0.015	15.0	5000	1.5	0	30	100	5	1500	150	5
88N-09	D-317312	340433	1071103	0.05	0	0.1	0.02	20.0	5000	1.5	0	10	700	5	150	7	5
88N-10	D-317313	340433	1071103	0.2	5	0.7	0.07	20.0	1500	3	30	30	1500	10	5000	10	50
88N-11	D-317314	340415	1071104	0.15	2	0.7	0.05	15.0	200	5	70	15	15000	7	5000	50	70
88N-12	D-317315	340415	1071104	0.1	10	0.5	0.3	3.0	700	1.5	20	150	200	30	500	5	30
88N-14	D-317317	340318	1071047	0.5	20	0.07	0.02	10.0	150	5	30	10	50	10	200	15	100
88N-15	D-317318	340325	1071049	0.05	0	0.05	.0150	7.0	5000	5	20	15	70	5	1000	30	20
88N-16	D-317319	340341	1071100	0.2	1	0.07	0.05	2.0	700	1.5	10	15	30	5	150	50	5
88N-17	D-317320	340350	1071107	2	5	0.07	0.02	15.0	700	5	20	15	1500	5	100	50	50
88N-18	D-317321	340358	1071102	0.05	0	0.02	0.01	20.0	5000	1	10	15	70	5	200	15	5
88N-19	D-317322	340400	1071101	0.07	0	0.03	0.03	30.0	5000	1.5	0	10	500	5	150	30	5
88N-20	D-317323	340400	1071101	0.3	0	0.05	0.02	2.0	5000	1.5	10	10	100	5	700	15	5
88N-21	D-317324	340540	1071125	0.7	1	0.1	0.1	20.0	700	2	10	20	150	5	700	20	7
88N-22	D-317325	340545	1071125	0.05	15	0.03	0.07	20.0	100	1.0 L	10	30	2000	15	3000	70	0
88N-23	D-317326	340535	1071133	0.05	15	0.07	0.07	10.0	100	1.5	15	30	3000	10	5000	15	7
88N-24	D-317327	340535	1071133	0.15	1	0.03	0.07	20.0	5000	2	10	10	1500	5	700	20	10
88N-25	D-317328	340550	1071145	0.1	7	0.1	0.01	70.0	150	1.5	15	10	10000	5	1500	5	5
88N-26	D-317329	340509	1071148	0.15	0	0.03	0.015	3.0	5000	2	0	10	100	5	150	5	5
88N-27	D-317330	340515	1071140	0.3	2	0.07	0.07	20.0	5000	1.5	10	30	30	5	300	15	10
88N-29	D-318411	340510	1071109	0.15	0	0.02	0.05	10.0	5000	1.5	0	10	50	5	300	5	7
88N-30	D-318412	340510	1071109	0.07	0	0.07	0.01	50.0	5000	2	0	10	30	5	1500	50	5
88N-31	D-318413	340421	1071111	0.3	2	0.15	0.10	7.0	1500	3	10	30	30	5	200	50	30
88N-32	D-318414	340435	1071113	0.2	1	0.15	0.10	15.0	5000	2	10	15	50	5	1500	30	10
88N-33	D-318415	340421	1071113	0.015	1	0.30	0.10	30.0	5000	3	20	30	150	10	2000	70	30
88N-35	D-318417	340339	1071149	0.2	5	0.20	0.07	70.0	700	3	20	15	15000	5	5000	50	30
88N-37	D-318419	340449	1071125	0.3	1	0.15	0.03	20.0	5000	2	10	20	700	5	1000	15	5
88N-38	D-318420	340438	1071140	0.07	1	0.15	0.05	2.0	2000	1	0	30	50	5	300	30	5
88N-39	D-318421	340438	1071140	0.05	0	0.07	0.01	30.0	5000	1	0	15	2000	5	500	50	5
88N-40	D-318422	340405	1071110	0.05	0	0.07	0.02	5.0	3000	1.5	0	10	30	5	500	70	5
88N-41	D-318423	340407	1071120	0.15	3	0.50	0.05	50.0	3000	3	15	30	3000	10	1000	300	15
88N-43	D-318402	340552	1071150	0.0	5	0.03	0.01	20.0	300	1.5	10	10	10000	5	1500	15	5
88N-44	D-318403	340552	1071150	0.0	1	0.02	0.01	15.0	300	1.5	10	10	700	5	3000	15	5
88N-45	D-318404	340325	1071115	0.1	0	0.03	0.01	1.5	5000	1.5	0	10	30	5	500	30	5
88N-46	D-318405	340525	1071115	0.2	0	0.1	0.02	10.0	5000	2.0	10	10	30	5	1500	70	5
88N-47	D-318406	340615	1071124	0.5	3	0.02	0.02	70.0	5000	2.0	0	10	150	5	200	10	5
88N-48	D-318407	340615	1071124	0.1	0	0.05	0.01	10.0	1000	2.0	0	10	150	5	2000	5	5
88N-49	D-318408	340615	1071124	0.1	10	0.1	0.01	1.5	700	15.0	20	10	15000	5	1500	10	20
88N-50	D-318409	340615	1071124	0.1	15	0.03	0.01	200.0	200	3.0	0	10	1500	20	150	20	5

Field	Lab#	Lat.	Long.	Pb ppm	Sc ppm	Sr ppm	V ppm	Y ppm	Zr ppm	As ppm	Bi ppm	Cd ppm	Sb ppm	Zn ppm	Au ppm
88N-01	D-317304	340300	1071045	15000	7	300	70	50	10	12	3	34.0	28	6700	0.1
88N-03	D-317306	340309	1071048	1500	5	0	15	30	100	5	2	23.0	2	18000	0.3
88N-04	D-317307	340309	1071048	500	20	0	70	50	200	11	2	39.0	3	9400	0.004
88N-05	D-317308	340310	1071050	1000	7	200	100	20	100	39	2	1.1	5	470	0.1
88N-06	D-317309	340455	1071052	15000	0	300	10	10	10	5	2	13.0	6	850	0.9
88N-08	D-317311	340453	1071054	2000	0	3000	30	20	10	7	2	7.6	6	1200	1
88N-09	D-317312	340433	1071103	7000	5	500	50	10	15	5	2	1.1	3	570	1.3
88N-10	D-317313	340433	1071103	5000	10	200	70	70	50	10	2	54.0	2	26000	0.4
88N-11	D-317314	340415	1071104	15000	15	0	50	70	20	46	2	28.0	2	23000	0.2
88N-12	D-317315	340415	1071104	500	15	100	150	70	300	500	2	2.4	4	430	0.05
88N-14	D-317317	340318	1071047	100	0	0	15	30	10	7	2	79.0	2	8000	0.006
88N-15	D-317318	340325	1071049	700	0	700	20	50	15	5	2	1.9	4	3900	0.3
88N-16	D-317319	340341	1071100	700	0	0	20	10	150	30	2	0.4	4	350	0.2
88N-17	D-317320	340350	1071107	2000	5	0	50	30	10	17	2	180.0	3	17000	0.2
88N-18	D-317321	340358	1071102	15000	0	300	10	10	10	7	2	1.1	9	220	0.3
88N-19	D-317322	340400	1071101	7000	0	1000	15	10	20	17	2	3.1	6	610	1.4
88N-20	D-317323	340400	1071101	700	0	500	15	10	10	5	2	17.0	2	4000	0.2
88N-21	D-317324	340540	1071125	10000	5	150	50	50	70	5	2	12.0	13	8700	0.1
88N-22	D-317325	340545	1071125	20000	5	0	70	15	10	35	7	45.0	120	11000	0.028
88N-23	D-317326	340535	1071133	3000	7	0	30	20	50	44	7	96.0	10	11000	0.012
88N-24	D-317327	340535	1071133	3000	0	150	15	20	50	58	2	17.0	9	2100	0.016
88N-25	D-317328	340550	1071145	20000	0	0	10	20	10	5	2	710.0	130	24000	0.4
88N-26	D-317329	340509	1071148	700	0	300	15	10	10	5	2	3.1	2	600	0.002
88N-27	D-317330	340515	1071140	300	5	500	20	15	70	5	2	1.4	2	210	0.002
88N-29	D-318411	340510	1071109	150	0	500	15	20	20	5	2	1.5	2	280	0.002
88N-30	D-318412	340510	1071109	1000	5	3000	20	15	10	5	2	0.9	6	640	0.002
88N-31	D-318413	340421	1071111	1500	5	300	70	50	70	7	2	2.1	3	280	0.028
88N-32	D-318414	340435	1071113	7000	5	300	70	30	70	10	2	1.5	3	530	0.25
88N-33	D-318415	340421	1071113	5000	5	100	100	20	70	48	2	3.4	5	2600	0.024
88N-35	D-318417	340339	1071149	20000	5	100	30	30	30	9	16	210.0	10	22000	0.036
88N-37	D-318419	340449	1071125	1000	0	1000	20	10	30	6	2	3.9	2	1900	0.1
88N-38	D-318420	340438	1071140	1000	5	0	30	30	20	32	2	0.8	3	390	0.012
88N-39	D-318421	340438	1071140	2000	0	0	20	15	10	5	33	3.6	150	410	0.6
88N-40	D-318422	340405	1071110	700	0	300	15	30	20	5	2	1.0	2	270	0.1
88N-41	D-318423	340407	1071120	20000	5	300	70	20	70	13	2	70.0	37	17000	2.1
88N-43	D-318402	340552	1071150	20000	0	0	15	20	10	9	5	530	0	22000	0.026
88N-44	D-318403	340552	1071150	20000	0	0	10	15	70	0	0	210	4	22000	0.006
88N-45	D-318404	340325	1071115	700	0	1500	20	20	30	0	0	0.6	0	140	0.034
88N-46	D-318405	340525	1071115	500	0	100	30	15	15	8	20	1.3	0	580	0.1
88N-47	D-318406	340615	1071124	20000	0	200	10	15	10	32	0	8.3	170	1200	0.15
88N-48	D-318407	340615	1071124	500	0	0	15	15	10	0	0	16	0	15000	0.004
88N-49	D-318408	340615	1071124	1500	15	0	10	30	10	0	18	96	0	24000	0.096
88N-50	D-318409	340615	1071124	20000	5	0	15	20	10	110	3200	14	140	5900	0.15

Geochemical analyses by Bondar-Clegg, Inc. Notes: Concentrations in ppm except where noted. Methods: ICP except Au (Fire ass -AA), Hg (Cold vapor AA), Ba & Sn (XRF) (1) Au concentrations in ppb (2) Fe concentrations in pct. (3) Ba interference due to Fe (4) Ba interference noted.

Sample #	Au(1)	Ag	Cu	Pb	Zn	Mo	Ni	Co	Bi	As	Sb	Hg	Fe(2)	Mn	Ba	Cr	W	Sn
92F02B	< 5	< 0.2	4557	9231	10.10%	80	22	13	61	9	16	0.164	> 10.00	2564	240(3)	44	1751	34
92F02C1	< 5	< 0.2	6	19	119	3	205	46	15	< 5	< 5	0.059	9.63	10256	390(4)	149	< 20	6
92F09B	< 5	< 0.2	30	18	187	2	72	69	16	< 5	< 5	0.020	> 10.00	197	40(4)	162	< 20	19
92F09D	< 5	< 0.2	21	16	130	1	20	7	6	< 5	< 5	0.026	2.53	1318	310	15	< 20	9
92F11A1	1859	15.1	29	680	269	27	10	2	< 5	< 5	< 5	0.025	1.18	406	90	454	< 20	10
92F11A2	337	3.3	203	1614	5526	109	37	15	16	85	24	0.095	9.10	2040	340(4)	360	< 20	17
92F11B1	298	7.1	27	306	161	58	12	2	< 5	13	< 5	0.026	1.42	113	240	502	< 20	10
92F11B2	11	1.9	9	110	96	33	8	2	< 5	< 5	6	0.013	0.63	296	110	341	< 20	17
92F11B3	192	4.4	24	385	240	51	15	3	< 5	5	< 5	0.024	2.07	393	100	483	< 20	10
92F11B4	292	3.7	14	173	93	43	9	1	< 5	< 5	< 5	< 0.010	0.94	65	40	483	< 20	14
92F11B5	< 5	1.6	26	170	123	31	11	2	< 5	< 5	< 5	0.017	0.62	695	50	416	< 20	12
92F11B6	507	6.0	30	381	237	52	7	1	< 5	7	6	0.017	1.71	42	80	212	< 20	10
92F11B7	703	13.1	24	463	219	91	12	2	< 5	6	11	0.014	1.56	154	60	486	< 20	< 5
92F11B8	167	5.1	277	5205	3861	115	35	11	11	214	15	0.057	8.45	523	40*	223	< 20	15
92F11B9	557	14.4	71	1294	912	137	20	6	5	30	12	0.035	3.81	679	50*	523	< 20	13
92F11C1	10	1.4	21	6850	1493	15	6	3	< 5	< 5	< 5	0.012	0.66	110	910	305	< 20	8
92F11C2	85	0.6	25	981	5070	47	11	4	9	< 5	< 5	0.017	0.67	120	330*	436	< 20	17
92F11C3	143	0.8	25	454	632	22	10	3	< 5	< 5	< 5	0.016	0.91	267	340	575	< 20	16
92F11C4	9	0.5	24	568	583	21	5	2	< 5	< 5	< 5	< 0.010	0.29	1176	200	151	< 20	16
92F11C5	< 5	11.5	180	0.94%	5352	153	7	3	11	7	10	0.040	0.61	427	200*	297	< 20	13
92F11C6	555	2.38opt	2002	1.99%	2.47%	43	6	3	29	15	14	0.067	0.74	966	300*	142	219	13
92F11C7	44	5.0	196	1528	2613	13	6	1	8	< 5	< 5	0.012	0.41	3645	140	182	< 20	15
92F11D	111	49.0	215	758	639	37	11	2	< 5	11	< 5	0.014	1.71	89	200	617	< 20	11

References

- Armstrong, A. K., 1958, The Mississippian of west-central New Mexico: New Mexico Bureau of Mines & Mineral Resources, Memoir 5, 32 pp.
- Armstrong, A. K., and Mamet, B. L., 1976, Biostratigraphy and regional relations of the Mississippian Leadville Limestone in the San Juan Mountains, southwestern Colorado: U.S. Geological Survey, Professional Paper 985, 25 pp.
- Armstrong, A. K., Mamet, B. L., and Repetski, J. E., 1992, Stratigraphy of the Mississippian System, south-central Colorado and north-central New Mexico: U.S. Geological Survey, Bulletin 1787, 22 pp.
- Azaroff, L. V., 1963, Role of x-ray intensities in crystal perfection studies; in Ramachandran, G. N. (ed.), *Crystallography and crystal perfection*: Academic Press, New York, pp. 190-124.
- Bagby, W. C., and Berger, B. R., 1985, Geologic characteristics of sediment-hosted, disseminated precious-metal deposits in the western United States; in Berger, B. R., and Bethke, P. M. (eds.), *Geology and geochemistry of epithermal systems*: Society of Economic Geologists, Reviews in Economic Geology, v. 2, pp. 169-202.
- Bagby, W. C., Menzie, W. D., Mosier, D. L., and Singer, D. A., 1986, Grade and tonnage model carbonate-hosted Au-Ag; in Cox, D. P., and Singer, D. A. (eds.), *Mineral deposit models*: U.S. Geological Survey, Bulletin 1693, pp. 175-177.
- Blakestad, R. B., Jr., 1978, Geology of the Kelly mining district, Socorro County, New Mexico: Unpublished M.S. thesis, University of Colorado, Boulder; and New Mexico Bureau of Mines & Mineral Resources, Open-file Report 43, 139 pp.
- Blankenberg, H.-J., von, and Berger, H., 1981, Kristallitgrossenuntersuchungen an Vulkanitachaten: *Chemie der Erde*, v. 40, pp. 139-154.
- Bobrow, D. J., Kyle, P. R., and Osburn, G. R., 1983, Miocene rhyolitic volcanism in the Socorro area of New Mexico: New Mexico Geological Society, Guidebook 34, pp. 211-217.
- Bowring, S. A., Kent, S. C., and Ward, S., 1983, Geology and U-Pb geochronology of Proterozoic rocks in the vicinity of Socorro, New Mexico: New Mexico Geological Society, Guidebook 34, pp. 137-142.
- Budding, A. J., and Broadhead, R. F., 1977, Igneous and metamorphic petrology of drill cuttings from the KCM No. 1 Forest Federal Well, Hidalgo County, New Mexico: New Mexico Bureau of Mines & Mineral Resources, Circular 152, pp. 29-35.
- Burnham, C. W., 1967, Hydrothermal fluids at the magmatic stage; in Barnes, H. L. (ed.), *Geochemistry of hydrothermal ore deposits*: Holt, Reinhart & Winston, New York, pp. 34-76.
- Carlsaw, H. S., and Jaeger, J. C., 1959, *Conduction of heat in solids*: Clarendon Press, Oxford, 510 pp.
- Cather, S. M., 1980, Petrology, diagenesis and genetic stratigraphy of the Eocene Baca Formation, Alamo Navajo Reservation, Socorro County, New Mexico: Unpublished M.S. thesis, University of Texas at Austin, 243 pp.
- Cather, S. M., 1986, Volcano-sedimentary evolution and tectonic implications of the Datil Group (latest Eocene-early Oligocene), west-central New Mexico: Unpublished Ph.D. dissertation, University of Texas at Austin, 484 pp.
- Cather, S. M., 1989, Post-Laramide tectonic and volcanic transition in west-central New Mexico: New Mexico Geological Society, Guidebook 40, pp. 91-97.
- Cather, S. M., and Chapin, C. E., 1989, Field guide to upper Eocene and lower Oligocene volcanoclastic rocks of northern Mogollon-Datil volcanic field; in Chapin, C. E., and Zidek, J. (eds.), *Field excursions to volcanic terranes in the western United States: Southern Rocky Mountains region*: New Mexico Bureau of Mines & Mineral Resources, Memoir 46, pp. 60-68.
- Chapin, C. E., 1989, Volcanism along the Socorro accommodation zone, Rio Grande Rift, New Mexico; in Chapin, C. E. and Zidek, J. (eds.), *Field excursions to volcanic terranes in the western United States: Southern Rocky Mountains region*: New Mexico Bureau of Mines & Mineral Resources, Memoir 46, pp. 46-57.
- Chapin, C. E., Chamberlin, R. M., Osburn, G. R., Sanford, A. R., and White, D. L., 1978, Exploration framework of the Socorro geothermal area, New Mexico; in Chapin, C. E., and Elston, W. E. (eds.), *Field guide to selected cauldrons and mining districts of the Datil-Mogollon volcanic field, New Mexico*: New Mexico Geological Society, Special Publication 7, pp. 115-129, plate in pocket.
- Condie, K. C., and Budding, A. J., 1979, Geology and geochemistry of Precambrian rocks, central and south-central New Mexico: New Mexico Bureau of Mines & Mineral Resources, Memoir 35, 58 pp.
- Cook, K., 1986, Conodont color alteration: A possible exploration tool for ore deposits: Unpublished M.S. thesis, New Mexico Institute of Mining & Technology, Socorro, 125 pp.
- Cox, D. P., and Singer, D. A. (eds.), 1986, *Mineral deposit models*: U.S. Geological Survey, Bulletin 1693, 379 pp.
- Cox, D. P., and Singer, D. A., 1990, Descriptive and grade-tonnage models for distal disseminated Ag-Au deposits. A supplement to U.S. Geological Survey, Bulletin 1693: U.S. Geological Survey, Open-file Report 90-282, 7 pp.
- Dunham, R. J., 1962, Classification of carbonates according to depositional texture; in Ham, W. E. (ed.), *Classification of carbonate rocks*: American Association of Petroleum Geologists, Memoir 1, pp. 108-121.
- Epstein, A. G., Epstein, J. B., and Harris L. D., 1977, Conodont color alteration-an index to organic metamorphism: U.S. Geological Survey, Professional Paper 995, 27 pp.
- Ewing, R. C., and Thompson, S., III, 1977, Thermal metamorphism of organic matter in drill cuttings from KCM No. 1 Forest Federal Well: New Mexico Bureau of Mines & Mineral Resources, Circular 152, pp. 49-51.
- Fournier, R. O., 1973, Silica in thermal waters-laboratory and field investigations; in Ingerson, E. (ed.), *Symposium on hydrogeochemistry and biogeochemistry*, Tokyo, 1970, Proceedings, v. 1, Hydrogeochemistry: The Clark Co., Washington, DC, pp. 122-139.
- Fournier, R. O., 1985, The behavior of silica in hydrothermal systems; in Berger, B. R., and Bethke, P. M. (eds.), *Geology and geochemistry of epithermal systems*: Society of Economic Geologists, Reviews in Economic Geology, v. 2, pp. 45-61.
- Griggs, D. T., and Blacic, J. D., 1964, The strength of quartz in the ductile regime: *EOS Transactions, American Geophysical Union*, v.45, pp. 102-103.
- Griggs, D. T., and Blacic, J. D., 1965, Quartz: Anomalous weakness of synthetic crystals: *Science*, v. 147, pp. 292-295.
- Guiraud, M., Sauniac, S., and Burg, J.-P., 1982, Precisions sur les conditions pressions-température lors de la mise en place de la nappe de Pardailhan (Montagne Noire), par la détermination des inclusions fluides: *C.R. Académie des Sciences, Paris*, v. 296, serie II, pp. 229232.
- Hanor, J. S., 1968, Frequency distribution of compositions in the barite-celestite series: *American Mineralogist*, v. 53, pp. 1215-1222.
- Harland, W. B., Armstrong, R. L., Cox, A. V., Craig, L. E., Smith, A. G., and Smith, D. G., 1990, *A geologic time scale 1989*: Cambridge University Press, Cambridge, U.K., 263 pp.
- Harrower, R., Norman, D. I., Savin, S. M., and Sawkins, F. J., 1982, Stable oxygen isotope and crystallite size analysis of the De Long Mountain, Alaska, cherts: An exploration tool for submarine exhalative deposits: *Economic Geology*, v. 77, pp. 1761-1766.
- Hathaway, J. C., 1972, X-ray mineralogy studies: Leg 11, pt 2; in Hollister, C. D., Ewing, J. I., and others, 1972, *Initial Reports, Deep Sea Drilling Project, v. 11*: U.S. Government Printing Office, Washington, DC, pp. 729-789.
- Hein, J. F., Scholl, D. W., Barron, J. A., Jones, M. G., and Miller, J., 1978, Diagenesis of late Cenozoic diatomaceous deposits and formation of the bottom simulating reflector in the southern Bering Sea: *Sedimentology*, v. 25, pp. 155-181.
- Henisch, H. K., 1988, *Crystals in gels and liesegang rings*: Cambridge University Press, Cambridge, U.K., 197 pp.
- Henry, N. F. M., Lipson, H., and Wooster, W. A., 1961, *The interpretation of x-ray diffraction photographs*: Macmillan & Co., London, 206 pp.
- Hoersch, A. L., 1981, Progressive metamorphism of the chert-bearing Dumess limestone in the Beinn an Dubhaich aureole, Isle of Skye, Scotland: A re-examination: *American Mineralogist*, v. 66, pp. 491-506.
- Holland, P. T., Beatty, D. W., and Snow, G. G., 1988, Comparative elemental and oxygen isotope geochemistry of jasperoid in the northern Great Basin: Evidence for distinctive fluid evolution in gold-producing hydrothermal systems: *Economic Geology*, v. 83, pp. 1401-1423.
- Hunt, A., 1983, Plant fossils and lithostratigraphy of the Abo Formation (Lower Permian) in the Socorro area and plant biostratigraphy of Abo red beds in New Mexico: New Mexico Geological Society, Guidebook 34, pp. 157-163.
- Idzikowski, S., 1977, The growth of crystalline grain in a-ferric oxide: *British Ceramic Society Publications*, v. 76, no. 4, pp. 74-81.
- Iovenitti, J., 1977, A reconnaissance study of jasperoid in the Kelly Limestone, Kelly mining district, New Mexico: New Mexico Bureau of Mines & Mineral Resources, Open-file Report 85, 200 pp.
- Iovenitti, J., and Renault, J., 1977, Crystallite size variation in cherts and jasperoids from the Magdalena mining district, Socorro County, New Mexico (abs.): *Geological Society of America, Abstracts with Programs*, v. 9, pp. 735.

- Johannsen, A., 1939, A descriptive petrography of the igneous rocks vol. 1 (2nd edition): University of Chicago Press, 318 pp.
- Jones, F. W., 1938, On measurement of particle size by x-ray methods: Proceedings of the Royal Society (London), v. 166A, pp. 16-43.
- Kappelmeyer, O., and Haenel, R., 1974, Geothermics with special reference to application: Gebrüder Borntraeger, Berlin, 211 pp.
- Keller, W. D., Stone, C. G., and Hoersch, A. L., 1985, Texture of Paleozoic cherts and novaculite in the Ouachita Mountains of Arkansas and Oklahoma and their geological significance: Geological Society of America Bulletin, v. 96, pp. 1353-1363.
- Kelley, S. A., Chapin, C. E., and Corrigan, J., 1992, Late Mesozoic and Cenozoic cooling histories of the flanks of the northern and central Rio Grande rift, Colorado and New Mexico: New Mexico Bureau of Mines & Mineral Resources, Bulletin 145, 39 pp.
- Klug, H. P., and Alexander, L. E., 1974, X-ray diffraction procedures: (2nd edition): John Wiley & Sons, New York, 292 pp.
- Krauskopf, K. B., 1967, Introduction to geochemistry: McGraw-Hill Book Co., New York, 721 pp.
- Kronenberg, A. K., Kirby, S. H., Aines, R. D., and Rossman, R. R., 1986, Solubility and diffusional uptake of hydrogen in quartz at high water pressures: Implications for hydrolytic weakening: Journal of Geophysical Research, v. 91, B12, pp. 12,723-12,744.
- Krukowski, S. T., 1988, Interim report on the conodont biostratigraphy of the Kelly Limestone (Mississippian), central New Mexico (abs.): New Mexico Geology, v. 10, p. 39.
- Loughlin, G. H., and Koschmann, A. H., 1942, Geology and ore deposits of the Magdalena mining district, New Mexico: U.S. Geological Survey, Professional Paper 200, 168 pp.
- Lovering, T. G., 1972, Jasperoid in the United States, its characteristics, origin, and economic significance: U.S. Geological Survey, Professional Paper 710, 154 pp.
- Lovering, T. G., and Heyl, A. V., 1974, Jasperoid as a guide to mineralization in the Taylor mining district and vicinity near Ely, Nevada: Economic Geology, v. 69, pp. 46-58.
- Lovering, T. G., and McCarthy, J. H., Jr., 1978, Detroit mining district; *in* Lovering, T. G., and McCarthy, J. H., Jr. (eds.), Conceptual models in exploration geochemistry; the Basin and Range Province of the western United States and northern Mexico: Journal of Geochemical Exploration, v. 9, pp. 168-174.
- Lucas, S. G., 1983, The Baca Formation and the Eocene-Oligocene boundary in New Mexico: New Mexico Geological Society, Guidebook 34, pp. 187-192.
- MacKenzie, K. J. D., and Melling, P. J., 1974, The calcination of titania: British Ceramic Society, Transactions, v. 73, pp. 23-27.
- Madrid, R. J., and Bagby, W. C., 1988, Gold occurrence and its relation to vein and mineral paragenesis in selected sedimentary-rock-hosted, Carlin-type deposits in Nevada, *in* Goode, A. D. T., and Bosma, L. I. (compilers), Bicentennial Gold 88, Extended Abstracts of Oral Program: Geological Society of Australia, Melbourne, Abstract Series no. 22, p. 161.
- Manrique, J., and Campbell, A., 1987, A fluid inclusion study of the Waldo-Graphic mine, Magdalena district, New Mexico: New Mexico Geology, v. 9, pp. 1-6.
- McGehee, R., and Renault, J. 1972, The use of standard deviation of x-ray diffraction lines as a measure of broadening in the Scherrer equation: A curve fitting method: Journal of Applied Crystallography, v. 5, pp. 365-370.
- McIntosh, W. C., Kedzi, L. L., and Sutter, J. F., 1991, Paleomagnetism and $^{40}\text{Ar}/^{39}\text{Ar}$ ages of ignimbrites, Mogollon-Datil volcanic field, southwestern New Mexico: New Mexico Bureau of Mines & Mineral Resources, Bulletin 135, 79 pp.
- McKee, E. D., 1967, Paleotectonic investigation of the Permian System in the United States, Arizona and New Mexico: U.S. Geological Survey, Professional Paper 515-J, pp. 199-223.
- Meyer, C., and Hemley, J. J., 1967, Ch. 6, Wall rock alteration; *in* Barnes, H. L. (ed.), Geochemistry of hydrothermal ore deposits (1st edition), Holt, Rinehart & Winston, Inc., New York, pp. 166-235.
- Meyers, W. J., 1978, Carbonate cements; their regional distribution and interpretation in Mississippian limestones of southwestern New Mexico: Sedimentology, v. 25, pp. 371-400.
- Meyers, W. J., 1988, Paleokarstic features in Mississippian limestone, New Mexico; *in* James, N. P., and Choquette, P. W. (eds.), Paleokarst: Springer-Verlag, New York, pp. 306-328.
- Mitra, G. B., and Misra, N. K., 1967, Line shape analysis of cold-worked magnesium: Acta Crystallographica, v. 22, pp. 454.
- Murata, K. J., and Norman, M. B., 1976, An index of crystallinity for quartz: American Journal of Science, v. 276, pp. 1120-1130.
- Nelson, C. E., 1990, Comparative geochemistry of jasperoids from Carlin-type gold deposits of the western United States: Journal of Geochemical Exploration, v. 36, pp. 171-195.
- Ohmoto, H., and Rye, R. O., 1979, Ch. 10, Isotopes in sulfur and carbon; *in* Barnes, H. L. (ed.), Geochemistry of hydrothermal ore deposits (2nd edition): John Wiley & Sons, New York, pp. 509-561.
- Osburn, G. R., 1978, Geology of the eastern Magdalena Mountains Water Canyon to Pound Ranch, Socorro County, New Mexico: Unpublished M.S. thesis, New Mexico Institute of Mining & Technology, Socorro, 160 pp.
- Osburn, G. R. (compiler), 1984, Socorro County geologic map: New Mexico Bureau of Mines & Mineral Resources, Open-file Report 238, 14 pp., map 1:200,000.
- Osburn, G. R., and Chapin, C. E., 1983a, Ash-flow tuffs and cauldron in the northeast Mogollon-Datil volcanic field: A summary: New Mexico Geological Society, Guidebook 34, pp. 197-204.
- Osburn, G. R., and Chapin, C. E., 1983b, Nomenclature for Cenozoic rocks of the northeast Mogollon-Datil volcanic field: New Mexico Bureau of Mines & Mineral Resources, Stratigraphic Chart 1, 7 pp., 1 sheet.
- Rejebian, V. A., Harris, A. G., and Huebner, J. S., 1987, Conodont color and textural alteration: An index to regional metamorphism, contact metamorphism, and hydrothermal alteration: Geological Society of America Bulletin, v. 99, pp. 471-479.
- Renault, J., 1979, Silica crystallite geothermometer: Initial calibration (abs.): Geological Society of America, Abstracts with Programs, v. 11, pp. 502.
- Renault, J., 1980, Application of crystallite size variation in cherts to petroleum exploration: Final Report for Grant #78-3315, New Mexico Energy Institute, 23 pp.
- Renault, J., and Iovenitti, J., 1978, Resolution of x-ray diffraction lines, a model of the 68-degree 20 quartz quintuplet (abs.): Geological Society of America, Abstracts with Programs, v. 10, pp. 236.
- Richards, T. L., 1970, Limiting crystallite size or lattice strain?: Journal of Applied Crystallography, v. 3, pp. 99.
- Riviere, M., Rautureau, M., Besson, G., Steinberg, M., and Alouri, M., 1985, Complémentarité des rayons-X et de la microscopie électronique pour la détermination des diverses phases d'une argile zincifère: Clay Minerals, v. 20, pp. 53-67.
- Ross, C. A., and Ross, J. P., 1985, Paleozoic tectonics and sedimentation in west Texas, southern New Mexico, and southern Arizona: West Texas Geological Society Field Conference, Publication 85-81, pp. 221-230.
- Sando, W. J., 1985, Revised Mississippian time scale, western interior region, conterminous United States: U.S. Geological Survey, Bulletin 1605-A, pp. 15-26.
- Seager, W. R., Hawley, J. W., and Clemons, R. E., 1971, Geology of San Diego Mountain area, Dona Ana County, New Mexico: New Mexico Bureau of Mines & Mineral Resources, Bulletin 97, 38 pp.
- Siemers, W. T., 1973, Stratigraphy and petrology of Mississippian, Pennsylvanian, and Permian rocks in the Magdalena area, Socorro County, New Mexico: New Mexico Bureau of Mines & Mineral Resources, Open-file Report 54, 133 pp.
- Silberman, M. L., and Berger, B. R., 1985, Relationship of trace-element patterns to alteration and morphology in epithermal precious-metal deposits; *in* Berger, B. R., and Bethke, P. M. (eds.), Geology and geochemistry of epithermal systems: Society of Economic Geologists, Reviews in Economic Geology, v. 2, pp. 230-232.
- Smallman, R. E., 1970, Modern physical metallurgy: Butterworths & Co., London, 544 pp.
- Smith, F. G., 1963, Physical geochemistry: Addison-Wesley Publishing Co., Reading, MA, 624 pp.
- Spurr, J. E., 1898, Geology of the Aspen mining district, Colorado, with atlas: U.S. Geological Survey, Monograph 31, 260 pp., atlas of 30 sheets folio.
- Taylor, R. G., 1979, Geology of tin deposits: Elsevier Scientific Publishing Co., New York, pp. 416-421.
- Theodore, T. G., and Jones, G. M., 1992, Geochemistry and geology of gold in jasperoid, Elephant Head area, Lander County, Nevada: U.S. Geological Survey, Bulletin 2009, 53 pp.
- Titley, S. R., 1959, Silication as an ore control, Linchburg mine, Socorro County, New Mexico: Unpublished Ph.D. dissertation, University of Arizona, Tucson, 153 pp.
- Titley, S. R., 1961, Genesis and control of the Linchburg orebody, Socorro County, New Mexico: Economic Geology, v. 56, pp. 695-722.
- Turcotte, D. L., and Schubert, G., 1982, Geodynamics: John Wiley & Sons, New York, 450 pp.
- Warren, B. E., and Averbach, B. L., 1950, The effect of cold-work

- distortion on x-ray patterns: *Journal of Applied Physics*, v. 21, pp. 595-599.
- Weidemann, K. E., Unnam, J., and Clark, R. K., 1987, Deconvolution of powder diffraction spectra: *Powder Diffraction*, v. 2, p. 130.
- Wilson, A. J. C., 1962, On variance as a measure of line broadening in diffractometry: General theory and small particle size: *Proceedings of the Physical Society (London)*, v. 80, pp. 286-294.
- Wilson, J. L., 1989, Lower and Middle Pennsylvanian strata in the Orogrande and Pedregosa basins, New Mexico: New Mexico Bureau of Mines & Mineral Resources, Bulletin 124, 16 pp.
- Wilpolt, R.H., MacAlin, A.J., Bates, R. L., and Vorbe, G., 1946, Geologic map and stratigraphic section of the Paleozoic rocks of the Joyita Hills, Los Pinos Mountains and northern Chupadera Mesa, Valencia, Torrance and Socorro Counties, New Mexico: U.S. Geological Survey, Oil and Gas Investigations Preliminary Map 61.
- Wood, W. A., 1939, The lower limiting crystallite size and internal strains in some cold-worked metals: *Proceeding of Royal Society of London, [A]*, v. 172, pp. 231-241.
- Wood, W. A., and Rachinger, W. A., 1949, Crystallite theory of metals: *Journal of the Institute of Metals*, v. 75, pp. 571-594.

Selected conversion factors*

TO CONVERT	MULTIPLY BY	TO OBTAIN	TO CONVERT	MULTIPLY BY	TO OBTAIN
Length			Pressure, stress		
inches, in	2.540	centimeters, cm	lb in ⁻² (= lb/in ²), psi	7.03×10^{-2}	kg cm ⁻² (= kg/cm ²)
feet, ft	3.048×10^{-1}	meters, m	lb in ⁻²	6.804×10^{-2}	atmospheres, atm
yards, yds	9.144×10^{-1}	m	lb in ⁻²	6.895×10^3	newtons (N)/m ² , N m ⁻²
statute miles, mi	1.609	kilometers, km	atm	1.0333	kg cm ⁻²
fathoms	1.829	m	atm	7.6×10^2	mm of Hg (at 0° C)
angstroms, Å	1.0×10^{-8}	cm	inches of Hg (at 0° C)	3.453×10^{-2}	kg cm ⁻²
Å	1.0×10^{-4}	micrometers, µm	bars, b	1.020	kg cm ⁻²
Area			b	1.0×10^6	dynes cm ⁻²
in ²	6.452	cm ²	b	9.869×10^{-1}	atm
ft ²	9.29×10^{-2}	m ²	b	1.0×10^{-1}	megapascals, MPa
yds ²	8.361×10^{-1}	m ²	Density		
mi ²	2.590	km ²	lb in ⁻³ (= lb/in ³)	2.768×10^1	gr cm ⁻³ (= gr/cm ³)
acres	4.047×10^3	m ²	Viscosity		
acres	4.047×10^{-1}	hectares, ha	poises	1.0	gr cm ⁻¹ sec ⁻¹ or dynes cm ⁻²
Volume (wet and dry)			Discharge		
in ³	1.639×10^1	cm ³	U.S. gal min ⁻¹ , gpm	6.308×10^{-2}	l sec ⁻¹
ft ³	2.832×10^{-2}	m ³	gpm	6.308×10^{-5}	m ³ sec ⁻¹
yds ³	7.646×10^{-1}	m ³	ft ³ sec ⁻¹	2.832×10^{-2}	m ³ sec ⁻¹
fluid ounces	2.957×10^{-2}	liters, l or L	Hydraulic conductivity		
quarts	9.463×10^{-1}	l	U.S. gal day ⁻¹ ft ⁻²	4.720×10^{-7}	m sec ⁻¹
U.S. gallons, gal	3.785	l	Permeability		
U.S. gal	3.785×10^{-3}	m ³	darcies	9.870×10^{-13}	m ²
acre-ft	1.234×10^3	m ³	Transmissivity		
barrels (oil), bbl	1.589×10^{-1}	m ³	U.S. gal day ⁻¹ ft ⁻¹	1.438×10^{-7}	m ² sec ⁻¹
Weight, mass			U.S. gal min ⁻¹ ft ⁻¹	2.072×10^{-1}	l sec ⁻¹ m ⁻¹
ounces avoirdupois, avdp	2.8349×10^1	grams, gr	Magnetic field intensity		
troy ounces, oz	3.1103×10^1	gr	gausses	1.0×10^5	gammas
pounds, lb	4.536×10^{-1}	kilograms, kg	Energy, heat		
long tons	1.016	metric tons, mt	British thermal units, BTU	2.52×10^{-1}	calories, cal
short tons	9.078×10^{-1}	mt	BTU	1.0758×10^2	kilogram-meters, kgm
oz mt ⁻¹	3.43×10^1	parts per million, ppm	BTU lb ⁻¹	5.56×10^{-1}	cal kg ⁻¹
Velocity			Temperature		
ft sec ⁻¹ (= ft/sec)	3.048×10^{-1}	m sec ⁻¹ (= m/sec)	°C + 273	1.0	°K (Kelvin)
mi hr ⁻¹	1.6093	km hr ⁻¹	°C + 17.78	1.8	°F (Fahrenheit)
mi hr ⁻¹	4.470×10^{-1}	m sec ⁻¹	°F - 32	5/9	°C (Celsius)

*Divide by the factor number to reverse conversions.

Exponents: for example 4.047×10^3 (see acres) = 4,047; 9.29×10^{-2} (see ft²) = 0.0929.

Editor: Jiri Zidek

Type face: Palatino

Presswork: Miehle Single Color Offset
Harris Single Color Offset

Binding: Saddlestitched with softbound cover

Paper: Cover on 12-pt. Kivar
Text on 70-lb White Matte

Ink: Cover—PMS 320
Text—Black

Quantity: 1,000